H.-S. Gwak[1]
S.-M. Youn[1]
U. Chang[1]
D. H. Lee[2]
G. J. Cheon[3]
C. H. Rhee[1]
K. Kim[4]
H.-J. Kim[4]

Usefulness of ^{18}F-Fluorodeoxyglucose PET for Radiosurgery Planning and Response Monitoring in Patients with Recurrent Spinal Metastasis

Abstract

Introduction: With the advancement and successful treatment of metastatic spinal cord disease, newer treatments are needed for the long-term survivors of recurrent disease. The lack of a standardized re-treatment regimen and the difficulty in delineating the tumor margins among patients who have received the treatment with metallic spinal fixation and conventional radiation are two of the challenges to be faced in recurrent metastatic spinal cord disease. In these patients, we applied hypofractionated stereotactic radiosurgery by defining the tumor margin with ^{18}F-fluorodeoxyglucose (FDG) positron emission tomography (PET). **Patients and Methods:** Three consecutive recurrent spinal metastasis patients underwent the CyberKnife treatment (Accuray, Inc., Sunnyvale, CA) from March 2004 to July 2004. A three-fraction schedule was applied at approximately 24 hour intervals. One patient had sarcoma and the other two patients had breast cancer. All patients had received previous conventional radiotherapy after operation ranging from 30 Gy to 45 Gy. CT-based planning was corrected by the FDG-PET hyperuptake area with the help of nuclear medicine. The mass responses were followed not only by MRI but also by FDG-PET, which was taken prior to treatment, and at one and six months after the treatment. The changes in standard uptake value (SUV) of serial PET were taken as a measure of response. To evaluate the relative SUV changes from different pretreatment values, we set a reduction index (RI), which represents the ratio of SUV change to pretreatment SUV. **Results:** No significant complications were noted during treatment with a mean follow-up of 13.3 months. The tumor volume on CT-based planning was 2.2 times larger than that of the CT-PET combined planning in case 1 of paraspinal muscle invasion. But the tumor volumes showed minimal changes in the other cases, in which the metastatic tumors were confined to the vertebral bodies. The SUV one month after treatment showed variable decreases and the RI ranged from 0.07 to 0.7. However, the SUVs at 6 months were well correlated with the clinical results. One patient showed marginal failure and the other two patients showed local control of the tumor, as their RI values were 0.65 and 0.87, respectively. **Conclusion:** To our knowledge, this is the first report using FDG-PET with radiosurgery in patients with recurrent spinal metastases hidden under metallic artifacts. The mass responses measured by SUV changes in FDG-PET correlated with the clinical results.

Key words

FDG-PET · recurrence · spinal metastasis · radiosurgery · planning · treatment response

Introduction

Spinal metastasis has a poor prognosis (6 months) despite surgical resection followed by radiation treatment [1]. Patient performance, tumor histology, location, systemic status of the cancer and the type of surgical approach are some of the variables that affect survival [2]. A subgroup of long-term survivors highlights

Affiliation
[1] Department of Neurosurgery, Korea Institute of Radiological and Medical Science, Seoul, Korea
[2] Department of Radiation Oncology, Korea Institute of Radiological and Medical Science, Seoul, Korea
[3] Department of Nuclear Medicine, Korea Institute of Radiological and Medical Science, Seoul, Korea
[4] Seoul National University Medical College, Seoul, Korea

Correspondence
Hyun-Jib Kim, M. D., Ph. D. · Department of Neurosurgery · Clinical Neuroscience Center · Seoul National University Bundang Hospital · 300 Gumi-dong · Bundang-gu · Sungnam-shi · Gyeonggi-do 463-707 · Republic of Korea · Tel.: +82/31/787/7166 · Fax: +82/31/787/4059 · E-mail: jibkim@snu.ac.kr

Bibliography
Minim Invas Neurosurg 2006; 49: 127–134 © Georg Thieme Verlag KG Stuttgart · New York
DOI 10.1055/s-2006-932181
ISSN 0946-7211

Table **1** Clinical characteristics of patients

Case	*Sex/Age*	*Pathology*	*Involved segment*	*Presenting symptoms*	*Previous treatment*	*Clinical result*
1	M/23	Sarcoma	C7-T1	Left arm pain and weakness	Posterior fusion + CRT 45 Gy at 39 months before	Marginal failure lead to 2nd operation; stationary at 16 months
2	F/55	Breast cancer	T1 – T2	Neck and shoulder pain, Left hand weakness	Anterior fusion + CRT 33 Gy at 20 months before	Complete response of treated lesion; improved at 12 months
3	F/50	Breast cancer	C7 – T1	Neck pain	Anterior fusion + CRT 30 Gy at 3 months before	Complete response but distant failure; worsened at 12 months

CRT = conventional radiation therapy

the need for a new protocol that can better estimate the expected survival and help in the selection of the most efficacious treatment [1]. The treatment of recurrent spinal metastatic disease after conventional therapy is difficult and a standardized treatment protocol does not exist. Recently, radiosurgery for recurrent spinal tumors was attempted in selected centers. The treatment had the advantage of being feasible and the short treatment time, and rapid symptomatic relief. However, the trials did not comment on the risk of radiation injury following previous irradiation or were the results of too short follow-ups [3,4]. In the case of re-irradiation using radiosurgery, it is necessary to delineate the tumor exactly in order for the planning software to calculate the correct tumor control dose, while reducing the hazardous radiation to the adjacent, normal spinal cord. Positron emission tomography (PET) has proven to be effective in differentiating the active tumor from non-specific inflammatory changes or necrosis and to be more useful when combined with CT.

We applied hypofractionated stereotactic radiosurgery (SRS) using the CyberKnife system (Accuray, Inc., Sunnyvale, CA) on three consecutive patients who had been previously treated by metallic spinal fixation and conventional radiation and had recurrent spinal metastatic disease. ^{18}F-Fluorodeoxyglucose (FDG) PET was used to define the tumor margin where the recurrent tumor was nearly invisible due to the metallic artifact. This study is the first report that combines FDG-PET with radiosurgery planning for recurrent spinal metastasis hidden under the metallic artifact. The mass responses were also followed by FDG-PET and the changes in standard uptake value (SUV) and the treatment was correlated with the clinical results.

Patients and Methods

Patient population

From April 2004 to July 2004, three patients who had previously undergone surgical decompression with metallic fusion followed by conventional radiation therapy, were transferred to our hospital to explore other treatment options for their recurrent lesions. Their demographic details are summarized in Table **1**. Although the diagnosis of recurrence was made from the presence of aggravating symptoms and a suspiciously increased mass extent on MRI, neither the exact extent of tumor involvement nor the tumor margins were shown on the images due to artifacts from the previous metal fixatives in all patients (Fig. **1**). Careful neurological examination revealed that no upper motor neuron signs (symptoms of spinal cord compression from the recurrent mass or radiation myelopathy from previous radiation therapy) were present in any patient.

Fig. **1** Serial photographs showing the process from diagnosis to radiosurgical planning; Axial gadolinium-enhanced MRI at the time of recurrence *(left)* in patients with previous metallic fixation and conventional radiation treatment reveals severe artifact from metallic fixatives and indistinct tumor margin. FDG-PET taken for tumor delineation *(center)* shows hyperuptake in the left-posterior portion of involved spinal segment, which was in correspondence to the patient's symptom of left arm pain. Radiosurgery planning CT image (*right*) shows the isodose line of the target volume (blue line), which was drawn from the information of the FDG-PET.

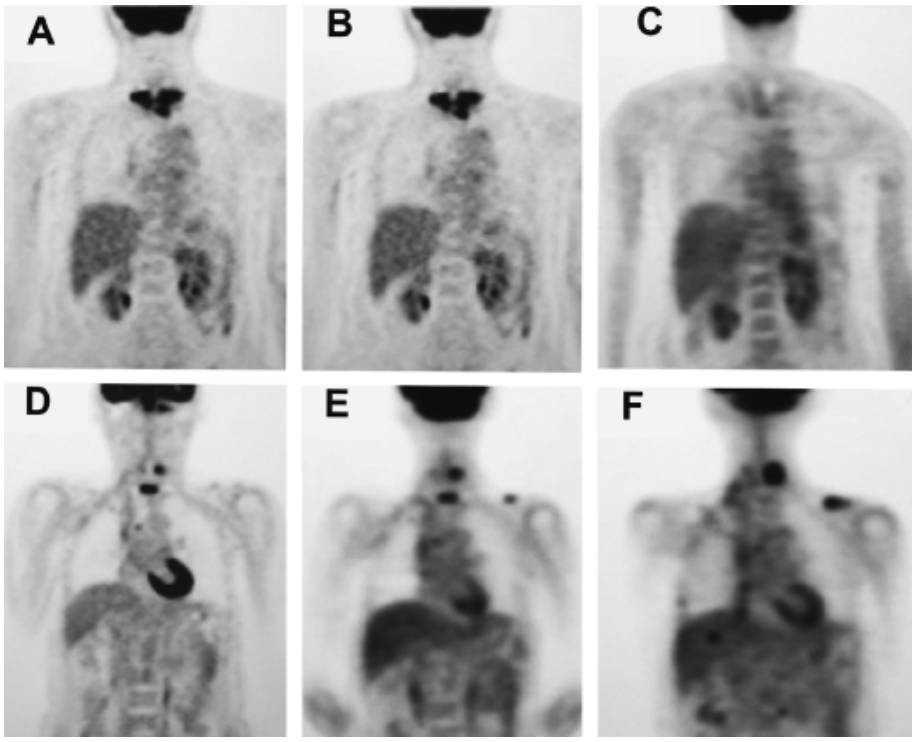

Fig. **2** Illustration of serial FDG-PET uptake changes after CyberKnife treatment in case 2 (**A**, **B** and **C**) and case 3 (**D**, **E** and **F**). In case 2, pre-treatment FDG-PET (**A**) shows intense uptake at involved region, which shows nearly no change at one month (**B**). However, at 6 months after the treatment (**C**), the uptake value has returned to normal meaning complete response of the treated lesion. In case 3, the hyperuptake of targeted T1 spinal body at both pre-treatment (**D**) and one-month after treatment FDG-PET (**E**) scans is normalized on the FDG-PET after 6 months (**F**) like case 2. However, hyperuptake at the C6 region, which was misdiagnosed as reactive bone change to operative fixation, becomes prominent with a newly developed left clavicular lesion as time goes by. This case is regarded as a distant failure.

Case 1 had a mixed sarcoma involving the T1 vertebrae 4 years ago. Extensive decompression from the C5 to T2 epidural space and a T1 corpectomy were followed by posterior pedicular screw fixation. Conventional radiation with 4500 cGy in 20 fractions was completed after the operation. His pre-operative right arm pain was abolished and right hand weakness was slightly improved from grade 4/5 to grade 4+/5 after the treatment. Three years after the treatment, the patient developed left hand weakness of grade 4/5 and follow-up MRI showed a recurrent mass extending into the C7-T1 left neural foramen (Fig. **1**).

Case 2 was a female patient who had been disease-free for 11 years since a modified radical mastectomy of her breast cancer. In November 2002, she felt progressive shoulder pain and was diagnosed with a solitary metastasis to C7 – T1. She had undergone radical corpectomy with posterior fusion followed by 3300 cGy conventional radiation in 11 fractions. After two and a half years of freedom from disease, followed by a bone scan, a CT scan revealed a recurrent mass on the T1 – T2 area. Although she maintained her performance in spite of significant pain of the posterior neck and shoulder, a whole-body PET revealed multiple bone metastases on the left humerus, right ilium and right clavicle in addition to the T1 – T2 recurrence (Fig. **2A**).

Case 3 was a patient who had undergone previous palliative chemotherapy for metastatic breast cancer 3 years ago. Her C6 metastatic lesion had progressed in spite of chemotherapy. She had undergone a C6 corpectomy and anterior fusion followed by 3000 cGy conventional radiation in 10 fractions three months before coming to our hospital. The follow-up MRI suggested a C7 – T1 recurrent lesion, which was marginally included in the previous radiation field. Whole-body PET showed a C7 – T1 recurrence and hyperuptake at the C6 level, which was diagnosed as a reactive change from decompression and fusion (Fig. **2A**).

CyberKnife hypofractionated SRS treatment

The CyberKnife is an image-guided, frameless radiosurgery system capable of fractionated treatment. This device consists of a lightweight 6-MV linear accelerator manipulated by a computer-controlled robotic arm, details of which have already been reported [5]. Non-invasive immobilization using an Aquaplast mask (WFR/Aquaplast Corp., Wyckoff, NJ) was applied during CT for planning and the whole course of fractionation therapy. In this series, a fiducial tracking method was adopted to locate the tumor [6]. Six fiducial makers made of gold seed (1.8 mm in diameter, 5 mm in length) were inserted deep into the space between the articular facet and the paravertebral muscle. Implantation of the markers was completed under local anesthesia with the use of fluoroscopy one week before treatment. Special attention was given not to overlap fiducial markers with the previous metallic implant. Thus, the location of each fiducial was confirmed with fluoroscopy at a 45-degree angle, which is the preset angle of the image-tracking camera. Image registration was accomplished by setting the region of interest (ROI) around the gold seed fiducials, filtering within each ROI to highlight the landmarks, and then calculating the center of intensity within each ROI to locate the landmark with respect to the center of the image. A digitally reconstructed radiograph (DRR) of the patient's lesion is generated from the thin slice (2.0 mm) CT data set. The ROIs were selected manually on the DRR before treatment. The Dynamic Tracking System (ver. 3.0, Accuray Inc., Sunnyvale, CA) was employed for delivering planned radiation. A rapid image-to-image registration, done by a computer workstation, enables the system to determine the exact location of the patient's lesion and to communicate changes to the robot with a stereotactic accuracy comparable to that of a frame-based system. The total root-mean-square targeting error has been presented previously as 1.0 to 1.2 mm and the observed overall error including one from the positioning was less than 1.5 mm at the

maximum [7]. The treatment protocol was approved by the Institutional Review Board of Korea Cancer Center Hospital. All patients signed an informed consent and were aware of being part of an investigational protocol. Each fraction was separated by approximately 24 hours and daily fraction dose was automatically determined by dividing the total dose by fraction numbers.

Radiosurgery planning

The non-isocentric inverse treatment planning (ver. 2.7, Accuray Inc., Sunnyvale, CA) technique was employed in all cases. Dose volume histograms of the target volume and all critical structures were produced for every patient. First, one physician had drawn the tumor margin on an axial image without the FDG-PET data. Second, it was reformatted into coronal and sagittal views. These initial tumor appearances were compared with axial and coronal views of FDG-PET scan (details given in the next section "Measurement of response by FDG-PET") with the help of nuclear medicine. The tumor was re-drawn until both the physician and nuclear medicine doctor agreed on the tumor margins. The planned dose delivered to the brain stem and/or spinal cord was less than 2310 cGy in total through 3 fractionations, in all cases after review by all the our CyberKnife center physicians. This spinal cord limiting dose was physically equivalent to 5600 cGy in a conventional 2 Gy fractionation schedule according to the linear quadratic formula but its biological effect and partial volume to be irradiated at this dose made it obviously different from conventional radiation. The dosimetric characteristics of our treatment were evaluated in terms of a conformity index, which was defined as the ratio of the prescribed isodose volume to the target volume and also by a coverage index representing the ratio of the isodose line completely encompassing the target to the prescribed isodose as Shaw et al. [8] suggested for assessing the quality assurance of radiosurgery. To assess the difference between CT-based planning and FDG-PET combined planning, the planned tumor volume was obtained from each and compared by non-parametric analysis (Mann-Whitney test) using SPSS software (ver. 11.0, Chicago, IL).

Measurement of response by FDG-PET

Whole-body FDG-PET was performed using the ECAT HR+ (Siemens, Knoxville, TN) system. Image spatial resolution was 5 mm (full width half maximum) with a slice thickness of 2.4 mm (axial field of view of 16.2 cm). After fasting for at least 6 hours and checking the blood glucose, an intravenous injection of 555 to 740 MBq (15 – 20 mCi) of ^{18}F-fluorodeoxyglucose (FDG) was performed, and whole-body PET images were obtained in 6 to 7 contiguous bed positions at 60 minutes after injection of FDG. The acquisition time was 8 min per bed position (40% transmission and 60% emission). Transmission scans, measured with rotating rod sources containing ^{68}Ge were obtained for attenuation correction. PET image reconstruction was performed by an iterative algorithm with ordered subset expectation maximization (OSEM). Standard uptake values (SUV), a semi-quantitative measurement of relative FDG uptake within the regions of interest (ROI), were calculated. The SUV was calculated according to the following formula:

SUV = radioactivity concentration in tissue [Bq/g]/(injected dose [Bq]/patient weight [g]).

To calculate the SUV, images were reviewed and the slice containing the tumor was selected. Three bed positions were generally acquired. To minimize partial volume effects, the maximum SUV within the ROIs was used for further calculation (hereafter SUV). Pretreatment maximum SUV were followed at one month and 6 months after the treatment at the same ROI.

To evaluate the amount of SUV changes from different pretreatment values, the authors tried to set a new index of the amount of SUV change to the pretreatment SUV as follows;

Reduction index (RI) = (Pretreatment SUV – Posttreatment SUV)/Pretreatment SUV.

Treatment failure was defined using the modified definition from Loeffler et al. [9] for analyzing malignant glioma after brachytherapy; 1) local – increased SUV values not more than 5 mm from the original tumor volume; 2) marginal – failure greater than 5 mm but no more than 3 cm from the original tumor volume; 3) distant – failure greater than 3 cm from the original tumor volume, other vertebrae or other organs. In the case of a recurrence on PET, MRI was also performed to confirm the pattern of recurrence.

Results

All patients were followed regularly. None were lost to follow-up. Follow-up period was 16 months in one patient and 12 months in the others.

Patient's compliance and acute side effects

All patients were treated at the outpatient department without hospital admission. No patient complained of difficulty from immobilization of about one hour and no difficulty was noted acquiring the same tumor location with each fraction schedule. At least 3 fiducials were traced among six implanted fiducials despite the masking by the metallic fixation device through all treatment procedures. Prophylactic dexamethasone at 3 mg per day was given to all three patients for the purpose of preventing acute radiation reaction during the course of fractionation. No acute side effects were observed during the treatment except grade I headache in case 3. All patients experienced improvement of their pain within 2 weeks after the treatment.

Treatment characteristics and tumor response

Radiotherapeutic characteristics including dosimetric indices are summarized in Table **2**. Tumor volume drawn on CT alone was 2.2 times larger compared to the CT-PET in case 1. But tumor volume was increased from 22.6 cm^3 to 29.0 cm^3 in case 2, from 4.7 cm^3 to 5.7 cm^3 in case 3 on CT-PET based planning. The reduction in tumor volume using CT-PET compared to CT alone in case 1 may be due to the elimination of the reactive change in the paraspinal muscles on CT/MRI, which showed no hyperuptake on FDG-PET (Fig. **1**). The minimal change of tumor volume in the other cases (1 and 2) resulted from the metastatic tumors confined to the vertebral bodies. The area to be irradiated was determined by the visual combination of CT and PET. Conformity index was 1.82 in case 1, 1.52 in case 2 and 1.41 in case 3 and these values met the standard protocol (1.0 – 2.0) of radiosurgery

Table **2** Radiotherapeutic characteristics of the patients

Case	*CT-based Tv* (cm^3)*	*CT-PET combined Tv* (cm^3)*	*Total dose/Fraction no.*	*Isodose line*	*Coverage index*	*Conformity index*	*PET SUV (RI) follow-up*		
							Pre-treatment	*1 month*	*6 months*
1	83.4	37.1	2700 cGy/3 fractions	81 %	0.98	1.82	2.9	2.7 (0.07)	3.1 (– 0.34)
2	22.6	29.0	2668 cGy/3 fractions	78 %	0.90	1.52	5.2	5.6 (– 0.08)	1.8 (0.65)
3	4.7	5.7	2834 cGy/3 fractions	77 %	0.99	1.41	9.9	3.0 (0.7)	1.3 (0.87)

* Abbreviations: Tv = tumor volume, RI (reduction index) = relative decrease of maximum SUV to pre-treatment SUV.

suggested by the Radiation Therapy Oncology Group. Concerning the coverage index, case 1 with 0.75 showed a major deviation (< 0.8) from the protocol, case 2 with 0.83 was in a range of minor deviation and only case 3 with 0.95 met the standard. The total dose delivered to the tumor margin was 2700 cGy at the 81 % isodose line in case 1, 2668 cGy at the 78 % isodose line in case 2 and 2834 cGy at the 77 % isodose line in case 3 in three fractions. The small differences of the total dose were due to the inverse plan under the rule of maximal allowable dose to the spinal cord as 2310 cGy.

The highest SUV in pretreatment FDG-PET was noted in case 3 (9.9). In case 2 it was 5.2 and in case 1 it was 2.9. At one month, the maximum SUV was calculated as 2.7 in case 1, 5.6 in case 2 and 3.0 in case 3. The reduction index (RI) corresponded to 0.07, – 0.08 and 0.70, respectively. The change of maximum SUV at 6 months was from 2.9 to 3.9 in case 1, from 5.2 to 1.8 in case 2 and from 9.9 to 1.3 in case 3. The change in RI at 6 months was – 0.34 in case 1, which means an increase of the SUV, 0.65 in case 2 and 0.87 in case 3. This corresponded to almost complete disappearance of uptake nearing the level of normal tissue uptake (Table **2**).

Pattern of failure and delayed radiation toxicity

In case 1, at 3 months follow-up, the MRI showed a recurrent mass 1 cm outside of the targeted lesion along the left paraspinal muscle. Follow-up at 6 months with MRI revealed further progression of the tumor. The SUV change at one month revealed no decrease. At 6 months follow-up, it showed a negative value of RI – 0.07 in the treated lesion and of RI – 0.34 in the paraspinal lesion, respectively (not shown in Table **2**). Thus, the treatment result was a marginal failure (Fig. **1**). Excision of the paraspinal mass was performed at 10 months after the CyberKnife treatment and was followed by systemic chemotherapy. Despite the recurrence of the mass, the pretreatment arm pain was much improved after one month following our treatment. In case 2, at one month after the CyberKnife treatment, the patient revealed a complete resolution of her neck pain despite a minimal change in SUV on PET. At 6 months follow-up, the PET showed a reduction of SUV to 1.8, which was not significantly higher than adjacent normal region (Figs. **2B** and **2C**). Thus, the patient had a complete response as she had undergone systemic chemotherapy during the follow-up period to control other bone metastasis. The reduction index was the largest at both one month and six months in case 3, which resulted in complete control of the treated lesion. At pretreatment PET, C6 vertebra had an increased uptake. However, it was determined at that time that this was due to a reactive bone formation around the metal screw inserted 3 months before. Hence, the C6 vertebra was excluded from the target volume and treatment. At 6 months follow-up after treatment, the SUV (7.1) revealed an increase in intensity of uptake on PET (Figs. **2E** and **2F**). The patient also revealed liver and abdominal lymph node metastasis during the follow-up period. She maintained her performance status with the virtue of systemic chemotherapy. Case 3 was regarded as a distant failure. All three patients revealed neither a new myelopathic symptom nor signal changes compatible with radiation necrosis on MRI.

Discussion

Feasibility of hypofractionated SRS for recurrent spinal metastases

The ability of the CyberKnife treatment system to deliver a precise high radiation dose in a fractionated schedule was already reported elsewhere [7]. Thus, detailed measurement of the accuracy of the system was not included here and is beyond the scope of this study. There is little difficulty in repositioning the patient at each fraction. A great reluctance to re-irradiate the central nervous system tissue exists among physicians in the belief that it has little capacity to recover from prior irradiation injury. Thus, there is very little information regarding the effects of irradiation to neural tissue that has been already irradiated in the past. Schiff et al. [3] reported their results of re-irradiation for malignant epidural spinal cord compression. In their study, a median dose of 30 Gy was used for the first radiation therapy, and the subsequent median cumulative dose of irradiation was 54.3 Gy. They concluded that re-irradiation was effective in maintaining the patient ambulatory with a minimal risk of radiation myelopathy. However, the short follow-up of 4.2 months may miss the true incidence of myelopathy. In animal studies, it has been shown that the time interval between irradiation [10], the amount of initial dose [11] and the volume of spinal cord to be irradiated [12] were important factors in determining the risk and latent period of radiation myelopathy in addition to the well-known total radiation dose and fraction size. Stereotactic radiosurgery could augment the "volume effect" by providing millimeter accuracy for reducing undesirable radiation to adjacent normal tissue. Also, fractionation has the radiobiological advantage in allowing the adjacent normal tissue to recover in between fractionations. This would minimize the risk of myelopathy, although the number of fractionations is limited in hypofrac-

tionation. Recent clinical trials using single session radiosurgery for spinal metastasis revealed both rapid symptomatic response and a very low incidence of myelopathy. However, these trials are confounded by inadequate follow-up periods to eliminate for delayed myelopathy [4], the dose to spinal cord was too small to be considerably risky [13], and radiosurgery was delivered as a boost to conventional therapy in a way of selecting minimal dose [14]. Moreover, it is difficult to calculate the biological effect of cumulative doses in patients who had already undergone the full course of conventional radiation. In a study by Ang et al. [11], the cervical spinal cords of rhesus monkeys were subjected to re-irradiation after earlier doses of either 44 or 70.4 Gy. The study revealed that the majority of the occult white matter injury recovered within 2 years among the subjects that received 44 Gy. However, when vascular injury occurred, the latent period little affected recovery. They suggested that the extrapolated ED_{50} for re-treatment after 44 Gy was ≥ 110 Gy, while the observed ED_{50} of the initial irradiation was 76 Gy. The extent of recovery due to the initial dose and the time interval is not known in humans. Although detailed dose-volume histogram data were not provided, the volume of spinal cord irradiated under the limit of 2310 cGy (which was 5600 cGy equivalent of conventional radiation of 2 Gy fraction size according to the linear quadratic formula) was 0.31 cm^3 in case 1, 0.12 cm^3 in case 2 and 0.01 cm^3 in case 3. A cumulative dose added to the dose of the previous radiation therapy is obviously smaller than ED_{50} from the animal data in each case and no patients showed clinical evidence of myelopathy during the follow-up period in our series.

Usefulness of PET in radiosurgery planning

To achieve conformal three-dimensional radiation, target and normal-tissue delineation should be precedent to an accurate radiation delivery system. When this concept was applied to primary cancers, the expected local control was not easily achieved due to the problems of defining the extent of disease from occult metastasis or lymph node involvement, which were not overtly defined by CT or MRI. It has been well known that functional information from FDG-PET is useful in differentiating inflammatory change and necrosis/fibrosis from malignant involvement of various tumors. The physiological information from PET could provide higher specificity and sensitivity for the staging of primary cancer [15] and be more useful to determine the postoperative treatment strategy [16]. The lack of anatomic detail from PET imaging could be corrected by coregistering of CT and PET. The hybrid PET-CT seems to be more beneficial than CT alone for radiation therapy planning. Mah et al. [17] reported that planning target volume (PTV) using coregistered CT and FDG-PET changed the treatment strategy from radical to palliative in 23 % of their lung cancer patients due to the detection of unexpected lesions or new nodal involvement. Most of the studies comparing CT/MRI target volumes to PET target volumes revealed a reduction in the target volume using PET targeting. Heron et al. [18] showed that the CT-based PTV in the primary lesion was about 1.5 times larger than the PET-based PTV due to the involvement of inflammatory changes and artifacts from metal dentures in head and neck cancer. In lymph node metastases, the PET-based PTV was 1.2 times larger than seen in CT because of new nodal involvement, although no significant change was made in target volume of individual nodes. On the other hand, Erdi et al. [19] reported the increase of the CT-PET-defined PTV compared to the CT-based PTV in radiotherapy planning for patients with non-small cell lung cancer. The main reason for the PTV increase was the incorporation of distant nodal disease while excluding atelectasis and trimming the target volume along the spinal cord by CT-PET. In our series, case 1, which was a primary spinal involvement of sarcoma, showed a 2.2-times larger CT-based PTV than PET-based PTV. The main causes of the significant volume increase were indistinct margins of paraspinal invasion and a metallic artifact. In contrast, the other two cases showed smaller CT-based PTV, 0.78 times in case 2 and 0.82 times in case 3. We postulate that in cases 2 and 3, tumors were mostly confined to the vertebral bodies of distinct margins, thus cryptic involvement of the vertebral body could not be reflected in the CT scan but could be done on PET.

Another way of easing the difficulty of defining the extent of disease is delivering boost radiation to the PET-defined active areas. Tralins et al. [20] tried this concept on glioblastoma, an example of a tumor that is difficult to control by radiation and normally has an occult infiltration. They applied a boost of 20 Gy to the FDG-PET hyperuptake area after delivery of 59.4 Gy to the MRI-defined target. Hence, they achieved a dose escalation up to 79.4 Gy. In their series, the FDG-PET target volume significantly predicted the time-to-progression of the tumor. From a practical point of view, functional information from PET needs to be registered to anatomic image, i. e., CT for radiation treatment planning. Registration could be made by either using well-defined fiducial markers or using contour fitting while the patient is immobilized. However, fixed fiducials, which were readily detectable on both CT and PET, are hard to find and immobilization of the patient during treatment in the same position to PET imaging is also difficult. The CyberKnife stereotactic radiosurgery prefers the patient to have the arms lifted in order to reduce the errors from penetration of the thick soft tissue of the lateral beam. In contrast, in PET the patient sets the arms beside the trunk. Moreover, this system needs thin slice imaging (less than 2.0 mm) to register to their image fusion software, which is not available on the current PET imaging technique. Thus, we had to use FDG-PET information without the aid of software which needed to be determined visually. We could expect, if we were to use a more sophisticated registration system, that we could possibly avoid marginal failure as in case 1.

Measurement of tumor response by FDG-PET

In the past decade, PET was used for diagnostic purposes rather than the quantitative measurement of treatment response. The established role of PET in monitoring the radiation response involves the differentiation of recurrence from radiation necrosis [21 – 23] or a significant factor for tumor grading [24]. The recent wide application of PET in cancer patients has brought some clues for quantitative monitoring of treatment response. Allal et al. [25] reported an inverse correlation of pretreatment SUV with both local control rate and progression-free survival in head and neck cancer. Their work concluded that SUV could reflect the biological aggressiveness of the tumor. Some authors have explored the use of PET in the prediction of earlier response time compared to CT/MRI. The authors assumed that metabolic changes could precede the morphological changes and would be better detected by PET. But the results of clinical trials failed to show either unanimity of early change or definite time of early response

even confined to radiation therapy. The transient increase of PET uptake due to radiation-induced inflammation during radiation therapy had been already reported [22]. Arslan et al. [26] reported that the SUV of posttreatment PET taken 4 weeks after chemoradiation therapy in esophageal cancer could not separate inflammation from residual tumor and the tumor volume on PET had a correlation with tumor response. On the contrary, Yao et al. [16] observed that, in the case of a negative postradiation PET, they found no viable tumor cells by needle or open biopsy even in enlarged lymph nodes in head and neck cancer. They postulated that postradiation PET had an accurate predictability for negative pathology. Some authors insisted that these problems could be solved by serial and sophisticated PET evaluation. Koike et al. [27] performed PET both prior to treatment and 10 days after radiation treatment in various malignant tumors and quantified the difference of SUV between early PET (1 hour after FDG injection) and delayed PET (3 hours after FDG injection) in terms of a "retention index". These retention indices were well correlated with the response on MRI taken 3 months after radiation. Also, the retention of FDG in malignant tumors could differentiate residual tumors from benign inflammatory changes. Sequential PET evaluation after radiation could be different according to not only tumor response but also to characteristics of the metastatic region. For example, brain tumor could show a different timetable of tumor response compared to spinal metastasis. Higashi et al. [28] confirmed the biphasic sequence of FDG PET uptake in an irradiated rodent bone marrow model. They gave 10 Gy to rodent femur and took PET on day 1, day 8 and day 18, which showed transient rise, fall and normalization, respectively. The mode of radiation (i.e., conventional fractionation versus radiosurgery) could affect a PET result at a certain time after treatment. Ericson et al. [29] analyzed the results of FDG PET uptake, which was used in cases of suspicious recurrence after gamma knife radiosurgery for brain metastases. Patient survival was prolonged significantly in the group of patients showing decreased PET uptake. However, the evaluation by PET varied from 3 months to 8.6 years. In order to exclude bias from the temporary radiation reaction, serial PET studies were needed. In our study, it is difficult to evaluate the utility of sequential changes of PET uptake on treatment because of the small number of patients enrolled. The PET SUV at one month after radiosurgery revealed no change in case 1, who failed to show local tumor control and a paradoxical increase in case 2, whose tumor showed complete control at 6 months PET. Thus, the early response of radiosurgery on a one-month PET scan seemed to be of little value in predicting further tumor control. At 6 months follow-up, PET results correlated with clinical outcome in all of our three patients. Although there is no concrete agreement on tumor response according to time sequence after radiosurgery, Lee et al. [30] reported similar results in glioma patients treated by gamma knife radiosurgery. The PET uptake value after the radiosurgery was well correlated with the later volume response in MRI.

Conclusion

Although the small number of patients precludes a definitive conclusion, we have shown that hypofractionated stereotactic radiosurgery combined with FDG PET planning is feasible in recurrent spinal metastatic patients with previous metallic fixation and conventional radiation treatment. FDG PET was helpful not only for planning radiosurgery but also for post-treatment response monitoring in our cases. These cases had severe metallic artifacts that made monitoring by anatomic imaging alone difficult. The changes in SUV 6 months after the treatment were correlated with both clinical results and the pattern of treatment failure.

References

[1] Bunger C, Laursen M, Hansen ES, Neumann P, Christensen FB, Hoy K, Helmig P. A new algorithm for the surgical treatment of spinal metastases. Curr Opin Orthop 1999; 10: 101 – 105

[2] Camins MB, Jenkins 3rd AL, Singhal A, Perrin RG. Tumors of the vertebral axis: benign, primary malignant, and metastatic tumors. In: Winn HR (ed). Youmans neurological surgery, volume 4, fifth edition. Philadelphia: Elsevier Inc, 2002: 4835 – 4868

[3] Schiff D, Shaw EG, Cascino TL. Outcome after spinal reirradiation for malignant epidural spinal cord compression. Ann Neurol 1995; 37: 583 – 589

[4] Hamilton AJ, Lulu BA, Fosmire H, Gossett L. LINAC-based spinal stereotactic radiosurgery. Stereotact Funct Neurosurg 1996; 66: 1 – 9

[5] Adler Jr JR, Murphy MJ, Chang SD, Hancock SL. Image guided robotic radiosurgery. Neurosurgery 1999; 44: 1299 – 1306

[6] Murphy MJ, Adler Jr JR, Bodduluri M, Dooley J, Forster K, Hai J, Le Q, Luxton G, Martin D, Poen J. Image-guided radiosurgery for the spine and pancreas. Comp Aid Surg 2000; 5: 278 – 288

[7] Ryu SI, Chang SD, Kim DH, Murphy MJ, Le QT, Martin DP, Adler Jr JR. Image-guided hypo-fractionated stereotactic radiosurgery to spinal lesions. Neurosurgery 2001; 49: 838 – 846

[8] Shaw E, Kline R, Gillin M, Souhami L, Hirschfeld A, Dinapoli R, Martin L. Radiation Therapy Oncology Group: radiosurgery quality assurance guidelines. Int J Radiat Oncol Biol Phys 1993; 27: 1231 – 1239

[9] Loeffler JS, Alexander 3rd E, Hochberg FH, Wen PY, Morris JH, Schoene WC, Siddon RL, Morse RH, Black PM. Clinical patterns of failure following stereotactic interstitial irradiation for malignant gliomas. Int J Radiat Oncol Biol Phys 1990; 19: 455 – 1462

[10] Wong CS, Hao Y. Long-term recovery kinetics of radiation damage in rat spinal cord. Int J Radiat Oncol Biol Phys 1999; 37: 171 – 179

[11] Ang KK, Price RE, Stephens LC, Jiang GL, Feng Y, Schultheiss TE, Peters LJ. The tolerance of primate spinal cord to re-irradiation. Int J Radiat Oncol Biol Phys 1993; 25: 459 – 464

[12] Kogel AJ van der. Dose-volume effects in the spinal cord. Radiother Oncol 1993; 29: 105 – 109

[13] Gerszten PC, Ozhasoglu C, Burton SA, Vogel WJ, Atkins BA, Kalnicki S, Welch WC. CyberKnife frameless stereotactic radiosurgery for spinal lesions: clinical experience in 125 cases. Neurosurgery 2004; 55: 89 – 98

[14] Ryu S, Fang Yin F, Rock J, Zhu J, Chu A, Kagan E, Rogers L, Ajlouni M, Rosenblum M, Kim JH. Image-guided and intensity-modulated radiosurgery for patients with spinal metastasis. Cancer 2003; 97: 2013 – 2018

[15] Dwamena BA, Sonnad SS, Angobaldo JO, Wahl RL. Metastases from non-small cell lung cancer: mediastinal staging in the 1990 s – meta-analytic comparison of PET and CT. Radiology 1999; 213: 530 – 536

[16] Yao M, Graham MM, Hoffman HT, Smith RB, Funk GF, Graham SM, Dornfeld KJ, Skwarchuk M, Menda Y, Buatti JM. The role of post-radiation therapy FDG PET in prediction of necessity for post-radiation therapy neck dissection in locally advanced head-and-neck squamous cell carcinoma. Int J Radiat Oncol Biol Phys 2004; 59: 1001 – 1010

[17] Mah K, Caldwell CB, Ung YC, Danjoux CE, Balogh JM, Ganguli SN, Ehrlich LE, Tirona R. The impact of ^{18}FDG-PET on target and critical organs in CT-based treatment planning of patients with poorly defined non-small-cell lung carcinoma: a prospective study. Int J Radiat Oncol Biol Phys 2002; 52: 339 – 350

[18] Heron DE, Andrade RS, Flickinger J, Johnson J, Agarwala SS, Wu A, Kalnicki S, Avril N. Hybrid PET-CT simulation for radiation treatment planning in head-and-neck cancers: a brief technical report. Int J Radiat Oncol Biol Phys 2004; 60: 1419 – 1424

[19] Erdi YE, Rosenzweig K, Erdi AK, Macapinlac HA, Hu YC, Braban LE, Humm JL, Squire OD, Chui CS, Larson SM, Yorke ED. Radiotherapy

treatment planning for patients with non-small cell lung cancer using positron emission tomography (PET). Radiother Oncol 2002; 62: 51 – 60
[20] Tralins KS, Douglas JG, Stelzer KJ, Mankoff DA, Silbergeld DL, Rostomily RC, Hummel S, Scharnhorst J, Krohn KA, Spence AM. Volumetric analysis of ^{18}F-FDG PET in glioblastoma multiforme: prognostic information and possible role in definition of target volumes in radiation dose escalation. J Nucl Med 2002; 43: 1667 – 1673
[21] Glantz MJ, Hoffman JM, Coleman RE, Freidman AH, Hanson MW, Burger PC, Herndon II JE, Meisler WJ, Schold Jr SC. Identification of early recurrence of primary central nervous system tumors by [^{18}F]fluorodeoxyglucose positron emission tomography. Ann Neurol 1991; 29: 347 – 355
[22] Chaiken L, Rege S, Hoh C, Choi Y, Jabour B, Julliard G, Hawkins R, Parker R. Positron emission tomography with fluorodeoxyglucose to evaluate tumor response and control after radiation therapy. Int J Radiat Oncol Biol Phys 1993; 27: 455 – 464
[23] Barker FG, Chang SM, Valk PE, Pounds TR, Prados MD. 18-Fluorodeoxyglucose uptake and survival of patients with suspected recurrent malignant glioma. Cancer 1997; 79: 115 – 126
[24] Sasaki M, Kuwabara Y, Yoshida T, Nakagawa M, Fukumura T, Mihara F, Morioka T, Fukui M, Masuda K. A comparative study of thallium-201 SPET, carbon-11 methionine PET and fluorine-18 fluorodeoxyglucose PET for the differentiation of astrocytic tumors. Eur J Nucl Med 1998; 25: 1261 – 1269
[25] Allal AS, Slosman DO, Kebdani T, Allaoua M, Lehmann W, Dulguerov P. Prediction of outcome in head-and-neck cancer patients using the standardized uptake value of 2-[^{18}F]fluoro-2-deoxy-D-glucose. Int J Radiat Oncol Biol Phys 2004; 59: 1295 – 1300
[26] Arslan N, Miller TR, Dehdashti F, Battafarano RJ, Siegel BA. Evaluation of response to neoadjuvant therapy by quantitative 2-deoxy-2-[^{18}F]fluoro-D-glucose with positron emission tomography in patients with esophageal cancer. Mol Imaging Biol 2002; 4: 301 – 310
[27] Koike I, Ohmura M, Hata M, Takahashi N, Oka T, Ogino I, Lee J, Umezawa T, Kinbara K, Watai K, Ozawa Y, Inoue T. FDG-PET scanning after radiation can predict tumor regrowth three months later. Int J Radiat Oncol Biol Phys 2003; 57: 1231 – 1238
[28] Higashi T, Fisher SJ, Brown RS, Nakada K, Walter GL, Wahl RL. Evaluation of the early effect of local irradiation on normal rodent bone marrow metabolism using FDG: preclinical PET studies. J Nucl Med 2000; 41: 2026 – 2035
[29] Ericson K, Kihlstrom L, Mogard J, Karlsson B, Lindquist C, Wilde Collins VP, Stone-Elander S. Postron emission tomography using ^{18}F-fluorodeoxyglucose in patients with stereotactically irradiated brain metastasis. Stereotact Funct Neurosurg 1996; 66: 214 – 224
[30] Lee JK, Liu RS, Shiang HR, Pan DH. Usefulness of semiquantitative FDG-PET in the prediction of brain tumor treatment response to gamma knife radiosurgery. J Comput Assist Tomogr 2003; 27: 525 – 529

H. Hirschberg[1, 2, 3]
S. Spetalen[4]
S. Carper[5, 6]
P. Hole[7]
T. Tillung[7]
S. Madsen[3, 5]

Minimally Invasive Photodynamic Therapy (PDT) for Ablation of Experimental Rat Glioma

Abstract

Objective: The feasibility of using ALA-mediated photodynamic therapy (PDT) tumor ablation as a minimally invasive treatment alternative for malignant brain tumors was evaluated in a rodent model. Treatment efficacy and side effects were evaluated with MRI, histopathology and survival rates. **Methods:** BT_4C orthotopic brain tumors were induced in BD-IX rats. At various time intervals following tumor induction the animals were given 5-aminolevulinic acid (ALA) and 4 hours later optical fibers were inserted directly into the tumor without mechanical debulking or cranial decompression. A 3-day course of steroid treatment was initiated immediately prior to PDT. **Results:** All untreated animals inevitably died within one month after tumor implantation (28.5 ± 2.5 days). Complete tumor eradication was achieved in only 1/17 rats, but a significant increase in survival was obtained in the group of animals receiving 125 mg/kg ALA and 26 Joules of light fluence. Histopathology revealed large areas of central tumor necrosis, although clusters of viable tumor cells were often found at the tumor periphery. Pronounced edema in the necrotic tumor center as well as in the surrounding brain, and along white matter tracts was evident in all the brains studied from PDT-treated animal. **Conclusion:** This study suggests that ALA-mediated PDT may become a promising alternative therapy for the minimally invasive treatment of brain tumors. A judicious choice of PDT regimens that minimizes inflammatory responses through the use multiple fractionated long-term treatment protocols would likely be required.

Key words

Glioma · tumor ablation · photodynamic therapy · rodent model

Introduction

Photodynamic therapy (PDT) involves the administration of a tumor-localizing, photosensitizing drug that is activated by light of a specific wavelength. This therapy results in a series of photochemical and photobiological events that cause irreversible damage to tumor tissues [1]. The novel second generation endogenous photosensitizer 5-aminolevulinic acid has many advantages over more traditional exogenous drugs [2,3].

PDT employing ALA-induced porphyrins has been previously found to selectively damage experimental brain tumors [4,5] with negligible effects on normal or adjacent, edematous brain [6], and is well suited for use in the brain since it has a threshold for necrosis in white matter that is significantly greater than for other drugs [7].

The combination of excellent tumor-to-normal brain tissue localization [8,9], short period of skin photosensitization (24 to 48 hours) and the possibility of oral administration also make ALA an excellent choice as photosensitizer.

Affiliation
[1] Department of Neurosurgery, Rikshospitalet, Oslo, Norway
[2] Beckman Laser Institute, University of California, Irvine, Irvine, CA, USA
[3] Department of Health Physics, University of Nevada, Las Vegas, NV, USA
[4] Department of Pathology, Ullevaal University Hospital, Oslo, Norway
[5] UNLV Cancer Research Center, University of Nevada, Las Vegas, NV, USA
[6] Department of Chemistry, University of Nevada, Las Vegas, NV, USA
[7] Interventional Center, Rikshospitalet, Oslo, Norway

Correspondence
Henry Hirschberg, M. D., Ph. D. · Department of Neurosurgery · Rikshospitalet · 0027 Oslo · Norway ·
Tel.: +47/230/74323 · E-mail: hhirschb@uci.edu

Bibliography
Minim Invas Neurosurg 2006; 49: 135–142 © Georg Thieme Verlag KG Stuttgart · New York
DOI 10.1055/s-2006-932216
ISSN 0946-7211

The current treatment of glioma patients is traditionally divided into surgical, radiotherapeutic, chemotherapeutic, and experimental treatments. Surgery is usually performed to either fully resect/debulk the gross contrast-enhancing portion of the tumor. Some deep-seated tumors, however, are considered inoperable due to their localization in "eloquent" areas of the brain. In these cases stereotactic biopsy is performed to establish diagnosis and tumor classification. Focal, minimally invasive interventional procedures, that allow brain tumor ablation under local anesthesia, can also be initiated in the same setting.

MR-guided stereotactic radiofrequency or laser thermal ablation of brain tumors, has been studied both experimentally and in clinical trials [10 – 15]. Thermal tumor ablation has the drawback that it lacks tumor specificity and must be carefully monitored during treatment, generally with MRI, to limit the extent of tissue destruction [11,13,14]. This greatly increases the complexity of this treatment modality.

The animal experiments reported here were designed to evaluate the feasibility of minimally invasive ALA-mediated PDT for the ablation of unresected BT_4C orthotopic brain tumors in BDIX rats. The optical fiber was placed directly into the tumor without mechanical debulking or cranial decompression. Treatment efficacy and side effects were evaluated with MRI, histopathology and survival rates.

Materials and Methods

Cell cultures

The BT_4C tumor was originally derived from transformed fetal BD-IX rat brain cells after exposure to ethylnitrosourea [16]. The BT_4C cells were grown as monolayers in RPMI medium with 10% heat-inactivated newborn calf serum (FCS) at 37 C and 5% CO_2. The cell line tested negative for viral agents in a rat antibody production test according to the Federation of Laboratory Animal Association (FELASA) recommendations.

Brain tumor model

Inbred BD-IX rats (Charles River, Lyon, France and Charles River Laboratories, Wilmington, MA, USA) of both sexes weighing at least 250 g were caged either alone or in pairs in Macrolon III cages. The animal holding rooms were maintained at constant temperature and humidity on a 12-hour light and dark schedule at an air exchange rate of 18 changes per hour. Animal care and protocol were in accordance with national legislation and institutional guidelines. The animals tested negative for parasitic, bacterial and viral agents according to the FELASA recommendations. For the surgical procedures, the rats were anaesthetized either with a combination of fentanyl/fluanisone and midazolam, or pentobarbital. Buphrenorphine was used as a post-operative analgesic.

A complete description of tumor establishment in this model has been provided elsewhere [17]. Briefly; anaesthetized rats were fixed in a stereotactic frame (David Kopf Instruments, Tujunga, CA, USA), the skin was incised and a 1.0-mm burr hole was made to fit the following coordinates: 3 mm posterior to and 2 mm to the right of the bregma and depth of 3 mm. The injection device consisted of a 30-G blunt cannula connected through a catheter (Small Parts, Miami Lakes, FL, USA) to an infusion pump (Harvard Apparatus, Holliston, MA, USA). The cannula was fixed in the electrode holder of the stereotactic frame, and then vertically introduced into the brain. A total of 10,000 cells in 5 μL of RPMI were injected into the brain during a period of 1 minute. The cannula was kept in place for 2 minutes, and slowly retracted to prevent the spread of tumor cells during cannula retraction. Closure was done with bone wax and sutures. Tumor take was 100%. The rats were euthanized with a lethal dose of pentobarbital. In the survival experiment, the rats were examined regularly and were euthanized with an overdose of pentobarbitone (100 mg/kg *i.p.*) when they showed a weight reduction of 10% and/or clinical signs of raised intracranial pressure such as reduced or impaired motor activity, and lethargy.

Magnetic resonance imaging

PDT-treated or control BD-IX rats were imaged in a 0.5 T open interventional MR scanner (GE Signa SP, GE Medical Systems, Waukesha, WI, USA). Animals were anesthetized, positioned in a custom-made restraining device and after subcutaneous injection of gadolinium contrast (1.0 mL of 0.5 mmol/mL Magnavist: Berlex Laboratories, Wayne, NJ, USA) were subjected to a T_1-weighted 3D gradient echo pulse sequence (TR = 34 ms; TE = 12 ms, slice thickness = 1.3 mm) using a receiver coil designed for scanning the human eye region. T_2 images, to determine areas and degree of edema, were obtained prior to contrast injection.

Monte Carlo calculations of light distributions in brain and tumor tissue

The distribution of light during interstitial light exposure was estimated from Monte Carlo simulation. Absorption and reduced scattering coefficients of 0.65 cm^{-1} and 29 cm^{-1} for normal brain, and 1.6 cm^{-1} and 6.9 cm^{-1} for tumor tissue, were used in the simulations. These tissue optical parameters were calculated from direct *in vivo* measurements of fluence rate in the model used here [18].

PDT ablation protocol

Tumors were induced intracranially in 41 rats. The animals were divided into the following groups:

Group 1: treatment nine days following tumor induction; ALA 60 (n = 8) or 125 (n = 9) mg/kg; light fluence 26 J.
Group 2: treatment 21 days following tumor induction; ALA 125 mg/kg; light fluence 26/13 J (n = 6).
Group 3: Six rats with tumors received ALA 125 mg/kg but no light and acted as untreated controls.
Group 4: Treatment, day 14; ALA 125 mg/kg; light fluence 26 J.

Animals in groups 1 – 3 were evaluated by survival time; those in group 4 were evaluated by histopathology.

All treatment groups of animals were administered ALA *i.p.* and subjected to light irradiation 4 – 5 hours later. Prior to irradiation, animals were anaesthetized and positioned in the stereotactic frame. The skin incision was opened and the bone wax removed from the burr hole. A 400-μm bare flat-end quartz fiber with numerical aperture 0.22 was introduced stereotactically directly into the brain using the same coordinates employed during

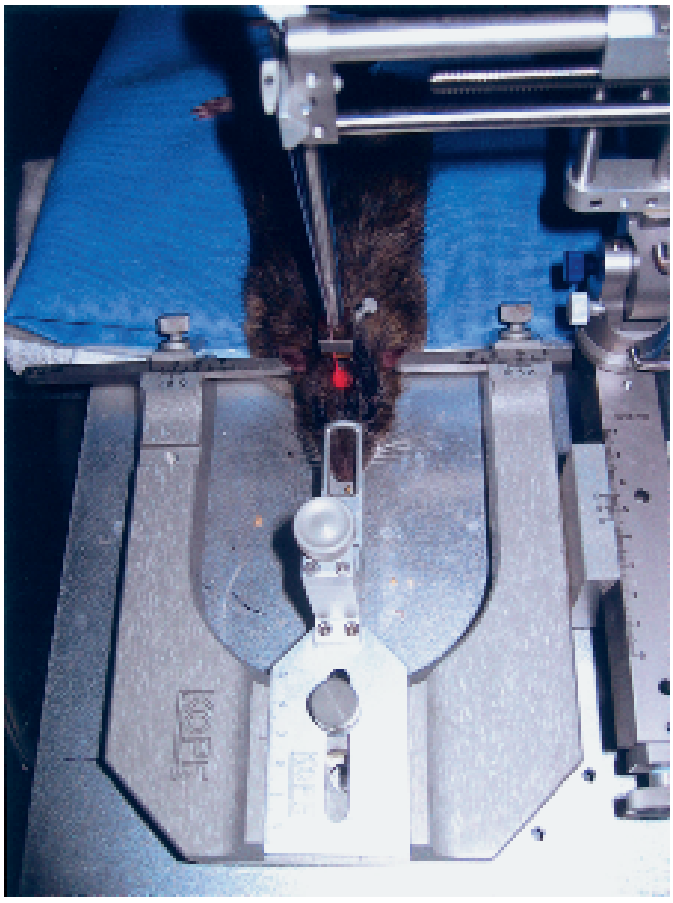

Fig. **1** Intratumor light delivery to an anesthetized rat via a stereotactically introduced bare fiber tip.

tumor induction. Light from a 632 nm diode laser (HPD, Inc) was delivered interstitially over a time interval of either 45 or 90 minutes. A typical treatment procedure is illustrated in Fig. **1**.

Following light exposure, the fiber was withdrawn and closure performed with bone wax and sutures. Thereafter the animals were released from the frame and buprenorphine was given as postoperative analgetic agent. In order to reduce post-treatment complications, steroids were administered to treated animals and controls (1 mg kg^{-1} methylprednisolone *i.p.*) immediately following treatment and for two subsequent days [8]. The rats were examined regularly and were euthanized with an overdose of pentobarbitone when they showed a weight reduction of 10% and/or clinical signs of raised intracranial pressure such as reduced or impaired motor activity, and lethargy. These clinical signs were subsequently considered as death events in the survival curves.

Histopathology

The animals in group 4 were euthanized 15 – 72 hours following treatment and the brains removed and prepared for histopathology. The brains were fixed in formaldehyde for 48 hours and were then halved coronally along the tumor injection track and embedded in paraffin. Microtome coronal sections were cut and stained with hematoxylin and eosin (H&E). Adjacent sections were immunostained with an antibody against the plasma protein fibrinogen (dilution 1 : 600, DakoCytomation, Glostrup, Denmark) to detect brain edema. Both tumor necrosis and neutrophil invasion, as determined from H&E stained sections through the tumor centers, were evaluated.

Table **1** Fluence and fluence rate calculated as a function of distance from optical fiber tip

Distance (mm)	*Fluence (J/cm^2)*[a]	*Fluence rate*[b]
0.0	820	150
1.0	300	55
2.0	130	30
3.0	50	9
4.0	18	3
5.0	6	1.1
6.0	2.4	0.4

[a] 26J delivered from fiber
[b] Fiber output power = 5 mW

Statistical analysis

Statistical analyses were done using an unpaired two-tailed Student's *t*-test. All results with a value of $p < 0.05$ were considered statistically significant.

Results

Light distribution simulation

The fluence and fluence rates at various distances from the center of a 4 – 5 mm tumor, a typical size at 21 days post-implantation, are summarized in Table **1** [9]. Here the input light dose rate was 5 mW delivered from the fiber tip. As can be seen from the table the entire tumor will be exposed to fluences in excess of 50 J/cm^{-2} if 26 J are delivered into the tumor. In this case the fluence rate in a zone 0.5 mm beyond the tumor's outermost border will be approximately 9 mW cm^{-2}. As also seen from the table, there is a very steep gradient in the light distribution due to the high attenuation of light in the tissue.

MRI appearance

Fig. **2a** shows a typical coronal image taken on the 18th day post-implantation.

On T_1 images with contrast, untreated tumors were easily visualized as high signal intensity areas at the site of injection. Neither spread of tumor cells to other brain areas nor central tumor necrosis was observed within untreated tumors. Fig. **2b** is a similar scan performed 24 hours following PDT treatment. The central portion of the tumor is now a low signal area indicating a lack of contrast enhancement, typical of central necrosis. A partial rim of hyperintense signal still remains indicating a disrupted BBB. Figs. **3a** and **3b** are axial scans, T_1-weighted with contrast and T_2 prior to contrast injection, respectively, of an untreated control tumor. The tumor is clearly visible as a contrast-rich area on the T_1 image. A ring-shaped high signal intensity area indicating peritumoral edema in the surrounding brain around tumor (BAT) is apparent on T_2 scans.

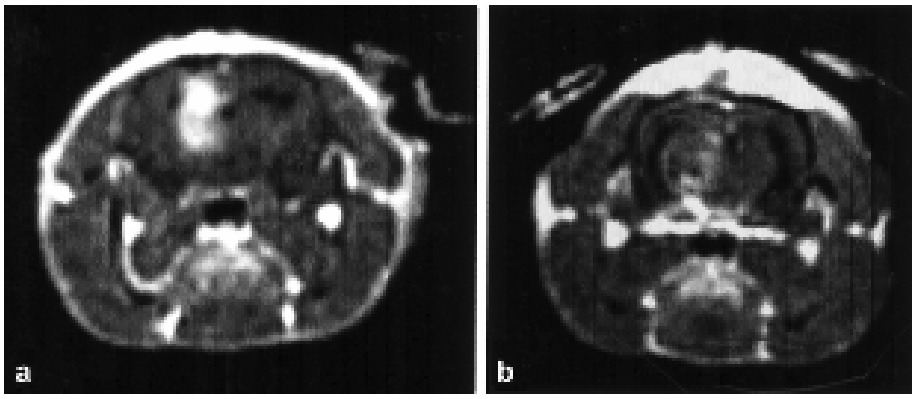

Fig. **2** T_1-weighted post-contrast coronal image, eighteen days following tumor cell implantation; **a** untreated tumor, **b** 24 hours after PDT treatment.

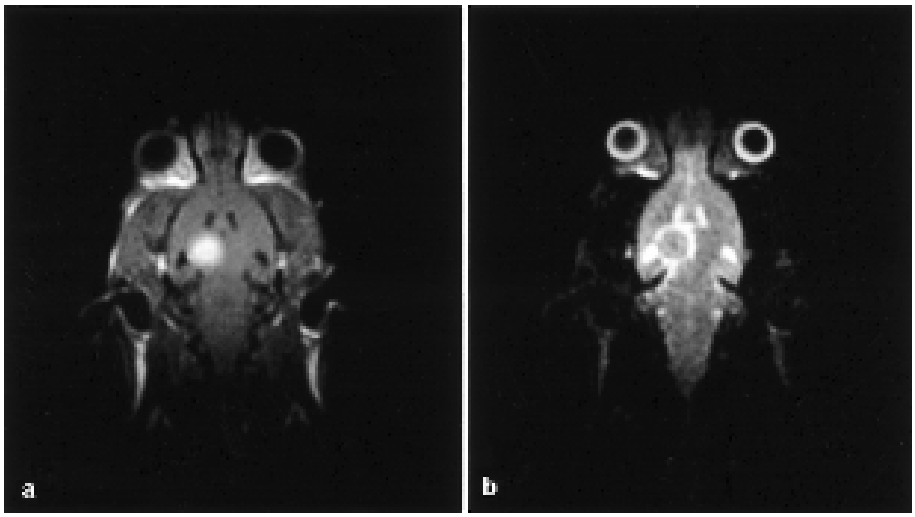

Fig. **3** Axial MR images of untreated tumor; **a** T_1-weighted post-contrast, **b** T_2-weighted pre-contrast. The peritumoral edema is clearly delineated.

Histopathology

Six rats received PDT treatment of 26 J 14 days following tumor induction (group 4). Fifteen to 72 hours after treatment the animals were sacrificed and the brains removed. Low magnification H&E stained sections from control and treated tumors are shown in Figs. **4a** and **4b**, respectively. On gross sections tumors were well defined, and no tumor necrosis was seen in sections from control animals. In contrast, in sections from PDT-treated tumors a central region of necrosis could be clearly discerned (Fig. **4b**). At higher magnification (Fig. **5** ×40) a more or less clearly defined border between tumor and normal brain was apparent in control animals (Fig. **5a**) with no observable capsule. In some regions there were limited signs of tumor infiltrating cell migration into the surrounding brain. On the other hand microscopically large areas of necrosis were seen in the PDT-treated tumors together with clusters of viable tumor cells often found at the tumor periphery (Fig. **5b**). Evidence of treatment induced damage to normal brain adjacent to tumor was also observed in several animals. These lesions consisted of areas of increased edema. Immunostaining to detect fibrinogen as an indication of brain edema was evaluated in sections obtained from these animals as well as from non-treated controls (Fig. **6**). Sections from non-treated animals revealed a 0.5 1 mm peritumoral edema pattern (Fig. **6a**). Pronounced edema in the necrotic tumor center as well as in the BAT, and along white matter tracts was evident in most of the brains studied (Fig. **6b**) from PDT treated animals.

Survival analysis

All the animals (n = 6) injected with BT_4C cells that received ALA but no light (control group 3) developed clinical symptoms of intracranial disease and had to be sacrificed between days 26 and 31. The mean survival time for this group was 28.5 days. ALA-mediated PDT was evaluated for its ability to prolong survival in this tumor model. Nine days after implantation with BT_4C tumor cells animals received either 60 mg/kg (n = 8) or 125 mg/kg (n = 9) ALA *i. p.* followed 4 h later by light treatment (26 J). All of the treated animals recovered under steroid treatment from the temporary effects of treatment, and all neurological sequelae resolved within the first 48 hours. The survival of these two groups of treated animals compared to controls is shown in the Kaplen-Meier curves (Fig. **7**). Survival was significantly increased in the group receiving 125 mg/kg ALA compared to controls (28.5 vs. 36 days mean; $p = 0.002$).

Although the group of animals receiving 60 mg/kg ALA showed an increased mean survival time of 37 days with one long-term survivor, this was not statistically significant compared to untreated animals ($p = 0.169$) due to the large variation in survival times (std. error: 5.4). Twelve animals were treated 21 days after tumor induction with 13 (n = 6) or 26 J (n = 6). At this time tumors were often about 8 mm in size. In both groups 5 of the six animals involved developed clear symptoms of increased intracranial pressure with weight loss and lethargy within the first post-treatment day. Two in each group were found moribund in

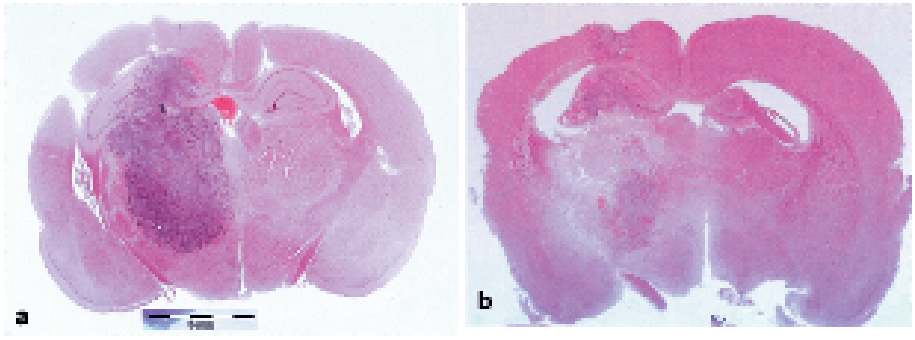

Fig. **4** Hematoxylin/eosin (H&E) stained coronal section of implanted BT_4C tumor under low magnification; **a** control tumor 14 days after implantation, no tumor necrosis is apparent; **b** treated tumor-containing brain, obtained 48 hours after PDT (26J @ 5 mW). Large areas of the tumor have been ablated.

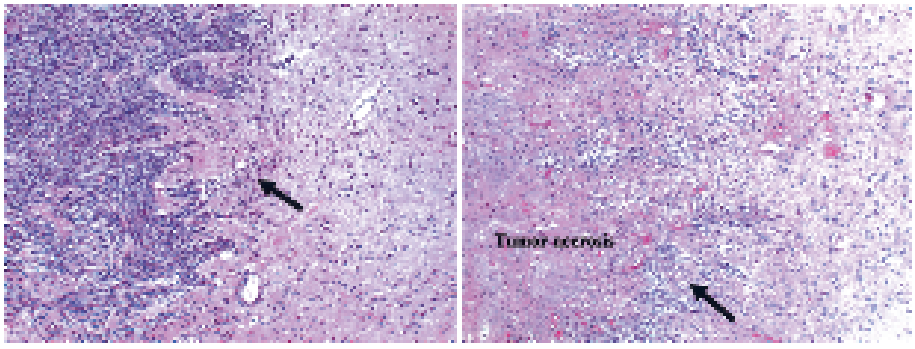

Fig. **5** Enlarged section of BT_4C tumor; **a** control tumor; arrow indicates migrating tumor cells; **b** treated tumor-containing brain; a large area of coagulation necrosis with cellular debris and associated edema are apparent; arrow indicates remaining tumor cells. Edema in brain adjacent to tumor is noted.

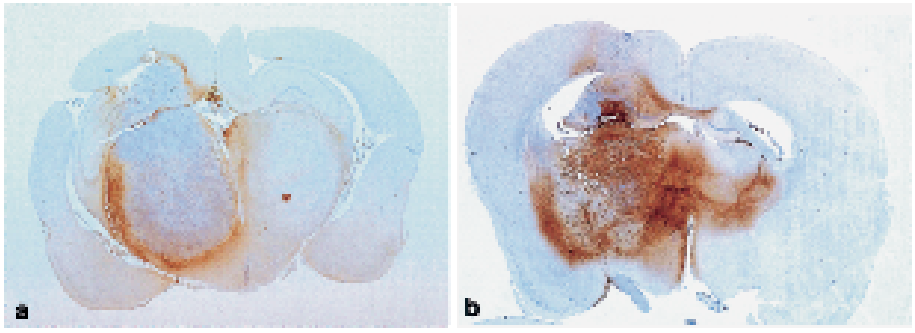

Fig. **6** Fibrinogen immunostained coronal sections of implanted BT_4C tumor under low magnification. Brown staining indicates the presence of plasma fluid indicative of cerebral edema; **a** control tumor 21 days after tumor implantation. The tumor associated vasogenic edema surrounding the tumor is clearly delineated. **b** Treated tumor-containing brain; pronounced edema in the necrotic tumor center as well as in the BAT, and along white matter tracts extending to the contralateral hemisphere is evident.

their cages within 48 h after PDT treatment and the remaining six were (3 in each group) euthanized also in this time period.

Discussion

The major indications for minimally invasive treatment modalities are small and/or deep-seated tumors, location in eloquent regions of the brain, elderly patients or patients with poor performance status. This type of treatment might also have advantages for the treatment of tumor recurrence compared to open surgery with its risk of postoperative complications.

The object of this study was to evaluate the feasibility of using ALA-mediated PDT tumor ablation as a minimally invasive treatment alternative for malignant brain tumors. The limited penetration of light in brain tissues and the increased uptake and retention of photosensitizer in tumor tissue makes PDT a highly localized treatment modality.

Although hematoporphyrin derivative (HpD), and its purified versions, porfimer sodium (Photofrin+) and dihematoporphyrin ether (Photofrin II+) have been used for photo-irradiation therapy in the brain their usefulness is somewhat limited by slow systemic clearance (resulting in prolonged skin photosensitivity) and poor tumor selectivity which often results in damage to normal brain tissue, as reported from preclinical studies [19–21]. These drawbacks restrict the clinical utility of Pf-based PDT, especially in the brain.

ALA, unlike hematoporphyrin derivatives, is not an exogenous photosensitizer. In the first step of the heme biosynthetic pathway 5-aminolevulinic acid (ALA) is formed from glycine and succinyl CoA. The last step is the incorporation of iron into protoporphyrin IX, and takes place in the mitochondria under the action of the enzyme, ferrochelatase. By adding exogenous ALA, the cellular synthesized protoporphyrin IX (PpIX) accumulates due to the limited capacity of ferrochelatase. Porphobilinogen deaminase is another enzyme of the heme synthesis pathway, catalyzing the formation of uroporphyrinogen from porphobilinogen. Its activity is higher in some tumors, while that of ferrochelatase is lower, so that PpIX accumulates with a high degree of selectivity in these tumors. Such selectivity has therefore been exploited for its application in fluorescent-guided resection of glial tumors

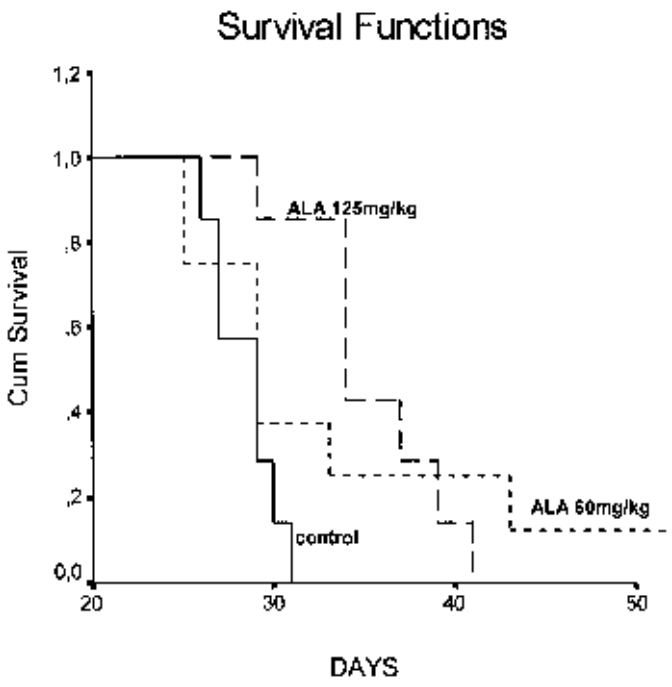

Fig. **7** Kaplan-Meier survival plot of control and PDT groups treated with 26 J of light over a 90 min interval, 9 days following tumor implantation. Mean survival after implantation: control (28.5 days), ALA 60 mg/kg (37 days), ALA 125 mg/kg (36 days).

[22,23]. Additionally PpIX-induced PDT has a threshold for necrosis in white matter that is significantly greater than for other drugs [7].

The anti-tumor efficacy of PDT is determined by the light energy delivered to the target tissue, the fluence rate at which the light is delivered, the sensitivity of the tissue to PDT and the concentration of the photosensitizer. Results from a previous study employing this model demonstrated a high degree of fluorescence observed in the tumors after *i.p.* administration of 60 – 250 mg kg^{-1} of ALA [9,24]. The tumor to normal brain ratio of PpIX was in the order of 200 : 1 indicating that the level of PpIX in tumor tissue is sufficient for a significant cytotoxic effect in the tumor while sparing normal tissue. The high PpIX level observed in tumor tissue is likely due to passive diffusion through a compromised BBB characteristic of the rapid angiogenesis associated with fast growing tumors as well as some of the factors already mentioned. This agrees well with the findings of Lilge and Wilson [25] who found ratios of 100 : 1 in a VX2 rabbit model. Additionally, extensive tumor PpIX fluorescence has been shown in patients undergoing surgery for glial tumors following the ingestion of 20 mg kg^{-1} of ALA [22,23]. Little or no fluorescence was found in areas of normal brain.

That the cell line the tumors are derived from is sensitive to ALA PDT has also been demonstrated. Multicell tumor spheroids, derived from the BT_4C cell line, were significantly growth inhibited in vitro following treatment, especially at low fluence rates [8,24,26]. Interestingly though, even at light fluence levels of 100 J/cm^2, 20% of the spheroids survived when followed for a 4-week period. As seen from Table **1**, a fluence level of 50 J/cm^2 would be reached in the periphery of a 6-mm diameter tumor. This total level is probably too low for the complete ablation of the tumor, since some tumor cells at the tumor periphery would survive treatment. That this is the case is seen from the histological sections showing pronounced central tumor necrosis surrounded by clusters of viable tumor cells (Fig. **5b**). One limiting factor for the efficacy of PDT is therefore most probably the inability to obtain an adequate fluence level due to the rapid attenuation of light in the brain. Simply increasing the total fluence level delivered to the tumor unfortunately has its limitations due in part to the relatively high levels of PpIX in the brain around tumor (BAT). Although the level of PpIX in normal brain is less than 1% of that found in the tumor, levels of sensitizer found in the BAT in our previous study were up to 20% of that found in bulk tumor [9]. This observation agrees well with the findings of others [27,28] and suggests a partial BBB breakdown in this region. Additionally, it is probable that PpIX produced in the tumor could be washed out into the BAT region by the net fluid outflow of the edema reaction found surrounding the tumor [29]. The resulting level of photosensitizer can cause damage to both the migrating cell infiltrating into the BAT and to normal brain tissue, following light treatment. More importantly PDT is known to induce a significantly increased edema reaction in the surrounding brain parenchyma, employing either hematoporphyrin derivatives [30,31], and to a lesser degree ALA [32]. Our results also clearly indicate the importance of this post-treatment edema reaction. The increased post-treatment morbidity and mortality observed when tumor ablation was undertaken in relatively large tumors is a limitation to the evaluation of this method in small animals. The small size of the intracranial space in rats, with its limited buffering volume, leads quickly to increased pressure, as a result of normal tumor progression and/or cerebral edema following PDT. In general, untreated tumor-bearing animals had to be euthanized within 48 hours following the first clinical signs (weight loss) due to tumor progression, typical for many rodent models. Furthermore, animals that showed no signs of disease were often found dead within 48 hours post-treatment (group 3), despite steroid support therapy if treatment was initiated more than 18 days post-implantation. Both the results of this study as well as that of other authors [32] have shown the limited effects steroid treatment has on this type of cytotoxic induced brain edema. The small dimensions of the rat brain also can lead to excessive fluence levels outside the tumor volume. The majority of PDT studies employing small animal models have been done with the incorporation of a relatively large craniectomy as a decompression measure [33] to mitigate some of the adverse effects of PDT. Since we were evaluating PDT as a minimally invasive treatment modality, to be performed directly following stereotactic biopsy, decompressive craniectomy was not undertaken in this series. The rapid attenuation of light in the much larger human brain, combined with a greatly increased buffering capacity compared with rodents, should make decompressive procedures in a clinical setting less important. In clinical trials employing Photofrin-mediated PDT as adjuvant treatment following surgical tumor resection post-treatment edema was not reported to be a serious problem [34].

The ultimate goal of tumor ablation is the total destruction of all pathological tissue. This was not achieved with the tolerable levels of fluence employed in these experiments, with only one long-term survivor (6%). This might in part be due to the rela-

tively high resistance to PDT of the chemically induced malignant cell line used in this study [24]. Employing a non-resected human cell line tumor (U87) in a nude rat model, and a different photosensitizer (HPPH), Lobel and co-workers have reported a long-term survival rate of 25 % [35].

In the above-mentioned previous study, as well as in the one reported here, PDT could induce a significant if not pronounced increase in survival time. Clinically it has been demonstrated that, even following gross total surgical resection, survival time is not dramatically increased [36, 37]. Recent publications employing mathematical models of glioma growth and invasion have pointed out some of the reasons for the inadequacies of current therapy, and that even large-scale treatment-induced destruction or surgical removal of the central portion of a rapidly growing tumor does not translate into a dramatic increase in survival [38, 39]. Different ablation treatment strategies will likely be required to achieve improved survival, e.g., the use of multiple fractionated long-term treatment protocols implemented by the use of implanted light applicators and portable lasers [8, 18, 40, 41].

Conclusion

The object of this study was to evaluate the feasibility of using ALA-mediated PDT tumor ablation as a minimally invasive treatment alternative for malignant brain tumors. PDT was well tolerated by the animals if treatment was initiated relatively early following tumor induction, i.e., when the tumors were relatively small. Although PDT could lead to a significant increase in survival time, complete ablation of the tumor proved difficult to achieve. Post-treatment-induced brain edema was the main cause of morbidity and early mortality in this tumor animal model despite steroid therapy.

Acknowledgements

This work has been supported by the Norwegian Cancer Society and the Norwegian Research Council, The Norwegian Radium Hospital Research Foundation, the UNLV Office of Research, the UNLV Cancer Research Center and the American Cancer Society. Portions of this work were made possible, in part, through access to the Laser Microbeam and Medical Program (LAMMP) at the Beckman Laser Institute, University of California, Irvine.

References

[1] Dougherty TJ, Gomer CJ, Henderson BW, Jori G, Kessel D, Korbelik M, Moan J, Peng Q. Review: Photodynamic therapy. J Nat Can Inst 1998; 90: 889 – 905
[2] Peng Q, Berg K, Moan J, Kongshaug M, Nesland JM. 5-Aminolevulinic acid-based photodynamic therapy: principles and experimental research. Photochem Photobiol 1997; 65: 235 – 251
[3] Peng Q, Warloe T, Berg K, Moan J, Kongshaug M, Giercksky K-E, Nesland JM. 5-Aminolevulinic acid-based photodynamic therapy: clinical research and future challenges. Cancer 1997; 79: 2282 – 2308
[4] Tsai J-C, Hsiao YY, Teng L-J, Chen C-T, Kao M-C. Comparative study on the ALA photodynamic effects of human glioma and meningioma cells. Lasers Surg Med 1999; 24: 296 – 305
[5] Hebeda KM, Saarnak AE, Olivo M. 5-Aminolevulinic acid induced endogenous porphyrin fluorescence in 9L and C6 brain tumours and in the normal rat brain. Acta Neurochirurgica 1998; 140: 503 – 513
[6] Olzowy B, Hundt CS, Stocker S, Bise K, Reulen HJ, Stummer W. Photoirradiation therapy of experimental malignant glioma with 5-aminolevulinic acid. J Neurosurg 2002; 97: 970 – 976
[7] Lilge L, Wilson BC. Photodynamic therapy of intracranial tissues: a preclinical comparative study of four different photosensitizers. J Clin Laser Med Surg 1998; 16: 81 – 82
[8] Hirschberg H, Angell-Petersen E, Peng Q, Madsen SJ, Sioud M, Sørensen D. Repetitive 5-aminolevulinic acid mediated photodynamic therapy of rat glioma. Proc SPIE 2004; 5312: 405 – 414
[9] Angell-Petersen E, Spetalen S, Madsen SJ, Sun C-H, Peng Q, Carper SW, Sioud M, Hirschberg H. Influence of light fluence rate on the effects of photodynamic therapy in an orthotopic rat glioma model. J Neurosurg 2006; 104: 109 – 117
[10] Marcus F. The use of radiofrequency energy for intracranial ablation: historical perspectives and results of experiments in animals. In: Breithardt G, Borggrefe M, Zipes D (eds). Non-Pharmacological Therapy of Tachyarrhythmias. Mount Kisco, NY: 213 – 219
[11] Anzai Y, Lufkin R, DeSalles A, Hamilton DR, Farahani K, Black KL. Preliminary experience with MR-guided thermal ablation of brain tumors. AJNR Am J Neuroradiol 1995; 16: 39 – 48
[12] Kahn T, Harth T, Bettag M, Schwabe B, Ulrich F, Schwarzmaier HJ, Modder U. Preliminary experience with the application of gadolinium-DTPA before MR imaging-guided laser-induced interstitial thermotherapy of brain tumors. J Magn Reson Imaging 1997; 7: 226 – 229
[13] Yi M, Ni Y, Yu J, Zhang H, Marchal G. Evaluation of radiofrequency ablation as an alternative for the treatment of brain tumor in rabbits. J Neurooncol 2002; 56: 119 – 126
[14] Leonardi MA, Lumenta CB, Gumprecht HK, Einsiedel GH von, Wilhelm T. Stereotactic guided laser-induced interstitial thermotherapy (SLITT) in gliomas with intraoperative morphologic monitoring in an open MR-unit. Minim Invas Neurosurg 2001; 44: 37 – 42
[15] Leonardi MA, Lumenta CB. Stereotactic guided laser-induced interstitial thermotherapy (SLITT) in gliomas with intraoperative morphologic monitoring in an open MR: clinical experience. Minim Invas Neurosurg 2002; 45: 201 – 207
[16] Laerum OD, Rajewsky MF, Schachner M, Stavrou D, Haglid KG, Haugen A. Phenotypic properties of neoplastic cell lines developed from fetal rat brain cells in culture after exposure to ethylnitrosourea in vivo. Z Krebsforsch Klin Onkol Cancer Res Clin Oncol 1977; 89: 273 – 295
[17] Mella O, Bjerkvig R, Schem BC, Dahl O, Laerum OD. A cerebral glioma model for experimental therapy and in vivo invasion studies in syngeneic BD-IX rats. J Neurooncol 1990; 9: 93 – 104
[18] Angell-Petersen E, Sørensen DR, Madsen SJ, Hirschberg H. Interstitial light application for repetitive photodynamic therapy in a rat brain tumor model. Proceeding SPIE, Vol. 5312; 2004: 415 – 423
[19] Chen Q, Chopp M, Madigan L, Dereski MO, Hetzel FW. Damage threshold of normal rat brain in photodynamic therapy. Photochem Photobiol 1996; 64: 163 – 167
[20] Dereski MO, Chopp M, Chen Q, Hetzel FW. Normal brain tissue response to photodynamic therapy: histology, vascular permeability and specific gravity. Photochem Photobiol 1989; 50: 653 – 657
[21] Ji Y, Powers SK, Brown TJ, Walsted D, Maliner L. Toxicity of photodynamic therapy with Photofrin in the normal rat brain. Lasers Surg Med 1994; 14: 219 – 228
[22] Stummer W, Stocker S, Wagner S, Stepp H, Fritsch C, Goetz C, Goetz AE, Kiefmann R, Reulen HJ. Intraoperative detection of malignant gliomas by 5-aminolevulinic acid-induced porphyrin fluorescence. Neurosurgery 1998; 42: 518 – 525
[23] Stummer W, Novotny A, Stepp H, Goetz C, Bise K, Reulen HJ. Fluorescence-guided resection of glioblastoma multiforme utilizing 5-ALA-induced porphyrins. A prospective study in 52 consecutive patients. J Neurosurg 2000; 93: 1003 – 1013
[24] Hirschberg H, Angell-Petersen E, Peng Q, Sorensen DR, Sun CH, Carper SW, Madsen SJ. ALA mediated Photodynamic Therapy of experimental malignant glioma in the BD-IX rat model. Proceeding SPIE; Vol. 6, no.1 2005: 513 – 521
[25] Lilge L, Portnoy M, Wilson BC. PDT-induced apoptosis in brain tissue in vivo: Apoptosis following PDT in normal and VX2 tumor-bearing rabbit brain. Proceedings SPIE,; Vol. 3592 1999: 28 – 36
[26] Hirschberg H, Sun CH, Tromberg BJ, Madsen SJ. Enhanced effects of concurrent 5-aminolevulinic acid-mediated photodynamic therapy by hyperthermia on glioma spheroids. J Neurooncol 2004; 70: 289 – 299

[27] Obwegeser A, Jakober R, Kostron H. Uptake and kinetics of 14C-labelled meta-tetrahydroxyphenylchlorin and 5-aminolevulinic acid in the C6 rat glioma model. Br J Cancer 1998; 78: 733 – 788
[28] Ji Y, Walstad DL, Brown JT, Powers SK. Relation between porphyrin distribution and blood brain barrier changes in the rat glioma model. Lasers Surg Med 1992; 12: 174 – 179
[29] Reulen HJ, Graham R, Spatz M, Klatzo I. Role of pressure gradients and bulk flow in dynamics of vasogenic brain edema. J Neurosurg 1977; 46: 24 – 35
[30] Ji Y, Powers SK, Brown TJ, Walsted D, Maliner L. Toxicity of photodynamic therapy with Photofrin in the normal rat brain. Lasers Surg Med 1994; 14: 219 – 228
[31] Kostron H, Obwegeser A, Jakober R. Photodynamic therapy in neurosurgery: a review. J Photochem Photobiol B 1996; 36: 157 – 168
[32] Ito S, Rachinger W, Stepp H, Reulen HJ, Stummer W. Oedema formation in experimental photo-irradiation therapy of brain tumours using 5-ALA. Acta Neurochir (Wien) 2005; 147: 57 – 65
[33] Ji Y, Walstad D, Brown JT, Powers SK. Improved survival from intracavitary photodynamic therapy of rat glioma. Photochem Photobiol 1992; 56: 385 – 390
[34] Muller P. PDT for primary brain tumors. Photodynamic News 1999; 2: 2 – 5
[35] Lobel J, MacDonald IJ, Ciesielski MJ, Barone T, Potter WR, Pollina J et al. 2-[1-Hexyloxyethyl]-2-devinyl pyropheophorbide-a (HPPH) in a nude rat glioma model: implications for photodynamic therapy. Lasers Surg Med 2001; 29: 397 – 405
[36] Kowalczuk A, Macdonald RL, Amidei C et al. Quantitative imaging study of extent of surgical resection and prognosis of malignant astrocytomas. Neurosurgery 1997; 41: 1028 – 1038
[37] Lacroix M, Abi-Said D, Fourney DR, Gokaslan ZL, Shi W, DeMonte F, Lang FF, McCutcheon IE, Hassenbusch SJ, Holland E, Hess K, Michael C, Miller D, Sawaya R. A multivariate analysis of 416 patients with glioblastoma multiforme: prognosis, extent of resection, and survival. J Neurosurg 2001; 95: 190 – 198
[38] Woodward DE, Cook J, Tracqui P, Cruywagen GC, Murray JD, Alvord Jr EC. A mathematical model of glioma growth: the effect of extent of surgical resection. Cell Prolif 1996; 29: 269 – 288
[39] Swanson KR, Bridge C, Murray JD, Alvord Jr EC. Virtual and real brain tumors: using mathematical modeling to quantify glioma growth and invasion. J Neurol Sci 2003; 216: 1 – 10
[40] Madsen SJ, Sun CH, Tromberg BJ, Hirschberg H. Development of a novel indwelling balloon applicator for optimizing light delivery in photodynamic therapy. Lasers Surg Med 2001; 29: 406 – 412
[41] Bisland SK, Lilge L, Lin A, Rusnov R, Wilson BC. Metronomic photodynamic therapy as a new paradigm for photodynamic therapy: rationale and preclinical evaluation of technical feasibility for treating malignant brain tumors. Photochem Photobiol 2004; 80: 22 – 30

K. Aydın[1]
C. Çokluk[1]
S. Kaplan[2]
C. Rakunt[1]
F. Çelik[1]

A Model of Unilateral Frontal Focal Cerebral Venous Occlusion in the Rat

Abstract

Objective: The aim of this experimental study was to create a new focal venous infarction model in rats. **Method:** 20-male Sprague-Dawley rats were used in this experiment. Unilateral frontal strip craniectomy was done in front of the coronal suture. Frontal veins were observed by using the operative microscope. In this study we used the bipolar coagulation method over the transparent dura mater for occlusion of the bridging veins for venous infarction. Specimens were evaluated by histopathological techniques. **Results:** Unilateral frontal hemispheric swelling, midline shift, brain edema, subcortical petechial hemorrhage, hemorrhagic infarction and necrosis were the histopathological findings on microscopic examination. **Conclusion:** Our results revealed that the bipolar coagulation method over the transparent dura mater for occlusion of the unilateral frontal cortical veins for venous infarction might be a new experimental model in the evaluation of brain damage after disturbance to the venous circulation.

Key words

Unilateral cortical veins · brain swelling · focal venous infarction model · rat brain

Introduction

Cerebral vein occlusion is a relatively common pathology in clinical practice [1 – 6]. Although numerous animal experiments had been conducted in the investigation of cerebral arterial obstruction, only few of them focused on venous occlusion [2, 7]. Experimental focal arterial ischemia models in animals generally use the proximal or distal segment of the middle cerebral artery for occlusion to produce ischemia [8 – 10]. However, the venous system is basically different because of the wide and complex anastomosis among the veins [11,12].

Anatomically, the cerebral veins can be divided into two groups; the superficial and the deep veins [11]. The superficial veins drain blood from the cortical and subcortical regions of the hemispheres into the sinuses [11,12]. The superficial group also can be divided into two groups as anastomotic veins and bridging veins. Four anastomotic veins had been defined in the literature; the anterior anastomotic vein (the vein of Trolard), the vein of Rolando, the posterior anastomotic vein (the vein of Labbe), and the vein or veins of Sylvius [11].

Brain edema, cerebral infarction, elevated intracranial pressure or intraparenchymal hemorrhage are common findings in patients suffering from cerebral venous occlusion [4]. In this experimental study we developed a new venous occlusion model in the rat brain using the bipolar coagulation method over the transparent dura mater for occlusion of the bridging veins for venous infarction. In this report we describe the technique and results including the histopathological examination.

Affiliation
[1] Department of Neurosurgery, Medical Faculty, Ondokuzmayıs University, Samsun, Turkey
[2] Department of Histology and Embryology, Medical Faculty, Ondokuzmayıs University, Samsun, Turkey

Correspondence
Keramettin Aydın, M. D. · Department of Neurosurgery · Medical Faculty · Ondokuzmayıs University · 55139 Samsun · Turkey · Tel.: +90/362/312/1919/3652 int. · Fax: +90/362/457/6041 · E-mail: kaydin@omu.edu.tr

Bibliography
Minim Invas Neurosurg 2006; 49: 143–146 © Georg Thieme Verlag KG Stuttgart · New York
DOI 10.1055/s-2006-944246
ISSN 0946-7211

Materials and Methods

Approval

The present study was approved by the local animal care committee at the Medical Faculty of Ondokuzmayis University (Ethical Committee).

Animal preparation

Twenty male Sprague-Dawley rats, each weighing between 280 and 320 grams, were used for this study. We used the bipolar coagulation method over the transparent dura mater for occlusion of the bridging veins for venous infarction.

Prior to surgery the animals were allowed free access to food and water in their cages with a 12-hour light/dark cycle and a temperature of 22 C.

Anesthesia

The rats were anesthetized with ketamine (4 mg/100 g) and xylazine (1.5 mg/100 g) administered intramuscularly. Hematocrit, pH, pO_2 and pCO_2 and blood pressure were monitored during surgery by using a femoral artery catheter. Rectal temperature was monitored at 37 C with a heating pad throughout the operation.

Surgery

Unilateral frontal vein occlusion: Each animal was placed in the prone position. A midline straight skin incision was made on the scalp from anterior to the coronal suture. The unilateral frontal bone was drilled. Dura mater and the unilateral frontal vein were exposed. The unilateral frontal vein can be visualized because the dura mater is transparent in rats. In this study we used the bipolar coagulation method over the transparent dura mater for occlusion of the bridging veins for venous infarction.

The frontal cortical veins were shown in a cadaveric rat brain (Fig. **1**).

Histological preparation

Three days after the operation, the rats were anesthetized with ketamine (4 mg/100 g) and xylazine (1.5 mg/100 g) administered intramuscularly. The rat brains were subjected to perfusion-fixation with 4% paraformaldehyde. The brains were removed from the skull and stored overnight at +4 C. The brains were embedded in paraffin to obtain coronal sections of the frontoparietal region. Sections were stained with hematoxylin and eosin.

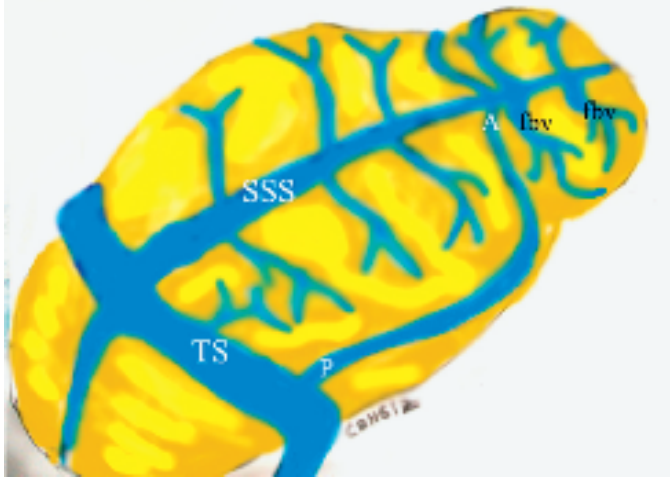

Fig. **1** Frontal cortical veins are shown in a cadaveric rat brain.

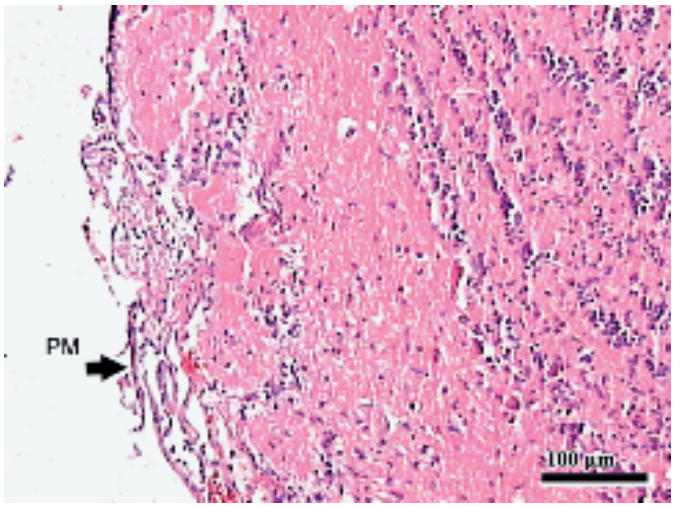

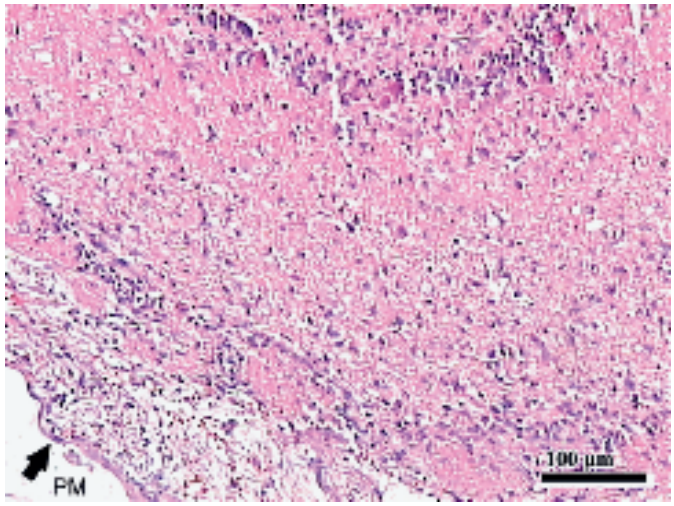

Fig. **2** **a**, **b** Histopathological appearance of the non-occlusion side. PM = pia mater.

Results

Physiological parameters

There were no significant changes in physiological variables (blood pressure, pulse, and blood gases) during the experiment.

Clinical observations

No death was noted in the experimental group.

Histopathological observations

The non-occlusion side is shown in Fig. **2**. Hemispheric swelling, brain edema, subcortical petechial hemorrhage, hemorrhagic infarction and necrosis were prominent histopathological findings on the microscopic examination. Petechial hemorrhage was generally located in the subcortical area. The venous infarction side was clear as poor stained areas in the brain slices stained with hematoxylin and eosin (Fig. **3**).

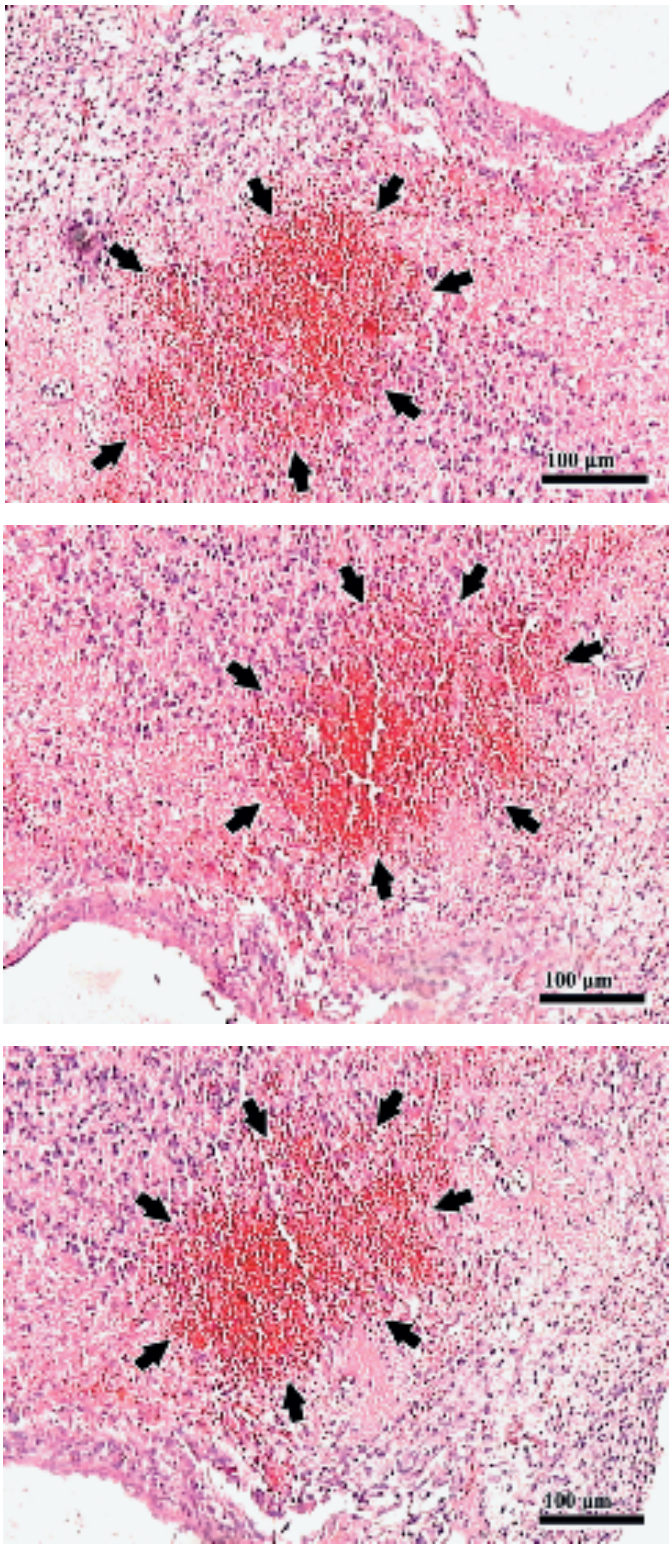

Fig. **3** **a – c** Histopathological appearance of the occlusion side.

Discussion

The new innovation in this experimental study was the surgical sacrifice of unilateral frontal drainage veins for evaluation of brain ischemia and infarction of venous origin. The evaluation of the hemorrhagic infarct area, calculation of cell number, estimation of infarct volume, demonstration of brain swelling and edema in small area may all be investigated with this experimental model. In this small area the effect of drugs on ischemia and/or infarction may be evaluated.

The cerebral venous anatomy of the rats is a very good model for studying venous occlusion diseases. The advantages of this model are the minimal venous variation and the similarity with the human cerebral venous circulation. At the same time, the identification of the frontal lobe was easy because of the prominent sulcus between the small frontal lobe and the relatively large parietal lobe in the rats.

Our observation on the rat brain revealed that the superficial veins in the rat brain can be divided into five subdivisions; 1) the frontal bridging veins group, 2) the anterior anastomotic vein, 3) the parietal and occipital bridging veins group, 4) the posterior anastomotic vein, and 5) the Sylvian veins group. The frontal bridging veins connect to the proximal part of the superior sagittal sinus in the frontal lobe. The anterior anastomotic vein drains venous blood into the superior sagittal sinus between the frontal and parietal lobes. The parietal and occipital bridging veins connect to the superior sagittal and transverse sinus behind the superior anastomotic vein in the parietal and occipital lobes. The posterior anastomotic vein drains into the sigmoid or transverse sinus.

Experimental models in the evaluation of venous occlusion generally used occlusion of the superior sagittal sinus and/or bridging veins [2,4,5,7]. The success of the occlusion of the superior sagittal sinus has some limitations because of the strong anastomotic organization. In rats, the frontal bridging veins do not have any anastomotic organization with other veins such as the anterior, posterior, Rolandic, and Sylvian veins. Because of this, in our model we used the unilateral frontal veins.

In the medical literature, there are many published experimental works on ischemia originating from focal arterial insufficiency or occlusion [8 – 10]. On the other hand, there are a few experimental studies on the ischemia originating from venous occlusion [2,4 – 7]. The cause of this dilemma is the lack of a model for venous occlusive diseases. It is difficult to produce a model of venous infarction because of the anatomic characteristics of venous structure.

The opening of a burr hole in the rat skull without any dural tear is an extremely important step in this model. A midline straight skin incision was made on the scalp from anterior to the coronal suture. The unilateral frontal bone was drilled. Dura mater and the unilateral frontal vein were exposed. The unilateral frontal vein can be visualized because the dura mater is transparent in the rat.

In this study we used the bipolar coagulation method over the transparent dura mater for occlusion of the bridging veins for venous infarction. This is a good and reliable technique for occlusion of the main cerebral veins. In some experimental studies, photochemically induced occlusion of the bridging veins was used for venous infarction. These two techniques may be used.

Brain swelling secondary to edema, cerebral ischemia, infarction and/or intraparenchymal hemorrhage are pathological findings in venous occlusion. According to our results brain swelling with a midline shift was a prominent finding in the hemisphere with unilateral frontal vein occlusion. Venous ischemia was most prominently located in the unilateral frontal lobe. Hemorrhage was located in the frontal pole. The success of this model is satisfactory in the aspect of pathological findings. The major difficulty is the necessity of microsurgical technique in the small rat brain.

Microneurosurgical techniques and the ability of using the operative microscope are necessary. One should make some practice before starting this experiment for improving his/her microsurgical ability and techniques.

Conclusion

We present a newly developed rat model, as demonstrated in this study, that can be very useful for further and more detailed investigations of the pathophysiological basis of cerebral venous infarction and for the experimental evaluation of therapeutic strategies. With this model, evaluation of the hemorrhagic infarct area, calculation of the cell number, estimation of the infarct volume, the demonstration of brain swelling and edema in a small area, and a precise evaluation the effect of drugs to the reduced brain area are possible.

References

[1] Kawaguchi T, Kawano T, Kaneko Y, Ooasa T, Masanori T, Ogasawara S. Classification of venous ischemia with MRI. J Clin Neurosci 2001; 8 (Supplement 1): 82 – 88

[2] Nakase H, Kakizaki T, Kazunori M, Hiramatsu K, Sakaki T. Use of local cerebral blood flow monitoring to predict brain damage after disturbance to the venous circulation: cortical vein occlusion model by photochemical dye. Experimental study. Neurosurgery 1995; 37: 280 – 286

[3] Benamer HTS. Cerebral venous thrombosis: anticoagulants or thrombolyic therapy? J Neurol Neurosurg Psychiatry 2000; 69: 427 – 430

[4] Fries G, Wallenfang T, Hennen J, Velthaus M, Heimann A, Schild H, Perneczky A, Kempski O. Occlusion of the pig superior sagittal sinus, bridging and cortical veins: multistep evolution of sinus-vein thrombosis. J Neurosurg 1992; 77: 127 – 133

[5] Nakase H, Kempski OS, Heimann A, Takeshima T, Tintera J. Microcirculation after cerebral venous occlusion as assessed by laser Doppler scanning. J Neurosurg 1997; 87: 307 – 314

[6] Forbes KPN, Pipe JG, Heiserman JE. Evidence for cytotoxic edema in the pathogenesis of cerebral venous infarction. AJNR Am J Neuroradiol 2001; 22: 450 – 455

[7] Schaller B, Graf R, Weinbard K, Heiss WD. A new animal model of cerebral venous infarction: ligation of the posterior part of the superior sagittal sinus in the cat. Swiss Med Wkly 2003; 133: 412 – 418

[8] Garcia JH, Liu KF, Yoshida Y, Lian J, Chen S, Del Zoppo GJ. Influx of leukocytes and platelets in an evolving brain infarct (Wistar rat). Am J Pathol 1994; 144: 188 – 199

[9] Narayanan U, Weiss HR, Liu X, Chi OZ. Exogenous endothelin-1 improves microvascular oxygen balance during focal cerebral ischemia in the rat. Regul Pept 2002; 105: 1 – 7

[10] Gomi S, Burnett MG, Karp A, Greenberg JH. Nimodipine does not affect the flow-metabolism couple in permanent cerebral ischemia. Exp Brain Res 2004; 155: 469 – 476

[11] Krayenbuhl H, Yasargil MG. Cerebral angiography, 2nd edn. Stuttgart: Georg Thieme Verlag, 1982: 181 – 235

[12] Yasargil MG. Microneurosurgery IVA. Stuttgart: Georg Thieme Verlag, 1994: 109 – 114

[13] Di Chiro G. Angiographic patterns of cerebral convexity veins and superficial dural sinuses. Am J Roentgenol 1962; 87: 308 – 321

[14] Delmas A, Chifflet J. Le sinus longitudinal superieur et les voies de drainage de la convexite cerebrale. Sem Hop Paris 1950; 26: 4888

S. Shabat[1]
Y. Pevsner[1]
Y. Folman[2]
R. Gepstein[1]

Pulsed Radiofrequency in the Treatment of Patients with Chronic Neuropathic Spinal Pain

Abstract

In recent years there has been debate among spinal surgeons, neurosurgeons and pain physicians regarding the efficacy of radiofrequency (RF) ablation when treating patients with a neuropathic pain source. It is usually considered as a treatment option after conservative treatment has failed. Twenty-eight patients with a minimal follow-up of 1 year were examined in our institution after they had undergone pulsed radiofrequency (PRF) procedures due to neuropathic spinal pain. Nineteen patients (68%) reported long-term pain relief (more than 1 year) which was defined as a reduction of the visual analogue score by at least 30%. No complications were found in this study except for mild discomfort in the treated area which spontaneously resolved up to 3 weeks after the procedure. We concluded that PRF is a safe and an effective procedure for patients who suffer from chronic neuropathic pain from spinal origin. It should be tried after conservative treatment has failed.

Key words

Pulsed radiofrequency · neuropathic spinal pain

Introduction

Radiofrequency (RF) procedures are an important part of complex minimal invasive treatment of chronic pain conditions and are used for reducing noxious transmission in the nervous system. Radiofrequency energy is a form of electromagnetic energy [1]. When applied to tissues, the rapidly oscillating electromagnetic field is believed to cause movements of charged particles, resulting in heat generation. Frictional or resistive heating of tissue around the probe tip, rather than the probe itself, is the primary source of heat. This heat probably cause a blockage of the transmission of pain stimuli from peripheral receptors to the central pain structures in case of pulsed RF (PRF). The effects of PRF are not clearly understood [2]. There are some attempts to explain the influence of PRF on the nervous structure. One of them is a reduction in pain reception by activation of the spinal and supraspinal mechanisms, as in the case of transcutaneous electrical nerve stimulation [2]. Another explanation is the induction of long-term depression in the spinal cord [2–4]. New investigations have shown that PRF could produce changes in the character of small non-myelinated fibers in the dorsal roots and horn [4].

There is no consensus in the literature of the recent years regarding the efficacy of pulsed radiofrequency for the treatment of patients with chronic neuropathic pain. Until lately, it was believed that neuropathic pain is usually a contraindication to the use of radiofrequency [5]. Lately some authors have shown beneficial effect of pulsed RF for these patients [2,4,6,7]. This contradiction in clinical outcomes led us to prospectively study our large group of patients under strict criteria in terms of pain improvement following the procedure for patients with neuropathic back pain.

Materials and Methods

Our study comprises 28 patients who underwent the RF procedure for neuropathic spinal pain between the years 2000 and

Affiliation
[1] Spinal Care Unit, Sapir Medical Center, Kfar-Saba, and Tel-Aviv Sackler Medical School, Israel
[2] Department of Orthopaedic Surgery, Hillel-Yafe Medical Center, Hadera, Israel

Correspondence
Shay Shabat, M. D. · Spinal Care Unit · Sapir Medical Center · 48 Tchernichovsky St. · 44281 Kfar-Saba · Israel · Tel.: +972/9/7472642 · Fax: +972/9/7410596 · E-mail: drshabat@hotmail.com

Bibliography
Minim Invas Neurosurg 2006; 49: 147–149 © Georg Thieme Verlag KG Stuttgart · New York
DOI 10.1055/s-2006-944238
ISSN 0946-7211

2002 and who were followed for at least 1 year. The patients were treated with pulsed radiofrequency (PRF) dorsal root ganglion (DRG) rhizotomy. There were 11 males (39%) and 17 females (59%). The age ranged from 24 to 72 (mean: 54) years.

Criteria for selection patients for RF treatment were: 6 months history of pain prior to the procedure, failure of any kind of conservative treatment and the absence of an absolute indication for surgical treatment.

The patients underwent pulsed radiofrequency rhizotomy (PRF) of the dorsal root ganglion with a standard approach [2,8]. Denervation was performed in an ambulatory outpatient setting under local anesthesia of the superficial tissue layers using lidocaine 1% and with fluoroscopic guidance. SMK-5, SMK-10, SMK-15 electrodes with 5 and 10 mm active tip (depending on the different level) and RFG-3C generator were used for localized targets. After sensor stimulation with 50 Hz and motor stimulation with 2 Hz, 0.5 mL of local anesthetic (lidocaine 2%) and depomedrol 80 mg were injected. For this procedure we used a core temperature of 42 degrees Celsius around the electrode tip for 120 seconds duration.

All patients were treated with non-steroidal anti-inflammatory drugs for 4–6 weeks after the procedures and underwent physiotherapy treatment for 1 month after the procedure.

A visual analogue scale (VAS) for evaluating the pain before and after surgery was used. A pain-free result was considered as a complete resolution of pain; a good result was considered to be at least 50% relief in pain; a moderate result relief in 30–50% of the pain prior to the procedure; and no effect was defined as less than 30% relief in pain. We considered pain free to be a good result and a moderate result as a significant reduction in pain.

The patients were examined in 4 intervals during the first year: after 4 weeks, after 3 and 6 months, and after 1 year.

Results

Twenty-eight patients suffering from chronic neuropathic pain (more than 6 months duration, 17 months on average) underwent PRF rhizotomy for dorsal root ganglion. Twenty patients were treated in the lumbar region while 8 were treated in the cervical region.

After 4 weeks, 24 patients (86%) reported an improvement in pain. In the second follow-up period (3 month after procedure) 23 patients (82%) reported significant pain relief: 2 patients had complete pain relief; 12 good relief and 9 moderate relief. Five patients (18%) experienced no effect in terms of pain relief.

Six months following the procedure 2 patients remained pain free, 7 patients had good results and 11 patients had moderate results. Three patients had a recurrence of symptoms, so overall 8 patients were classified as no effect (29%).

In the next evaluation, which was performed 1 year after the procedure, only one additional patient was deteriorated to have no effect, so 19 patients had significant pain relief (68%) while for 9 patients (32%) there was no effect.

No complications were observed after all PRF procedures. However, 6 patients (21%) developed post-procedure discomfort in the same innervated region, which was resolved spontaneously within a 3 week period.

The results for this group of patients are summarized in Table **1** and Table **2**.

Table **1** Results after pulsed radiofrequency of the 28 patients

	Pain free	*Good*	*Moderate*	*Total with pain relief*	*No effect*
1 month	2	12	10	24 (86%)	4 (14%)
3 months	2	12	9	23 (82%)	5 (18%)
6 months	2	7	11	20 (71%)	8 (29%)
12 months	2	6	11	19 (68%)	9 (32%)

Table **2** Mean visual analogue scale before and after PRF treatment of the 28 patients

	Before	*After*	*Difference*
1 month	8.8 (range 7–10)	4.1 (range 0–10)	4.7
3 months	8.8 (range 7–10)	4.2 (range 0–10)	4.6
6 months	8.8 (range 7–10)	4.8 (range 0–10)	4.0
12 months	8.8 (range 7–10)	4.9 (range 0–10)	3.9

Discussion

We evaluated patients suffering from neuropathic pain for at least 6 months and who had failed to respond to conservative treatment (mean symptomatic period until the procedure was 17 months). Spontaneous resolution of pain after being symptomatic for so long is almost never detectable [9]. The method that was used in these patients was a non-destructive method of radiofrequency procedure-pulsed RF of the dorsal root ganglion [2]. The effect of this treatment in terms of pain relief was measured by a standard pain scale (visual analogue scale – VAS) and it was found to be successful. The patients had substantial reduction in pain following the procedures. After 1 year follow-up 68% of the patients still showed significant improvement and the average reduction in VAS was 3.9 points. In addition, no complication in this treatment modality was seen, except for mild discomfort in 6 patients after the procedure, which resolved spontaneously after 3 weeks.

In most papers, a significant reduction in pain is defined as a reduction in 2 points or more than 30% in the visual analogue score [10]. In this study we used only the second part of these criteria, which means only reduction of pain by at least 30% in comparison with the pain before the treatment. This criterion is even

stricter than those used elsewhere, and if we had used either of the above criteria we would have ended up with even better results.

The mechanism by which pulsed RF works is unclear. Several mechanisms were suggested. One of them is the activation of both spinal and supraspinal mechanisms similar to the way transcutaneous electrical nerve stimulation works, thus reducing pain stimulation [11]. It is also more interesting and yet unclear how it achieves long-term depression in the spinal cord. Pulsed RF is usually delivered at 1 – 2 Hz. This frequency is similar to what was suggested to induce long-term depression in the spinal cord [3,4].

In this study we used a core temperature of 42 degrees Celsius around the electrode tip for 120 seconds duration. This was based on the study of Slappendel et al. [12] who showed a similar effect of pulsed RF given at low temperature (around 40 degrees Celsius) in comparison with higher temperature (67 degrees Celsius).

We did not use any diagnostic blocks prior to the treatment in any of the patients. The issue of prognostic blocks prior to the definitive procedure was questioned in previous articles [13,14]. In the past, we used to perform prognostic blocks of the treated region before every radiofrequency procedure. With time, we changed this approach. We realized that we could rely on a combination of accurate history taking, physical examination and imaging studies for doing RF procedures without confirmation of the diagnosis by blocks prior to the procedure. In addition, there are up to 25 % of false positive and false negative results of blocks, increased waiting time and additional hospitalizations.

In conclusion, the results of this study which examined the effect of pulsed RF on patients with chronic neuropathic pain for up to 1-year follow-up are encouraging. No major complications were noted except for mild discomfort in the minority of the patients which was resolved spontaneously in a 3 week period. Still, additional studies in this subject are needed in order to understand the exact way the pulsed RF causes pain relief in the chronic neuropathic patients. As for now, this procedure is recommended only after conservative treatment has failed.

References

[1] Hecht P, Hayashi K, Lu Y, Fanton GS, Thabit 3rd G, Vanderby Jr R, Markel MD. Monopolar radiofrequency energy effects on joint capsular tissue: potential treatment for joint instability. An in vivo mechanical, morphological, and biochemical study using an ovine model. Am J Sports Med 1999; 27: 761 – 771

[2] Munglani R. The longer-term effect of pulsed radiofrequency for neuropathic pain. Pain 1999; 80: 437 – 439

[3] Pockett S. Spinal cord synaptic plasticity and chronic pain. Anesth Analg 1995; 80: 173 – 179

[4] Sandkuhler J, Chen JG, Cheng G, Randic M. Low-frequency stimulation of afferent Adelta-fibers induced long-term depression at primary afferent synapses with substancia gelatinosa neurones in the rat. J Neurosci 1997; 17: 6483 – 6491

[5] Patt RB, Cousins MJ. Techniques for neurolytic blockade. In: Cousins MJ, Bridenbaugh (Eds.). Neural Blockade, third edition. Philadelphia: Lippencott Raven, 1998: 1007 – 1062

[6] Wijk RM Van, Geurts JW, Wynne HJ. Long-lasting analgesic effect of radiofrequency treatment of the lumbosacral dorsal root ganglion. J Neurosurg 2001; 94: 227 – 231

[7] Yin Y, Willard F, Carreiro J, Dreyfuss P. Sensory stimulation-guided sacroiliac joint radiofrequency neurotomy: technique based on neuroanatomy of the dorsal sacral plexus. Spine 2003; 28: 2419 – 2425

[8] Kleef M van, Barendse GA, Kessels AH, Lousberg R, Sluijer M. Radiofrequency lesion adjacent to the dorsal root ganglion for cervical pain: a prospective double blind randomized study. Neurosurgery 1996; 38: 1127 – 1132

[9] Borenstein DG. Epidemiology, etiology, diagnostic evaluation, and treatment of low back pain. Curr Opin Rheumatol 1999; 11: 151 – 157

[10] Farrar JT, Young Jr JP, LaMoreaux L, Werth JL, Poole RM. Clinical importance of changes in chronic pain intensity measured on an 11-point numerical pain rating scale. Pain 2001; 94: 149 – 158

[11] Bowsher D. Mechanics of acupuncture. In: Filshie J, White A (Eds.). Medical Acupuncture. Edinburgh: Churchill Livingstone, 1998: 69 – 82

[12] Slappendel R, Crul BJ, Braak GJ, Geurts JW, Booij LH, Voerman VF, do Boo T. The efficacy of radiofrequency lesioning of the cervical dorsal root ganglion in a double-blind randomized study: no difference between 40 and 67 C treatments. Pain 1997; 73: 159 – 163

[13] North RB, Han M, Zahurak M, Kidd DH. Radiofrequency lumbar facet denervation: analysis of prognostic factors. Pain 1994; 57: 77 – 83

[14] Sapir DA, Gorup JM. Radiofrequency medial branch neurotomy in litigant and nonlitigant patients with cervical whiplash: a prospective study. Spine 2001; 26: 268 – 273

Stereotactic Radiotherapy for the Treatment of Pituitary Adenomas

M. T. Selch[1]
A. Gorgulho[2]
S. P. Lee[1]
C. Mattozo[2]
T. D. Solberg[1]
N. Agazaryan[1]
A. A. F. DeSalles[2]

Abstract

Purpose: The aim of this study was to retrospectively review local control and morbidity following stereotactic radiotherapy (SRT) for pituitary adenoma. **Methods:** Between 1997 and 2004, 39 patients with pituitary adenomas received SRT. Median age was 56 years (range: 13 to 90 years). Thirty-three patients underwent incomplete transsphenoidal surgery prior to SRT and six had unresectable tumors. The largest tumor dimension varied from 1.7 to 6 cm (median: 3 cm). Tumor volume varied from 1.2 to 56 mL (median 10.5 mL). Thirty-five tumors were ≤ 1 mm from the optic chiasm/nerve. Thirty-three tumors were non-functional. SRT was delivered by a dedicated linear accelerator (Novalis, Heimstetten, Germany). Beam collimation was achieved by a fixed circular collimator (five patients) or a micro-multileaf collimator (34 patients). Total dose varied from 4500 to 5040 cGy (median: 4860 cGy) and was prescribed at the 90% isodose line. **Results:** After a median follow-up of 32 months (range: 12 to 94 months), the local control rate was 100%. Tumor size was stable in 26 patients and decreased in 13 patients. Hormone normalization did not occur following SRT. New endocrine deficiency occurred in six patients. No patient developed cranial nerve injury or second malignancy following treatment. **Conclusions:** SRT achieves a high rate of local control and a low rate of treatment-induced morbidity. SRT is applicable to pituitary adenomas in close proximity to the optic apparatus and tumors in excess of three centimeters in the greatest dimension. Further follow-up is necessary to establish the long-term outcome following SRT for pituitary adenomas.

Key words

Stereotactic radiotherapy · pituitary adenoma

Introduction

Pituitary adenomas are benign tumors of the adenohypophysis and account for 10% of adult intracranial neoplasms [1]. Patients may suffer deterioration of vision or hypopituitarism due to a tumor mass effect. Secretory adenomas may cause profound metabolic disturbance. Total surgical removal is the treatment of choice for patients with non-functional adenomas and functional tumors other than prolactinomas [2]. Patients with residual tumors are at risk for progressive neurological complaints and recurrent endocrinopathy. Initial medical management with a dopamine agonist is recommended for patients with symptomatic prolactinomas [3]. Agonist therapy may result in tumor volume reduction and a decrease in serum prolactin [4,5]. Some patients do not respond to medical management or prove intolerant of agonist therapy. Cessation of medical management results in tumor regrowth and recurrent hyperprolactinemia [3].

Conventional external beam irradiation can control growth of pituitary adenomas. Reported 10-year local control rates following radiotherapy vary from 85 to 90% [6–10]. Radiotherapy may alleviate hormone hypersecretion, although a latency of many months is required for biochemical remission [8]. Conventional radiotherapy for pituitary adenomas has been associated with rare, but serious, long-term morbidity including second neoplasms, cognitive impairment, optic atrophy and hypopituitarism [11].

Affiliation
[1] Department of Radiation Oncology, David Geffen School of Medicine at UCLA, Los Angeles, California USA
[2] Division of Neurosurgery, David Geffen School of Medicine at UCLA, Los Angeles, California USA

Correspondence
Michael T. Selch, M. D. · Department of Radiation Oncology · David Geffen School of Medicine at UCLA · 200 Medical Plaza · Suite B-265 · Los Angeles, CA 90095–6951 · USA · E-mail: selch@radonc.ucla.edu

Bibliography
Minim Invas Neurosurg 2006; 49: 150–155 © Georg Thieme Verlag KG Stuttgart · New York
DOI 10.1055/s-2006-944240
ISSN 0946-7211

Stereotactic radiosurgery (SRS) is a method for delivering a large single dose of ionizing irradiation to an intracranial site [12]. The inherently steep dose gradient produced by SRS affords physical protection of normal tissue adjacent to the target lesion. Control of tumor growth and hormonal hypersecretion has been reported in 86 to 100% and 50 to 96%, respectively, following SRS for pituitary adenomas [13].

Despite the dosimetric advantages of SRS, use of this innovative technique for pituitary adenomas may be limited by tumor size or proximity to the optic apparatus. SRS is typically recommended for pituitary adenomas ≤ 3 centimeters in size and located several millimeters from the optic apparatus [13].

Stereotactic radiotherapy (SRT) combines the physical dose localization advantages of SRS with the radiobiological benefits of dose fractionation [14]. A fractionated dose of irradiation known from conventional radiotherapy experience to be effective for pituitary adenomas and tolerated by the optic apparatus can be delivered by the SRT technique to a markedly reduced volume of the central nervous system. Several groups have documented the efficacy and safety of SRT pituitary adenomas [15 – 22].

We retrospectively report our initial clinical experience with SRT using a dedicated linear accelerator for the treatment of pituitary adenomas. Patient outcome was analyzed with regard to local tumor control and morbidity.

Table **1** Patient and tumor characteristics of 39 patients with pituitary adenomas treated with SRT

Characteristic		*Value*
Age (years)	Range	13 – 90
	Median	56
Gender		
	Male	27
	Female	12
Initial secretory status		
	Non-functional	33
	Growth hormone	2
	Prolactin	2
	Growth hormone/prolactin	2
Size		
	> 3 cm	19
	≤ 3 cm	20
Timing of SRT		
	Residual disease after initial surgery	16
	Recurrent disease after previous surgery	17
	Inoperable tumor	6
Tumor location at SRT		
	Intrasellar only	3
	Sella/cavernous sinus	8
	Cavernous sinus only	10
	Sella/suprasellar extension	11
	Sella/suprasellar/cavernous sinus	7

Patients and Methods

Between February 1997 and November 2004, 39 patients with pituitary adenoma received SRT in the UCLA Department of Radiation Oncology. Patient and tumor characteristics are shown in Table **1**. Thirty-three patients underwent incomplete transsphenoidal surgery prior to SRT. Sixteen of these patients received SRT within three months of surgery for stable, residual adenoma. Seventeen patients received SRT for pituitary adenoma recurring after initial incomplete surgery. The interval from initial surgery to image-documented recurrence varied from one to nine years (median: three years). Six patients were not candidates for transsphenoidal surgery and underwent primary SRT. Thirty-three tumors were non-functional and six demonstrated hypersecretion of either growth hormone or prolactin or both hormones. All patients with functional tumors demonstrated persistent or recurrent hypersecretion unresponsive to suppressive medication following initial surgery. Tumor was confined to the sella in only three patients at the time of SRT. The remainder demonstrated involvement of the cavernous sinus or suprasellar region or both areas. Tumor was ≤ 1 mm from the optic chiasm or nerve in 35 patients. Pituitary function was entirely normal in eight patients immediately prior to SRT. One or more replacement hormones were required in the remainder, including complete anterior pituitary failure in seven patients.

The technique of SRT has been described elsewhere [23]. Patients were immobilized with a custom-fitted thermoplastic face mask (U-PLAST, BrainLAB, Munich, Germany). Tumors were localized with contrast-enhanced MR and CT scans performed with compatible fiducial localizers. Axial slice thickness through the region of interest was 3 mm. CT-MR image fusion by the mutual information technique was used during treatment planning in all cases. Three-dimensional isodose treatment plans were generated using a BrainLAB planning system (versions 3.5 – 5.1, BrainLAB, Munich, Germany). Gross tumor volume was defined as the contrast-enhancing tumor demonstrated on axial, coronal and sagittal MR. At the time of SRT, tumor diameter, defined as the largest tumor dimension in any MR plane, varied from 1.7 to 6 cm (median: 3 cm) and tumor volume varied from 1.2 to 56 mL (median: 10.5 mL). Planning target volume was defined as the gross tumor volume plus a margin of normal tissue varying from one to 4 mm (median: 2 mm). Prescription isodose was defined as the largest isodose encompassing the planning target volume.

Treatment was delivered to a single isocenter by a dedicated linear accelerator (Novalis, Heimstetten, Germany). Beam collimation was achieved by a fixed circular collimator in five patients. These patients were irradiated with four to six non-coplanar arcs at unique treatment couch angles. In the remaining 34 patients, field-shaping with a micro-multileaf collimator (mMLC) was used to optimize dose distribution for non-spherical targets. This collimator consists of 26 pairs of leaves varying in thickness from 3 to 5.5 mm. These patients were treated with seven to 15 static shaped beams (16 patients) or, more recently, four to six dynamic non-coplanar arcs (17 patients).

Dose was prescribed at the 90% isodose line (Fig. **1**). Daily and total dose to the optic apparatus was restricted to ≤ 200 cGy and

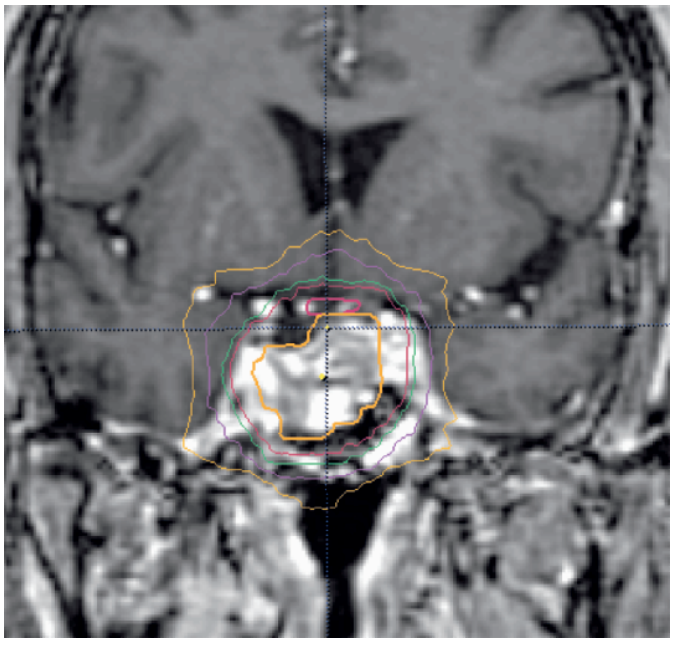

Fig. **1** Coronal contrast-enhanced T_1-weighted MR image demonstrates pituitary adenoma and superimposed LINAC stereotactic radiotherapy isodose lines. Isodose lines displayed, from the adenoma (heavy yellow) and chiasm (heavy red) are: 90% (red), 80% (green), 50% (purple), 30% (yellow), respectively.

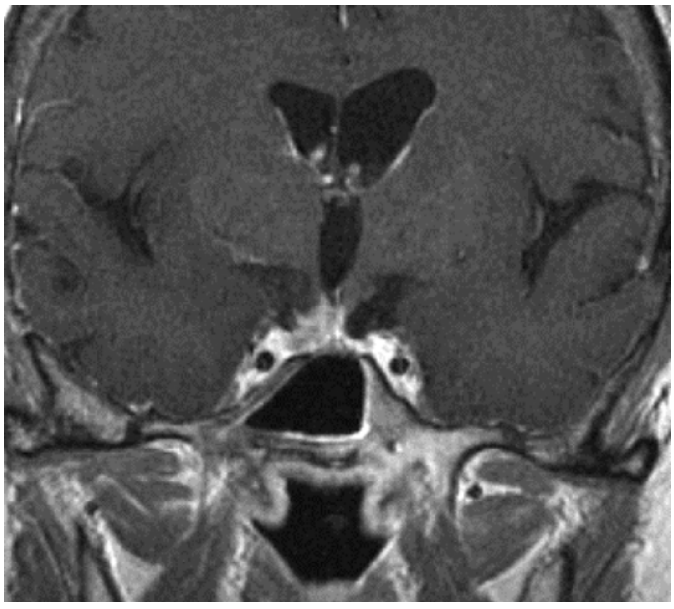

Fig. **2** Coronal contrast-enhanced T_1-weighted MR image of the patient shown in Fig. **1** taken 24 months after stereotactic radiotherapy.

≤ 5200 cGy, respectively. As a consequence, prescribed target dose varied from 4500 to 5040 cGy (median: 4860 cGy). Reproducibility of patient positioning was evaluated using the depth helmet method of Kooy et al. [24].

Overall and local progression-free survival rates were calculated from the completion of SRT by the actuarial method of Kaplan and Meier. Patients were followed every six months after SRT by clinical examination, laboratory analysis and MR. Complete response was defined as absence of contrast-enhancing tumor on MR. Progression was defined as any enlargement in the size of the contrast-enhancing tumor. The impact of patient, tumor and treatment variables upon outcome was assessed using the log-rank test.

Results

All patients were available for clinical and imaging follow-up evaluation. The median follow-up was 32 months (range: 12 to 94 months). Tumor responded to SRT in 13 patients although no response was complete. The largest tumor dimension decreased by more than 50% in two patients 24 and 48 months after treatment (Fig. **2**). Eleven tumors demonstrated lesser degrees of reduction. Tumor was radiographically stable in the remaining 26 patients. One patient died of myocardial infarction 84 months after SRT. The remaining 38 patients are alive. The two- and four-year actuarial overall and local progression-free survival rates were each 100%.

Two patients with growth hormone-secreting tumors demonstrated no reduction in either ICF or serum growth hormone one year after SRT. One patient with a prolactinoma demonstrated no change in serum prolactin 18 months after SRT. Serum prolactin declined from 232 ng/mL to 118 ng/mL (normal: 20 ng/mL) 88 months after treatment in the other patient with prolactinoma. No change in growth hormone, ICF or prolactin was noted one year after SRT in two patients with mixed growth hormone/prolactin-secreting adenomas.

Seven patients had impairment of visual fields prior to SRT. Six remained unchanged after treatment and one patient improved 24 months after SRT. Four patients, including one who was blind, had impaired visual acuity prior to SRT. None improved after treatment.

There was no acute toxicity during daily immobilization or SRT. No patient developed new cranial nerve injury, symptomatic perilesional edema or second malignancy. New endocrine deficiency occurred in six patients at risk for pituitary failure (19%). One patient with normal hormonal status required thyroid hormone replacement 36 months after SRT. One patient with initially normal function was noted to have low growth hormone 24 months after SRT but was asymptomatic and did not receive supplementation. One other patient with normal function developed panhypopituitarism 48 months after SRT. The remaining three patients required one or more hormone supplements prior to treatment and developed new thyroid insufficiency at 24 to 60 months after SRT. Prospective assessment of cognitive function was not performed.

Discussion

It is axiomatic in the radiotherapy of pituitary adenomas that reducing the volume of normal parenchyma exposed to treatment must not result in eventual tumor relapse. Pituitary adenoma regrowth following conventional radiotherapy is associated with a doubling of mortality compared to patients with controlled tu-

mors [25]. The target volume for SRT in our series included gross tumor depicted on imaging plus an additional two millimeters of normal tissue to account for imaging uncertainties and patient relocation variances. This planning approach results in substantial reduction of the volume of normal parenchyma included within the high-dose region compared to conventional techniques [7,26]. The local control rate of 100% demonstrates that SRT utilizing a micromultileaf collimator to irradiate an intracranial tumor with minimal normal tissue exposure is a viable alternative for pituitary adenomas.

The local control rate in our series is similar to other SRT series (Table **2**). Colin et al. reported an eight-year local control rate of 99% in a series of 110 patients followed a median of 82 months [22]. Milker-Zabel et al. reported actuarial 5- and 10-year control rates of 93% and 85%, respectively, in a series of 63 patients followed-up for a mean of 39 months [19]. Paek and associates reported a five-year actuarial control rate of 98% in a group of 68 patients followed a median of 30 months [21]. Control rates of 85 to 100% have been reported in smaller series followed 9 to 62 months [15–19].

Further follow-up is required to fully assess the long-term local control rate in our series. The median follow-up duration in our series is 32 months and 13 patients have been followed two years or less. Locally progressive pituitary adenoma has been reported 24 to 33 months following SRT elsewhere. Late relapses of pituitary adenoma have been documented as long as 20 years following conventional radiotherapy [6,27].

The small number of patients and absence of relapse precludes analysis of factors predictive of local control. Local control in the 19 patients with adenomas > 3 centimeters indicates SRT is a viable option for tumors traditionally considered too large for SRS. In the literature, SRT is equally efficacious for patients with unresectable/inoperable pituitary adenomas compared to those managed after incomplete transnasal surgery [21,22]. There is no difference in control rates between functional or non-functional adenomas [19,20].

Table **2** Results of stereotactic radiotherapy for pituitary adenomas

Series	*No. of patients*	*No, of functional tumors*	*Median follow-up (months)*	*% Local control*	*% Hormone normalization*	*% Visual morbidity*
Coke	19	5	19	100	–	0
Mitsumori	30	18	36	85	54	0
Welsh	9	9	62	100	75	0
Jalali	22	9	9	100	22	0
Milker-Zabel	63	26	39	85	15	6
Milker-Zabel	20	20	60	100	80	0
Paek	68	0	30	98	–	2
Colin	110	47	82	99	42	0
Selch	39	6	32	100	0	0

Pituitary adenomas are modestly sensitive to fractionated irradiation. In our series, reduction in tumor size was noted in 13 patients (33%). In only two patients was the largest tumor dimension reduced by more than 50% and no patient demonstrated a complete response. Response rates following SRT of 26% to 38% have been reported elsewhere [16,19,21]. The low response rates of pituitary adenomas following SRT may be a reflection of limited follow-up. In the large series of Colin et al., patients were followed-up for a minimum of four years. This group documented 36% complete response and 89% objective response, defined as at least 30% reduction in the largest tumor dimension [22]. Tumor response kinetics were noted to be slow. Median time to objective response was four years and nearly eight years for complete resolution. According to Collin et al., suprasellar extension greater than 20 mm was an unfavorable prognostic factor for achieving complete response (univariate $p = 0.01$). Response is not influenced by patient age, gender or functional status of the tumor or tumor volume [22].

No patient in our series with hormonally active adenoma demonstrated endocrine normalization following SRT. Others have reported frequent hormonal normalization following SRT, perhaps as a consequence of longer follow-up. Normalization of hypersecretion is known to be delayed several years after conventional radiotherapy [8]. Mitsumori et al. reported normalization in seven of 13 patients with an overproduction of various hormones prior to SRT [16]. Average interval to normalization was 18 months. Milker-Zabel et al. reported normalization of growth hormone secretion in 16 of 20 patients after a 26 month median latency [20]. Finally, Colin et al. reported 42% complete response in 47 patients with persistent secretion prior to irradiation [22]. Median interval to normalization of ACTH was two years and greater than five years for growth hormone. Normalization of hypersecretion occurs more rapidly following SRS. Landolt et al. reported a median latency to growth hormone normalization of 1.4 years after SRS compared to seven years after conventional radiotherapy [28]. In the literature, there is no significant effect of gender, tumor volume, tumor size or degree of suprasellar extension on the rate of hormone normalization following SRT [22].

The rate of serious morbidity was low in our experience. Pituitary function declined in six patients at risk for endocrine failure (19%) but only one developed panhypopituitarism. No patient developed impaired vision despite the tumor approaching within one millimeter of the optic apparatus in 35 cases, again demonstrating the viability of SRT for pituitary adenomas unsuitable for SRS. No patient developed a second intracranial malignancy. Although a prospective neurocognitive evaluation was not performed, no patient demonstrated obvious dementia.

Similar low rates of sequelae have been reported elsewhere. Mitsumori et al. reported a three-year rate of freedom from adverse central nervous system effects of 100% following SRT compared to 72% ($p < 0.02$) after SRS in a non-random experience [16]. The authors noted abnormal contrast enhancement in temporal lobe parenchyma following SRS for adenomas extending into the cavernous sinus. It is noteworthy that 25 patients in our series received SRT for adenomas with cavernous sinus extension and none demonstrated parenchymal injury. Colin et al. observed deficiency of ACTH, TSH and FSH-LH in 28.6%, 32% and 13.9%, re-

spectively, following SRT [22]. Pituitary insufficiency following irradiation may be more a consequence of injury to the stalk or hypothalamus than a direct effect on pituitary parenchyma [29]. Hyperprolactinemia following conventional radiotherapy is considered an indicator of hypothalamic injury by ionizing irradiation [30]. Following conventional irradiation, where the stalk and hypothalamus receive a dose equivalent to the adenoma, the rate of pituitary function decline varies from 20 to 50% [7–9, 31, 32]. Following SRS, the rate of panhypopituitarism is significantly lower when < 770 cGy is delivered to the stalk compared to higher doses [33]. The absence of post-treatment hyperprolactinemia in our series indicates that SRT using mMLC beam-shaping permits irradiation of an adenoma with simultaneous exclusion of the stalk/hypothalamus and consequent reduction in the rate of injury to the hypothalamic-pituitary axis. Finally, Paek et al. reported a 98% actuarial rate of preserving visual function [21]. Both patients in their series developing blindness received treatment delivered to more than one isocenter. The rare visual complications noted by Paek et al. may be a function of dose inhomogeneities that invariably accompany use of more than a single isocenter for stereotactic irradiation. Nedzi et al. demonstrated that dose inhomogeneity is the most significant predictive factor for complications following SRS [34]. Use of a single isocenter and a shaped field in our series resulted in a conformal and homogeneous dose distribution compared to either a large circular collimator or multiple isocenters.

Longer follow-up is needed to assess the ultimate safety of SRT. Late sequelae typically occur after a latency of many years following conventional irradiation for parasellar tumors. Minniti et al. reported that the cumulative risk of a second intracranial neoplasm was 2% at 10 years and 2.4% at 20 years in a group of 426 patients irradiated for pituitary adenoma [35]. According to Colin et al. there was no plateau in the incidence of pituitary insufficiency following SRT for nearly eight years [22]. All cases of pituitary function decline in our series occurred 24 or more months after treatment.

In summary, SRT is a safe and effective alternative for management of pituitary adenomas, particularly those where SRS is contraindicated due to tumor size and/or proximity to the optic apparatus. Use of an mMLC permits a conformal and homogeneous dose distribution resulting in exclusion of critical parasellar tissue from the high-dose volume. Further clinical experience and long-term follow-up is required to determine the eventual role of SRT compared to other forms of radiotherapy for pituitary adenomas.

References

[1] Ezzat S, Asa SL, Couldwell WT, Couldwell WT, Barr CE, Dodge WE, Vance ML, McCuthcheon IE. The prevalence of pituitary adenomas. A systematic review. Cancer 2004; 101: 613–619

[2] Ebersold MY, Quast LM, Laws ER, Scheitauer B, Randall RV. Long-term results in transphenoidal removal of non-functioning pituitary adenomas. J Neurosurg 1986; 64: 713–719

[3] Leavens ME, McCutcheon IF, Samaan NA. Management of pituitary adenomas. Oncology 1992; 6: 69–80

[4] McGregor AM, Scanlon Hall K, Cook DB, Hall R. Reduction in size of a pituitary tumor by bromocriptine therapy. N Engl J Med 1979; 300: 291–293

[5] Thorner MO, Martin WH, Rogol AD, Morris JL, Perryman RL, Conway BP, Howards SS, Wolfman MG, MacLeod RM. Rapid regression of pituitary prolactinomas during bromocriptine treatment. J Clin Endocrinol Metab 1980; 51: 438–445

[6] Grigsby PW, Simpson JR, Emami B, Fineberg BB, Schwartz HG. Prognostic factors and results of surgery and postoperative irradiation in the management of pituitary adenomas. Int J Radiation Oncol Biol Phys 1989; 16: 1411–1417

[7] Tsang RW, Brierly JD, Panzarella T, Gospodarowicz MK, Sutcliffe SB, Simpson WJ. Radiation therapy for pituitary adenoma: treatment outcome and prognostic factors. Int J Radiation Oncol Biol Phys 1994; 30: 557–565

[8] Zierhut D, Flentje M, Adolph J, Erdmann J, Raue F, Wannenmacher M. External radiotherapy of pituitary adenoma. Int J Radiation Oncol Biol Phys 1995; 33: 307–314

[9] Zaugg M, Adaman O, Pescia R, Landolt AM. External irradiation of macroinvasive pituitary adenomas with telecobalt: a retrospective study with long-term follow-up in patients irradiated with doses mostly of between 40–45 Gy. Int J Radiation Oncol Biol Phys 1995; 32: 671–680

[10] McCord MW, Buatti JM, Fennell EM, Mendenhall WM, Marcus RB, Rhoton AL, Grant MB, Freidman WA. Radiotherapy for pituitary adenoma: long-term outcome and sequelae. Int J Radiation Oncol Biol Phys 1997; 39: 437–444

[11] Al Mefty O, Kersh JE, Routh A, Smith RR. The long-term side effects of radiation therapy for benign brain tumors in adult. J Neurosurg 1990; 73: 502–512

[12] Leksell L. The stereotactic method and radiosurgery of the brain. Acta Chirug Scan 1951; 102: 316–391

[13] Sheehan JP, Niranjian A, Sheehan JM, Jane JA, Laws ER, Kondziolka D, Flickinger J, Landolt AM, Loeffler JS, Lunsford LD. Stereotactic radiosurgery for pituitary adenomas: an intermediate review of its safety, efficacy and role in the neurosurgical treatment armamentarium. J Neurosurg 2005; 102: 678–691

[14] Tome WA, Mehta M, Meeks SL, Buatti JM. Fractionated stereotactic radiotherapy: a short review. Tech Cancer Res Treat 2002; 1: 153–172

[15] Coke C, Andrews DW, Corn BW, Werner-Wasik M, Downes B, McCune C, Curran WJ. Multiple fractionated stereotactic radiotherapy of residual pituitary macroadenomas: initial experience. Stereotac Funct Neurosurg 1997; 69: 183–190

[16] Mitsumori M, Shrieve DC, Alexander E, Kaiser UB, Richardson GE, Black PM, Loeffler JS. Initial clinical results of linac-based stereotactic radiosurgery and stereotactic radiotherapy for pituitary adenomas. Int J Radiation Oncol Biol Phys 1998; 42: 573–580

[17] Welsh JS, Wharam MD, Nauta H, Jackson J, Williams JA. Stereotactic radiotherapy for Cushing's disease and prolactinoma. J Radiosurgery 1999; 2: 23–29

[18] Jalali R, Brada M, Perks JR, Traish D, Burchell L, McNair H, Thomas DGT, Robinson S, Johnston DG. Stereotactic conformal radiotherapy for pituitary adenomas: technique and preliminary experience. Clin Endocrinol 2000; 52: 695–702

[19] Milker-Zabel S, Debus J, Thilmann C, Schlegel W, Wannenmacher M. Fractionated stereotactically guided radiotherapy and radiosurgery in the treatment of functional and nonfunctional adenomas of the pituitary gland. Int J Radiation Oncol Biol Phys 2001; 50: 1279–1286

[20] Milker-Zabel S, Zabel A, Huber P, Schlegel W, Wannenmacher M, Debus J. Stereotactic conformal radiotherapy in patients with growth hormone secreting pituitary adenoma. Int J Radiation Oncol Biol Phys 2004; 59: 1088–1096

[21] Paek SH, Downes MB, Bednarz G, Keane WM, Werner-Wasik M, Curran WJ, Andrews DW. Integration of surgery and fractionated stereotactic radiotherapy for the treatment of nonfunctioning pituitary macroadenomas. Int J Radiation Oncol Biol Phys 2005; 61: 795–808

[22] Colin P, Jovenin N, Delemer B, Caron J, Grulet H, Hecart AC, Lukas C, Bazin A, Bernard MH, Scherpereel B, Peruzzi P, Nakib I, Reon C, Rousseaux P. Treatment of pituitary adenomas by fractionated stereotactic radiotherapy: a prospective study of 110 patients. Int J Radiation Oncol Biol Phys 2005; 62: 333–341

[23] Dunbar SF, Tarbell NJ, Kooy HM, Alexander E, Black PM, Barnes PD, Goumnerova L, Scott RM, Pomeroy SL, La Vally B, Sallan SE, Loeffler JS. Stereotactic radiotherapy for pediatric and adult brain: preliminary report. Int J Radiation Oncol Biol Phys 1994; 30: 551–559

[24] Kooy HM, Dunbar SF, Tarbell NJ, Mannarino E, Ferarro N, Shustermann S, Bellerive M, Finn L, McDonough CV, Loeffler JS. Adaptation and ver-

ification of the relocatable Gill-Thomas-Cosman frame in stereotactic radiotherapy. Int J Radiation Oncol Biol Phys 1994; 30: 685 – 691
[25] Erfurth EM, Bulow B, Nordstrom CH, Mikoczy Z, Hagmar L, Stromberg U. Doubled mortality rate in irradiated patients reoperated for regrowth of a macroadenoma of the pituitary gland. Eur J Endocrinol 2004; 150: 497 – 502
[26] Sohn JW, Dalzell JG, Suh JH, Tefft M, Schell M. Dose-volume histogram analysis of techniques for irradiating pituitary adenomas. Int J Radiation Oncol Biol Phys 1995; 32: 831 – 837
[27] Grigsby PW, Simpson JR, Fineberg B. Late regrowth of pituitary adenomas after irradiation and/or surgery. Hazard function analysis. Cancer 1989; 63: 1308 – 1312
[28] Landolt AM, Haller D, Lomax N, Schubiger O, Siegfried J, Wellis G. Stereotactic radiosurgery for recurrent surgically treated acromegaly: comparison with fractionated radiotherapy. J Neurosurg 1998; 88: 1002 – 1008
[29] Constine LS, Woolf PD, Cann D, Mick G, McCormick K, Raubertas RF, Rubin P. Hypothalamic-pituitary dysfunction after radiation for brain tumors. N Engl J Med 1993; 328: 87 – 94
[30] Trampe EA, Lundell G, Lax I, Werner S. External irradiation of growth hormone producing pituitary adenomas: prolactin as a marker of hypothalamic and pituitary effects. Int J Radiation Oncol Biol Phys 1991; 20: 655 – 660
[31] Rush S, Cooper PR. Symptom resolution, tumor control and side effects following postoperative radiotherapy for pituitary macroadenomas. Int J Radiation Oncol Biol Phys 1997; 37: 1031 – 1034
[32] McCollough WM, Marcus RB, Rhoton A, Ballinger WE, Million RR. Long-term follow-up of radiotherapy for pituitary adenoma: the absence of late recurrence after > 4500 cGy. Int J Radiation Oncol Biol Phys 1991; 21: 607 – 614
[33] Fiegl GC, Bonelli CM, Berghold A, Mokry M. Effects of gamma knife radiosurgery of pituitary adenomas on pituitary function. J Neurosurg 2002; 97 (Suppl 5): 415 – 421
[34] Nedzi LA, Kooy H, Alexander E, Gelman RS, Loeffler JS. Variables associated with the development of complications from radiosurgery of intracranial tumors. Int J Radiation Oncol Biol Phys 1991; 21: 591 – 599
[35] Minniti G, Traish D, Ashley S, Gonsalves A, Brada M. Risk of second brain tumor after conservative surgery and radiotherapy for pituitary adenoma: update after an additional 10 years. J Clin Endocrinol Metab 2005; 90: 800 – 804

The Microsurgical Anatomy of the Ciliary Ganglion and its Clinical Importance in Orbital Traumas: An Anatomic Study

Y. Izci
E. Gonul

Original Article

Abstract

The ciliary ganglion can easily be injured during surgery for the repair of orbital fractures and laterally situated intraorbital mass lesions. The aim of this study is to elucidate the microsurgical anatomy of the ciliary ganglion and to emphasize its clinical importance in orbital traumas and surgeries. The orbits of 10 adult cadavers were fixed with 10% formalin and dissected under the microscope with special attention to the presence and location of the ciliary ganglion. The motor (parasympathetic), sympathetic, and sensory roots, and the short ciliary nerves were exposed. Its relationship with other intraorbital neural and vascular structures were investigated. Some anatomic landmarks were determined and the distances between these landmarks were measured. The ciliary ganglion is an intraorbital neural structure approximately 3 mm in size, situated near the orbital apex, posterolateral to the globe in loose areolar tissue between the optic nerve and lateral rectus muscle. The mean distance between the ganglion and the optic nerve was 2.9 mm (range: 2.70 – 3.10 mm) and the mean distance between the lateral rectus muscle and the ganglion was 10.4 mm (range: 9.20 – 11.20 mm). Six to 10 short ciliary nerves arise from the ganglion and run forward in a curving manner with the ciliary arteries above and below the optic nerve. The ciliary ganglion should be taken into the account especially during lateral approaches to the orbit and the patients should be warned before the surgery about possible mydriatic or tonic pupils as a complication.

Key words

Ciliary ganglion · orbit · surgery · trauma

Introduction

The ciliary ganglion (CG) lies close to the lateral aspect of the optic nerve. It normally receives the parasympathetic (motor) root from the oculomotor nerve to the inferior oblique muscle. The shape of the ganglion varies (ovoid or rectangular shape with its largest diameter paralleling the axis of the optic nerve) among the specimens and with the level of sectioning within any specimen [1,2].

Since the CG is located in close proximity to very important neurovascular structures, such as optic nerve, branches of the oculomotor nerve, ophthalmic artery, abducens nerve, and nasociliary nerve [1,3], it is obvious that lesions of the CG may also affect these nearby structures and conversely, lesions of the neighbouring structures may affect the ganglion [2]. Injury to the CG may lead to Argyll-Robertson pupil [4] or to Adie's tonic pupil [5]. Therefore, knowledge of the various ramifications and branches of the ganglion is useful during the orbital surgery.

Although many papers about the microsurgical anatomy of the orbit have been previously published, there is no specific and detailed study about the morphological aspects of this fine ganglion. We describe, herein, the microsurgical anatomy of the CG and its relationship with intraorbital nerves, arteries and veins. We also emphasize its importance in orbital trauma and surgery.

Affiliation
Department of Neurosurgery, Gulhane Military Medical Academy, Ankara, Turkey

Correspondence
Yusuf Izci, M. D. · Department of Neurosurgery · Gulhane Military Medical Academy · 06018 Etlik · Ankara · Turkey · Tel.: +90/312/304/5318 · Fax: +90/312/304/5300 · E-mail: yusufizci@yahoo.com

Bibliography
Minim Invas Neurosurg 2006; 49: 156–160 © Georg Thieme Verlag KG Stuttgart · New York
DOI 10.1055/s-2006-944241
ISSN 0946-7211

Materials and Methods

This study was performed in the microsurgical laboratory of Gülhane Military Medical Academy. Twenty orbits in 10 adult cadavers were dissected specially to reveal the CG. The whole orbital content was removed and fixed with 10% formalin. The arteries and veins were perfused with coloured latex and silicone to facilitate the dissection. The orbits were dissected and examined under 3- to 20-fold magnification. The ganglion was exposed through the orbitozygomatic craniotomy, in which the supraorbital rim and lateral wall were removed with a frontal bone flap. The remaining posterior part of the orbital roof was removed using a rongeur. The periorbita was opened and the orbital fat was removed so that the muscles, nerves and vessels were clearly displayed. After the identification of the CG the location of the ganglion itself was found. Following this, the other roots of the ganglion and the short ciliary nerves were dissected.

Once the CG was exposed, morphometric measurements were made according to some landmarks as defined in Table **1**. These landmarks are also shown in Fig. **1**. The measurements were performed using a micrometer. Then, the number, length and diameter of the short ciliary nerves were determined. The size of each CG was also measured. The distance between the ganglion and optic nerve and the distance between the ganglion and lateral rectus muscle were also measured to determine the risk of injury to this fine structures during the surgical approaches and trauma to the orbit.

Results

Neural relationship

To find the location of the CG, one must first find the nerve to the inferior oblique muscle which runs parallel and close to the inferior border of the lateral rectus muscle and follow it backwards up to the motor root of the ganglion.

Some of the ascending sympathetic fibres and also a bundle of which collect together to form the sympathetic root of the CG course as an independent branch surrounded by orbital fat and exit the carotid artery in the cavernous sinus and pass through the most medial part of the fissure and oculomotor foramen to reach the CG and globe. The fibres forming the sympathetic root of the CG run forward and upward along the medial margin of the abducens nerve to reach the area lateral to the inferior division of the oculomotor nerve, where they pass through the central sector of the fissure. Some sympathetic fibres join the ophthalmic division and are distributed to the pupil in the long ciliary nerves that arise from the nasociliary nerve in the orbit. Others may pass directly through the fissure and orbit to the globe. The mean distance between the posterior end of the globe and the anterior edge of the CG was 12 mm (range: 7.75 – 19.80 mm) according to our measurements.

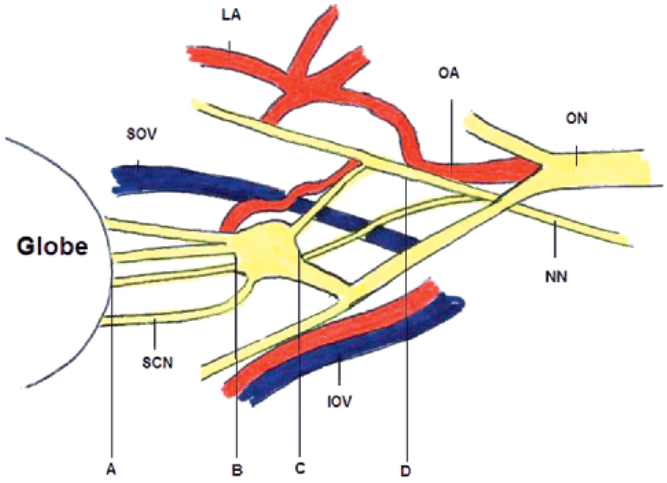

Fig. **1** Line drawing of a right orbit depicting the landmarks and the distances measured in this study. A = posterior end of the globe, B = anterior edge of the ciliary ganglion, C = posterior edge of the ciliary ganglion, D = site of the ophthalmic artery crossing the lateral side of the optic nerve, NN = nasociliary nerve, OA = ophthalmic artery, LA = lacrimal artery, ON = oculomotor nerve, SOV = superior ophthalmic vein, IOV = inferior ophthalmic vein, SCN = short ciliary nerve.

Table **1** The landmarks of the morphometric measurements

Distance	*from*	*to*
A – B	Posterior end of the globe	Anterior edge of the ciliary ganglion
B – C	Anterior edge of the ciliary ganglion	Posterior edge of the ciliary ganglion
C – D	Posterior edge of the ciliary ganglion	Site of the ophthalmic artery crossing the lateral side of the optic nerve
A – C	Posterior end of the globe	posterior edge of the ciliary ganglion
A – D	Posterior end of the globe	Site of the ophthalmic artery crossing the lateral side of the optic nerve

The ophthalmic artery, superior ophthalmic vein and nasociliary nerve which are situated on the lateral side of the optic nerve at the orbital apex cross between the nerve and superior rectus muscle to reach the medial part of the orbit. The measurements between the neurovascular structures which are related to CG are summarized in Table **2**. The mean distance between the CG and superior ophthalmic vein was 5.1 mm (range: 4.70 – 5.60 mm) and the mean distance between the CG and inferior ophthalmic vein was 4.5 mm (range: 3.70 – 4.90 mm). The mean distance between the posterior edge of the CG and the site of the ophthalmic artery crossing the lateral side of the optic nerve was 4.1 mm (range: 3.25 – 9.70 mm).

The inferior division of the oculomotor nerve gives rise to three branches. Two are directed forward to reach the inferior rectus and inferior oblique muscles and one passes medially below the optic nerve to enter the medial rectus muscle. In addition, the branch to the inferior oblique muscle gives rise the motor (parasympathetic) root to the CG.

The parasympathetic fibres synapse in the ciliary ganglion (which gives rise to the short ciliary nerve) and pierce the sclera to reach the ciliary body and iris.

Table **2** Measurements of the anatomic structures related to the CG

Measurement sites	*Mean [mm]*	*Range [mm]*
A – B	12	7.75 – 19.80
B – C	5.25	4.15 – 6.45
C – D	4.1	3.25 – 9.70
A – C	18.08	12.80 – 23.50
A – D	18.16	15.10 – 23.50
Width of CG	3.04	2.75 – 3.40
CG – ON	2.90	2.70 – 3.10
CG – SOV	5.1	4.70 – 5.60
CG – IOV	4.5	3.70 – 4.90
CG – LRM	10.4	9.20 – 11.20
Number of SCN	7	6 – 10

CG = ciliary ganglion, ON = optic nerve, SOV = superior ophthalmic vein, IOV = inferior ophthalmic vein, LRM = lateral rectus muscle, SCN = short ciliary nerves.

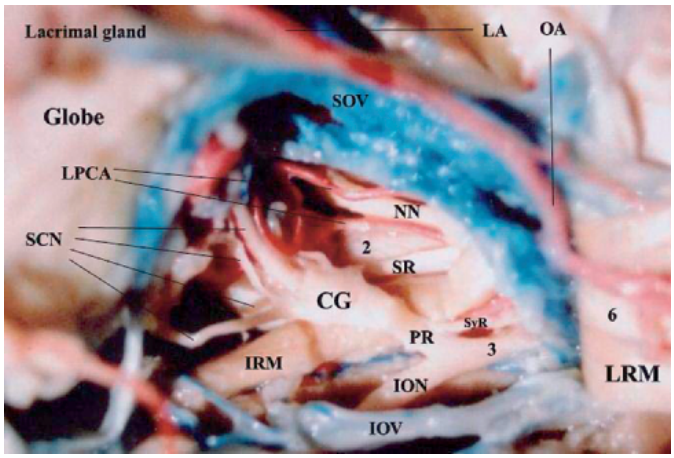

Fig. **2** Cadaver dissection showing neural and vascular structures around the ciliary ganglion. The lateral rectus muscle has been retracted to expose the ganglion. CG = ciliary ganglion, PR = parasympathetic root, SyR = sympathetic root, SR = sensory root, SCN = short ciliary nerves, SOV = superior ophthalmic vein, IRM = inferior rectus muscle, IOV = inferior ophthalmic vein, ION = inferior oblique muscle branch of oculomotor nerve, LPCA = lateral posterior ciliary arteries, NN = nasociliary nerve, OA = ophthalmic artery, LA = lacrimal artery, 2 = optic nerve, 3 = inferior division of the oculomotor nerve, 6 = abducens nerve lying on the lateral rectus muscle.

The abducens nerve passes through the annulus inferolateral to the oculomotor and nasociliary nerves then enter the medial surface of the lateral rectus muscle. The nasociliary nerve enters the orbit through the medial part of the superior orbital fissure and passes through the annulus between and lateral to the inferior and superior divisions of the oculomotor nerve. The nasociliary nerve crosses the optic nerve with the ophthalmic artery and superior ophthalmic nerve and gives rise to the anterior and posterior ethmoidal and infratrochlear nerves, was not exposed in this study. The nasociliary nerve also gives off several long ciliary nerves (which pass to the globe) and a sensory root to the CG. The fibres from the sensory root are distributed to the globe with the short ciliary nerves and convey sensation from the cornea and globe.

Arterial relationship

In our observations, the ophthalmic artery runs through the optic canal inferiorly to optic nerve and between its dural sheath and periosteum of the optic canal. The ophthalmic artery gives branches of the central retinal artery just before or on entering the orbit, and it gives the posterior lateral ciliary artery and the lacrimal artery into the orbit. It is directed toward the inner wall by making a curve over the optic nerve. The lacrimal artery derived from the ophthalmic artery reaches the lacrimal gland laterally and gives its branches. On the other hand, the posterior lateral ciliary artery goes on making convolutions and before entering ocular bulb gives branches of the longus and the brevis at the mediosuperior side of the optic nerve and adjacent to the CG, and its efferent nerve fibres. The lateral and upper aspects of the relations between the CG and the local arterial system are demonstrated in Fig. **2**.

Venous relationship

The superior ophthalmic vein passes backward within the superolateral part of the extraocular muscle cone. At the apex of the orbit, it exits the muscle cone by passing between the origin of the superior and lateral rectus muscles from the annular tendon. After exiting the muscle cone, it courses downward along the part of the lateral surface of the annular tendon while hugging the edge of the lateral margin of the fissure. It turns backward through the inferior sector of the fissure. It does not reach the lower margin of the fissure but turns medially below the annular tendon and the lower edge of the ophthalmic and abducens nerves to empty into the cavernous sinus an average of 2.8 mm above the lower margin of the fissure.

The inferior ophthalmic vein drains the inferomedial part of the orbit and courses backward within the muscle cone toward the superior orbital fissure. It exits the intraconal area by coursing between the origin of the lateral and inferior rectus muscles. It then courses below the annular tendon and through the inferior sector of the fissure to empty into the anterior inferior part of the cavernous sinus. It often joins the superior ophthalmic vein before emptying into the cavernous sinus.

Discussion

Knowledge of the microsurgical anatomy of the orbit is very important for preservation of the neurovascular structures during intraorbital procedures [6]. Fallopius and Willis described a nerve plexus belonging to the oculomotor nerve in the orbit in the 17th century. Schacher was the first to describe the CG in 1701. In the last century, only sporadic studies on the CG have been published [2].

The CG of man is known to have three nerve roots; sensory, sympathetic and motor (parasympathetic). The findings in our study indicate that this mode of connection is rather exceptional [4, 7 – 9].

The CG in a man was attached directly to the nerve for the inferior oblique muscle or was connected by a motor root. It gave off six to ten short ciliary nerves. Ganglion cells were also distributed into the sensory root and the motor root, and both roots gave off short ciliary nerves [10].

Sympathetic fibres come from the superior cervical ganglion which is situated at the base of the skull between the internal jugular vein and the internal carotid artery. The nervus caroticus internus divides into two as the internal carotid plexus and a cavernous plexus and goes to the orbit. All of the sympathetic fibres to the eye itself enter the globe by the way of the ciliary nerves [7].

Because the fat was not removed from these specimens as it is in gross anatomic dissections, the true spatial relationship of the CG became apparent. The ganglion may be so close to the optic nerve that it nearly touches it. The mean distance between the CG and optic nerve was 2.9 mm and this proximity together with variations in shape and position, make the ganglion vulnerable to surgical damage, especially when the optic nerve is approached through a lateral orbitotomy [11 – 13].

According to Johnston and Parkinson, they could not identify a branch that passed directly from the carotid plexus to the CG. They suggested that the sympathetic fibres to the CG joined the abducens nerve and were distributed with the branches of the ophthalmic nerve [10]. Sinnreich and Nathan were able to define a separate sympathetic root in 22 of 30 specimens. In 20 specimens, it originated directly from the plexus of the carotid sympathetic plexus. In the remaining two specimens, it originated in the orbit from the plexus that surrounds the ophthalmic artery or one of its branches [2]. Natori and Rhoton, in 3 of 20 orbits, there were sympathetic roots from both sources. In their study, a fine sympathetic root or rootlets was identified in 27 of 30 specimens and all 27 it arose directly from the carotid sympathetic plexus. In 5 of the 27, there was a second root from the plexus that surrounds the ophthalmic artery [14]. In our study, all sympathetic roots originated from the carotid sympathetic plexus.

A dissection of the lateral aspect of the orbit demonstrates the orbital lobe of the lacrimal gland and its nerve. The lateral rectus muscle and the sixth nerve are retracted to demonstrate the CG and the short ciliary nerves. The mean distance between the CG and lateral rectus muscle was 10.4 mm and this measurement showed that the ganglion was closer to the optic nerve than to the lateral rectus muscle. The CG contains not only the synapses of the parasympathetic fibres to the iris and ciliary body from the third cranial nerve, but also the efferent (and non-synapsing) sympathetic fibres to the ocular blood vessels. Afferent sensory fibres from the cornea, iris and ciliary body pass through the ganglion to the nasociliary branch of the ophthalmic nerve [4].

The parasympathetic pupillary constrictor fibres originate from the Edinger-Westphal nucleus. The fibres exit the midbrain in the oculomotor nerve, spreading out in the cavernous sinus, and follow the inferior division of the nerve in the superior orbital fissure. The fibres enter the nerve to the inferior oblique muscle, travelling adjacent to the lateral border of the inferior rectus muscle, and synapse in the CG. The fibres leave the ganglion as the short ciliary nerves, penetrating the sclera near the optic nerve to arrive at their end organ destinations, the iris and ciliary body [4,15]. 93 – 97 % of these parasympathetic fibres go on to supply the ciliary body resulting in the stimulation of accommodation. The remaining 3 – 7 % innervate the pupillary sphincter allowing constriction of the pupil in response to light [16,17].

Lesions to the parasympathetic fibres in the nerve to the inferior oblique muscle, CG, or short ciliary nerves could account for this isolated unilateral mydriasis; however, one would expect an oval asymmetric dilation if the lesion was at the level of some of the ciliary nerves. Mydriasis after operative repair of orbital floor fracture has been attributed to manipulation of the inferior oblique muscle. The posterior location of the fractures suggests that surgical manipulation of or near the ciliary ganglion may account for these phenomena. Patients should be warned before posterior orbital floor repair about possible mydriatic or tonic pupils as a complication [18].

Lateral microorbitotomy provides excellent exposure of the superior, lateral and inferior intraconal compartments. The majority of orbital tumours, however, can be removed using this cosmetically acceptable approach. It is possible to obtain safe, adequate exposure of masses superior, lateral and inferior to the optic nerve through a 35-mm skin incision or using a coronal scalp flap. Although this approach is simple and not associated with the potential complications of an intracranial operation, it carries some risks for intraorbital structures. The lateral rectus muscle must be retracted superiorly or inferiorly during this approach to visualize the lateral part of the orbit. Following retraction of the lateral rectus muscle, there are no structures blocking access to the CG, two-thirds of the anterior optic nerve and the lateral surface of the globe [11,12]. There is a risk of damage to the intraorbital connective tissue which contains CG and ciliary nerves during this approach.

Gonul et al. advocated a transmaxillary approach to the orbit in cases of inferomedial posterior intraconal and inferolateral lesions. Although this provides an extradural approach and seems safe, it carries some risks for the CG, especially the lateral route of approach. Neural structures, especially the motor route of the CG often escape notice within the orbital fat and are easily damaged during surgery [19].

Following injury to the ciliary ganglion or the short ciliary nerves, observations may include: light near dissociation (LND); tonicity of both the pupillary light reaction and accommodation; segmental palsy of the iris sphincter; and denervation hypersensitivity to the dilute cholinergic agents [15]. In the eight to 12 weeks following injury to the CG, surviving ganglion cells sprout collaterals to re-innervate both the ciliary body and the pupil. This re-innervation results in a pupil that constricts more to near stimulation than to light. This is LND. The tonic pupil also dilates poorly due to inappropriate tone secondary to aberrant re-innervation. Segmental palsy results from the fact that the sphincter is made up of 70 to 80 separate motor units, each served by a separate parasympathetic nerve fibre. Unlike LND, which takes weeks to months to develop, hypersensitivity can be observed within days to weeks [16,17].

Four cases of mydriasis after repair of the orbital floor were reported by Hornblass [20] and cases were also reported by Stillwater and Levine [21]. All involved fractures of the posterior orbital floor. Stromberg and Knibbe [22] did not mention the location of the fracture in their case. Additionally, two cases were reported by Bodker and associates [18]. Arai et al. reported one patient in whom a tonic pupil developed postoperatively, with a cavernous angioma located on the deep lateral side of the optic nerve, which was resected through the inferior route. It was thought that either short ciliary nerves or the ciliary ganglion was damaged during surgery [6].

Presumably, intraoperative manipulation of the nerve to the inferior oblique muscle, inferior rectus muscle, CG, or short ciliary nerves, causing stretching, contusion, edema or hematoma formation to the parasympathetic fibres with subsequent transient conduction block, would account for the mydriatic pupil [18].

In conclusion; the CG and its nerve roots often escape notice within the orbital fat and are easily damaged during surgery. A detailed knowledge of the microanatomy of the CG is very important and greatly facilitates the preservation of this fine structure. Physicians should warn their patients of these complications when they repair posterior orbital floor fractures or perform a lateral microorbitotomy for intraorbital lesions.

References

[1] Gray H. Anatomy: Descriptive and Surgical. London: Parragon, 1994: p 500
[2] Sinnreich Z, Nathan H. The ciliary ganglion in man (anatomical observations). Anat Anz Jena 1981; 150: 287 – 297
[3] Morard M, Tcherekayev V, Tribolet N. The superior orbital fissure: A microanatomical study. Neurosurgery 1994; 35: 1087 – 1093
[4] Duke-Elder ST. System of Ophthalmology, Vols 2 and 12. London: H. Kimpton, 1971: p 662
[5] Walsh FB, Hoyt WF. Clinical Neuro-Ophthalmology. 3rd edn, Vol. 4. Baltimore: The Williams & Wilkins Company, 1969: p 496
[6] Arai H, Sato K, Katsuta T, Rhoton AL. Lateral approach to intraorbital lesions. Anatomic and surgical considerations. Neurosurgery 1996; 39: 1157 – 1163
[7] Demiroğlu U, Esen AN, Arvas S. Anatomy of the orbit and clinical importance in traumas. Turk J Med Biol Res 1990; 1: 170 – 178
[8] Kuchiiwa S, Kuchiiwa T, Suzuki T. Comparative anatomy of the accessory ciliary ganglion in mammals. Anat Embryol 1989; 180: 99 – 205
[9] Sacks JG. Peripheral innervation of extraocular muscles. Am J Ophthalmol 1983; 95: 520 – 527
[10] Johnston JA, Parkinson D. Intracranial sympathetic pathways associated with the sixth cranial nerve. J Neurosurg 1974; 39: 236 – 243
[11] Gonul E, Timurkaynak E. Lateral approach to the orbit: An anatomical study. Neurosurg Rev 1998; 21: 111 – 116
[12] Gonul E, Timurkaynak E. Inferolateral microsurgical approach to the orbit: An anatomical study. Minim Invas Neurosurg 1999; 42: 137 – 141
[13] Natori Y, Rhoton AL. Transcranial approach to the orbit: Microsurgical anatomy. J Neurosurg 1994; 81: 78 – 86
[14] Natori Y, Rhoton AL. Microsurgical anatomy of the superior orbital fissure. Neurosurgery 1995; 36: 762 – 775
[15] Gurwood A, Lehn L. Tonic pupils. Optometry today 1999; 39: 37 – 39
[16] Slamovits TL, Glaser JS. The pupils and accommodation. In: Glaser JS (Ed). Neuro-Ophthalmology. Philadelphia: JB Lippincott, 1990
[17] Slamovits TL, Glaser JS. The pupils and accommodation. In: Tasman W, Jaeger EA (Eds). Duane's Clinical Ophthalmology CD ROM. Philadelphia: JB Lippincott, 1998
[18] Bodker FS, Cytryn AS, Putterman AM, Marschall MA. Postoperative mydriasis after repair of orbital floor fracture. Am J Ophthalmol 1993; 115: 372 – 375
[19] Gonul E, Erdogan E, Duz B, Timurkaynak E. Transmaxillary approach to the orbit: An anatomic study. Neurosurgery 2003; 53: 935 – 942
[20] Hornblass A. Pupillary dilatation in fractures of the floor of the orbit. Ophthalmic Surg 1979; 10: 44 – 46
[21] Stillwater LB, Levine PA. Anisocoria with orbital floor fractures. Worry and wait. Otolaryngol Head Neck Surg 1981; 89: 882 – 888
[22] Stromberg BV, Knibbe M. Anisocoria following reduction of bilateral orbital floor fractures. Ann Plast Surg 1988; 21: 486

A. Pavez[1,2]
C. Salazar[1]
R. Rivera[1,2]
J. Contreras[1]
A. Orellana[1]
C. Guzman[2]
O. Iribarren[2]
H. Hernandez[2]
J. Elzo[2]
D. Moraga[2]

Description of Endoscopic Ventricular Anatomy in Myelomeningocele

Abstract

Objective: The purpose of this work is to present our endoscopic neuroanatomical findings of a series of myelomeningocele and hydrocephalus patients, treated with endoscopic third ventricular cisternostomy (ETVC), in order to describe ventricular configuration abnormalities in this group of patients, in which this neurosurgical procedure has limited performance. **Method:** We checked the videos of 10 endoscopic third ventricular cisternostomies of myelomeningocele patients taken during 24 months as from December 1998. A previous guideline is designed to record anatomic variables in the lateral ventricles, IIIrd ventricle, and basal cisterns. The topic is analyzed in view of the necropsy and imaging background data. **Results:** The ETVC of lateral ventricles showed: absence of septum (9/10); absence of anteroseptal vein (8/10); absence of choroid plexus and thalamostriate vein (0/10); absence of fornix (1/10): small foramen of Monro (4/10). The ETVC of the IIIrd ventricle showed: impossibility of recognizing any mammillary bodies (4/10); presence of septations (5/10); presence of atypical veins in the floor (6/10); translucent floor (5/10); floor umbilications (5/10); absence of infundibulum (4/10); arachnoid adherences (7/10); and visual contact of basilar artery (4/10). **Conclusion:** There are categorical structural alterations in the ventricular system of myelomeningocele patients that are well correlated with previous necropsy and imaging reports. The ventricular system of dysraphic children presents severe anatomic alterations, which alter the reference points of the classical endoscopic third ventricular cisternostomy.

Key words

Myelomeningocele · neuroendoscopy · hydrocephalus · neuroanatomy

Introduction

After several conceptual and technological stages that started in the early years of the 20th century, endoscopic third ventricular cisternostomy (ETVC) is nowadays the best treatment for obstructive hydrocephalus [1–8]. Nevertheless, the value of this tool may be questioned in the case of spinal dysraphia-associated hydrocephalus, even though this condition has mainly an obstructive basis [2].

The selection of children who may benefit of ETVC, may be difficult because of the several factors which contribute to the etiology of hydrocephalus in myelomeningocele patients.

On the other hand, there are no formal reports on any specific endoscopic description regarding ventricular configuration alterations in this group of patients. There is no doubt that performing a standardized procedure of ETVC with its classical benchmarks with patients that may have substantial structural brain variations is more than enough to put its success at risk.

The purpose of this work is to present our endoscopic neuroanatomic findings of a series of myelomeningocele and hydrocepha-

Affiliation
[1] Servicio de Neurocirugia del Hospital Van Buren Hospital, Universidad de Valparaiso, Valparaiso, Chile
[2] Departamento de Neurociencias, Escuela de Medicina, Universidad Católica del Norte, Coquimbo, Chile

Correspondence
Dr. Alonso Pavez · Servicio de Neurocirugia · Departamento de Neurociencias · Escuela de Medicina · Universidad Católica del Norte · Larrondo 1281 · Coquimbo · Chile · Tel.: +56/51/224/998, +56/51/209/825 · Fax: +56/51/217/364 · E-mail: apavez@ucn.cl

Bibliography
Minim Invas Neurosurg 2006; 49: 161–167 © Georg Thieme Verlag KG Stuttgart · New York
DOI 10.1055/s-2006-932193
ISSN 0946-7211

lus patients, treated with ETVC, in order to describe ventricular configuration alterations in this group of patients. We hope that this report may be a starting point to improve the success of the neurosurgical ETVC procedure in this type of patients and also be a first step to study this matter in more depth.

Material and Methods

We designed our neuroanatomic descriptive study to collect data of high relevance. Anatomic structures were classified as present or absent. The size evaluations were performed based on the instrument used in the procedure (4.7-mm outer diameter), exposing each case to the independent evaluation of two observers. The variables studied were as follows:

Lateral ventricles
- Absence of septum pellucidum
- Absence of anteroseptal vein
- Absence of thalamostriate vein
- Absence of choroids plexus
- Absence of fornix
- Comparative size of foramen of Monro

Third ventricle
- Identification of mammillary bodies
- Presence of intraventricular septations
- Presence of atypical vessels
- Translucence of ventricular floor
- Alterations of ventricular floor
- Presence of infundibulum
- Arachnoids adherences
- Visual contact with basilar artery

Ten ETVC videos taken between December 1998 and December 2002 in dorsolumbar myelomeningocele patients were analyzed. The technical style of our center has already been described [7].

Results

The neuroanatomic findings of a series of ETVC myelomeningocele and hydrocephalus patients showed that the lateral ventricle presents substantial anatomic alterations, with the absence of septum being the most relevant of them, found in 9 out of 10 cases (Table **1**).

Table **1** Summary of lateral ventricle findings

Absence of septum	9/10
Absence of anteroseptal vein	8/10
Absence of thalamostriate vein	0/10
Absence of choroids plexus	0/10
Absence of fornix	1/10
Size of foramen of Monro: small	4/10
Symmetry of foramen of Monro	9/9

The neuroanatomic malformation in this type of patients gives a unique opportunity to visualize through the ETVC the entire ventricular cavity, including both thalami, foramen of Monro and choroids plexus in the early stages of the procedure (Fig. **1a**). The absence of the anteroseptal vein in 8 out of 10 patients that may probably be associated to the absence of septum is a very important fact because it is a classical point of reference in the execution of the procedure. On the contrary, the structure of choroid plexus was present in all the cases, sometimes with an absolutely sagittal position and very close to the counter lateral plexus, showing a parallel disposition in those cases, and far away from the common convergent modality of the normal brain (Fig. **1b**). The thalamostriate vein followed the choroid plexus very closely in a similar manner. The choroid plexus is an anatomic element that allows the immediate three-dimensional orientation and navigation to the IIIrd ventricle (Fig. **1c**). In the 9 cases where the septum was absent, both foramina of Monro were observed, presenting symmetrical diameters (Fig. **1d**). This is interesting because in two cases (probably due to the angular or spatial arrangement of foramina of Monro and the position of the instrument), it was easier to continue with the endoscopy through the counter-lateral foramen of Monro, without further incidents or difficulties.

The neuroanatomical ETVC findings in the third ventricle showed also substantial differences from the normal parameters (Table **2**).

Table **2** IIIrd ventricle findings

Unrecognizable mammillary bodies	4/10
Presence of septations	5/10
Presence of abnormal veins	6/10
Translucent floor	5/10
Floor umbilications	5/10
Absence of infundibulum	4/10
Arachnoidal adherences	7/10
Visual contact with basilar artery	4/10

The first aspect that stands out is the opalescence of the ventricular floor in 5 cases (Figs. **2a I** and **2a II**) with the subsequent impossibility to recognize the underlying cistern or dorsum sellae. This atypical aspect is associated to intraventricular septations in 5 patients (Fig. **2b**). In a crosswise direction and similar in colour to the thalamic wall, their presence increased the difficulty of recognizing the mammillary bodies, which were completely unrecognizable in 4 cases (Fig. **2a I**). Following a crosswise path, six patients presented a vein-like blood vessel located deep in the ventricular floor, behind the infundibulum, when recognizable. On the contrary, the fenestration was done behind this vein, falling in the interpeduncular cistern, without further incidents. Finally, it is important to mention that the presence of floor umbilications was seen in 5 cases, and all of them were located in the mean line. This anomaly of the ventricular floor did not represent a major difficulty to choose the location of the stoma, regardless of its coexistence with other floor alterations.

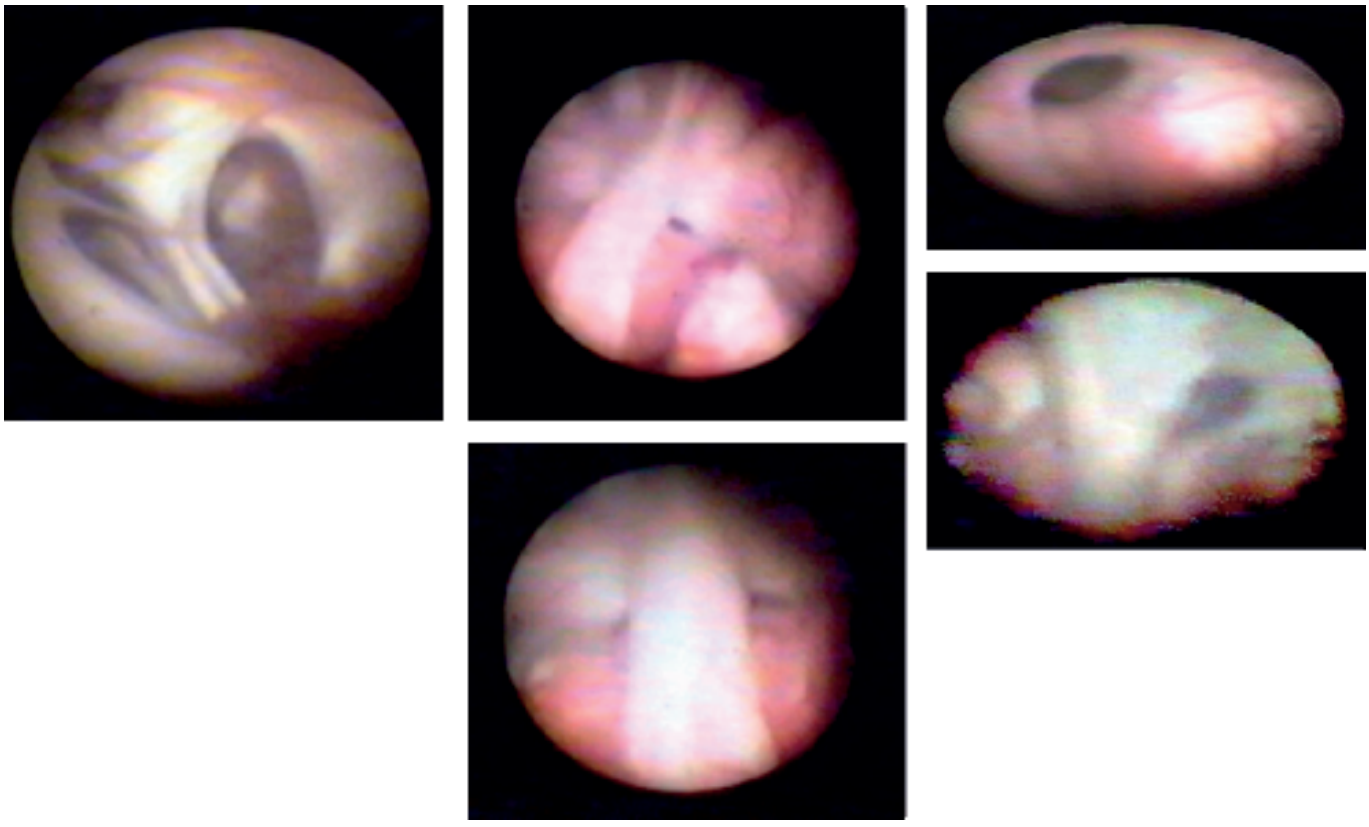

Fig. **1** **a** Unique ventricular cavity, showing larges foramen of Monro, thalamus, both fornix, and the cavity of the third ventricle. **b I** View of both fornix in absence of septum pellucidum. Note the absence of the anteroseptal vein. **b II** View of the parallel disposition of the choroid plexuses. **c** The choroid plexus of the right lateral ventricle in direction to the foramen of Monro and the third ventricle. It remain as a benchmark in the execution of the procedure. **d** The symmetry of foramina Monro allow to choose, in this instance of the prodedure, the easier way to continue the procedure.

After the fenestration, 7 cases showed an arachnoidal band adhering to the ventricular floor that had to be fenestrated (Fig. **2c**), a simple operation in 5 of the 7 patients, in order to have visual contact with the basilar artery, which was feasible in 4 cases only.

In accord with all other reports, it is important to clarify that a bidirectional flow of cerebral spinal fluid was documented in all 10 cases.

Discussion

Hydrocephalus associated with myelomeningocele could be the result of several factors that in one way or another may be implied in the development of dysraphia. These factors may have an obstructive or communicating pattern (Arnold-Chiari malformation, maturing state of the arachnoidal hairiness, aqueduct stenosis, neural tissue infections), whose final balance is the nature of hydrocephalus, and thus the opportunity of performing an ETVC [2]. The results have been discouraging according to several authors [1, 3, 4, 6]. After checking 69 patients, Teo and Jones [2] established the clinical and radiological selection criteria with performance rates above 70 – 80 %.

Now, the neural tube defects and the associated neuroaxial malformations have been subject to anatomical analysis under the aspects of different disciplines related to the specialty [5, 9 – 11]. Therefore, it seems proper to address the discussion in the search for existing congruencies, in terms that offer a more solid base for debate by eliminating much of the subjectivity of looking through the endoscope.

Pathological correlation

Ventricular malformations are frequently described in autopsy series (50 – 90 %), the main ones being ostenosis, deformations and atresia of the IIIrd and IVth ventricles deformations, and Sylvian aqueduct abnormalities.

Gilbert et al. [5] reported the complete or nearly complete thalamic fusion with different degrees of neuronal hypoplasia, which is consistent with Walker's [12] considerations, stating that ventricular floor malformations are related to abnormal degrees of hypothalamus fusion. Nevertheless, no postoperative hypothalamic dysfunctions were observed for us in any of the fenestrated cases with severe floor alterations. For this reason, it is more likely that the anomalies described in this article were intraventricular septations (or floor thickening, arachnoidal adherences or "second membranes", as they are called by other authors). These anomalies could arise from atypical vessels during embryonic development resulting in aberration of heterotopic diencephalons, and are probably not related to iatrogenic effects. As a matter of fact, Kawamura et al. [13] has recently reported an abnormally elevated position of the hypothalamus with normal function.

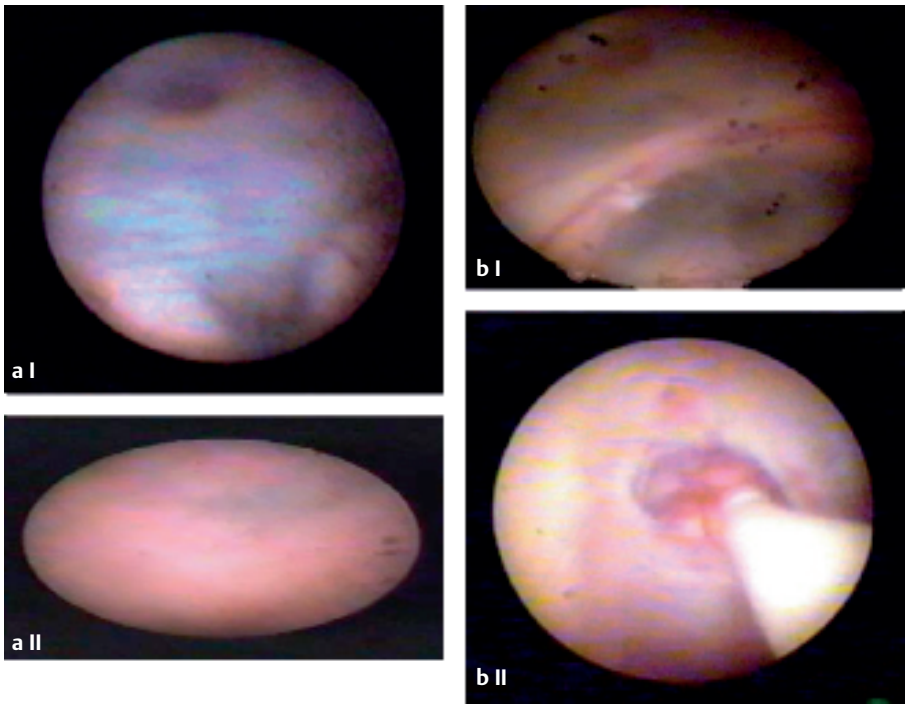

Fig. **2** **a I** Partial translucent floor of the third ventricle. **a II** Total opalescence of the ventricular floor. Note how difficult is the recognition of the mammillary bodies. **b I** View of a septation in the floor of the third ventricle. **b II** Fenestration and ballooning of the floor behind the septation (on the left side of the picture). No hypothalamic alteration were observed in our study.

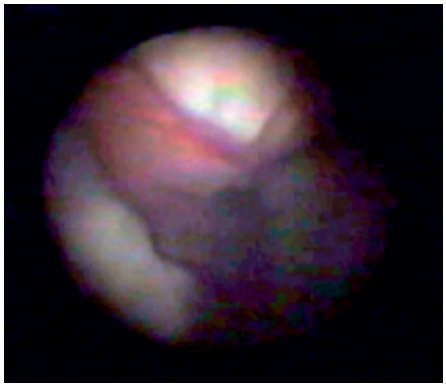

Fig. **3** The enlarged atrium offered the view of choroids plexus "climing up" from the temporal horn.

We did not include the presence of mean line floor umbilications in the set of variables studied because the reports by Morota et al. describe a "red spot" in an adult case instead of the tuber and infundibulum, interpreted as the glandular vestige of the hypophysis.

More than a dysplastic element, the absence of a septum pellucidum has been interpreted as the consequence of a prolonged ventricular hypertension during intrauterine development. Nevertheless, there is evidence of corpus callosum agenesis in a considerable group of patients with seal defects associated to an actual absence of the girus cingularis [9]. This agrees completely with recent reports about the MRI evaluation of cerebral alterations described below.

Sonographic correlation

The partial or total absence of a septum pellucidum, as well as the presence of cavum septi, is described in patients with MMC associated hydrocephalus [9,10], even when the latter has no direct relation with the Arnold-Chiari malformation.

The architecture of the lateral ventricles can present several alterations, the most relevant of which are morphological modifications of the frontal horns [10] and the asymmetrical anterior-posterior growth with frank atrio-occipital predominance, which may be observed in congenital hydrocephalus with another etiology. Since ETVC is a procedure that, in addition to other advantages, seeks to reduce the anesthesia times, it is difficult to clearly establish the endoscopic confirmation of these findings. However, there were two specific cases in which the posterior cavity could be explored, observing a large space, with an extremely enlarged atrium that clearly exposed the choroid plexus climbing from the temporal horn (Fig. **3**).

A moderate IIIrd ventricle dilatation is described in a major group of patients, reaching exceptionally severe ballooning [9,14]. The presence of a medial mass in the Arnold-Chiari malformation is cited as a rare finding in ultrasonographic exploration. Whenever it is present, it is near the foramen of Monro, and occasionally it can cause the obstruction of the foramen with the development of ipsilateral ventriculomegaly. In this respect, it is important to say that none of the cases in this series presented any characteristic structure.

Some of the findings described in ultrasonographic reports are ventricle hernias to parasellar or quadrigeminal cisterns, and the enlargement of the suprapineal recess. We did not find similar conditions. Nevertheless, it is interesting to refer to the aspect of the ventricular floor. There is documentation showing an empty sellae and ventricular floor hernia to the prepontine cistern in adults with hydrocephalus [15]. In the light of the topometric work of Lang et al. [8], this situation presumes the doubling or tripling of the fenestration target zone, varying between 4 and 9 mm in normal brains (from the posterior infundibulum margin to the anterior mammillary process margin). Such a situation would be easily recognized during the endoscopic proce-

dure, even in the presence of dysplastic floors. Therefore, it is reasonable to think that the embryological alterations in our patients could have an influence on the absence of this hernia pattern, as its exposure to a ventricular hypertension could also date from long before.

Tomographic correlation

The findings of cerebral alterations in the CT scans of patients examined for myelomeningocele reach more than 90%. Ventricular malformations are by far the most frequent.

The first aspect is the descending location of the IVth ventricle, attaining a substantial meaning in the tomographic diagnosis of Arnold-Chiari malformation [10].

The partial or total absence of the septum pellucidum in lateral ventricles is once again one of the first findings to be described. It is not necessary to insist on its correlation with sonographic, anatomopathological and currently endoscopic reports which, as mentioned before, gives it a first visual connotation that can be easily identified when entering the lateral ventricle cavity with the endoscope.

The axial sections report what Zimmerman called the "vampire bat" configuration is formed by a sum of morphological alterations. In the first place, the described echographic morphology of the "anterior pointing" and the medial biconcavity in the frontal horns are also seen in the CT with incredible accurateness. When the CT scan reports of dysraphic patients were prepared, the technology did not provide yet all the features present today to execute coronary sections and, for this reason, it is not easy to find the correlation of the "inferior pointing" described in the previous section. The second element is the result of the almost constant enlargement of the occipital horns in these patients, adopting a sharp form similar to the frontal horn. Documents support that the presence of these alterations is not related to the growth of the temporal horns stigmatized as a sensible and specific parameter of active hydrocephalus. Moreover, the clinical follow-up of some of these patients shows the tendency of the occipital horns to keep their morphology and size, independent from the valve function or hydrocephalus activity. Another factor to consider is that the topographic value of the patients shows the presence of active hydrocephalus "rounds" the architecture specifically of the frontal horns which, after decompression, recover their original shape. Nevertheless, this modification is not seen in the occipital horns. This suggests that morphological alterations of the lateral ventricles are part of cerebral dysgenesis, and not a consequence of hydrocephalus.

There is less correlation between the variances described for the IIIrd ventricle. The necropsy description refers to moderate dilatation with certain frequency, and ventriculographic findings suggested the coexistence of aqueduct stenosis. However, the topographic correlation lacks strength in this sense.

The description of the prominent medial mass is anecdotal, which seems somewhat reasonable because it was not possible to identify such structures with the endoscope. The thickening of the interthalamic commissure described by the pathologist could correspond to the septations mentioned in the results. These are structures that have a greater diameter than the fenestration (the inflated balloon of a Fogarty 4 gives a diameter of 6 – 7 mm), and should not measure less than 5 mm, and therefore, can be detected by the current CT scan. Whether its absence in the radiological descriptions is due to technological or anatomical reasons is still unknown.

Magnetic resonance (MRI) correlation

A recent report about an MRI evaluation of cerebral abnormalities in patients with neural tube closure defects [13] included the values of 10 patients with myelomeningocele, which establishes an interesting correlation with intellectual evaluations.

The first thing to point out is the 8/10 ratio where the authors describe the presence of cerebral alterations in this group of patients, compared to the 9/10 of this series. Obviously, the imaging report includes alterations of the parenchyma, whereas ours selects cases with active hydrocephalus (a condition present in 7 of the MRI series cases).

The most relevant extraventricular findings are discrete to moderate cerebral hemisphere hypoplasia (3/10), predominantly parietal-occipital polymicrogiria (3/10), and hypoplasia of the cerebral falx with circumvolution interdigitation. Partial corpus callosum agenesis, greatly associated with polymicrogiria, is described in 6 out of 8 patients with cerebral alterations, which correlates with the 9/10 septum-absent described in this study. Seven of the 8 patients with MRI MMC presented hydrocephalus for which shunts were installed without any problems. The sharpened aspect of the frontal horns associated with ventricular dilatation appeared in 4 cases, confirming the descriptions from ultrasonic and tomographic findings.

There is a complete or almost complete IIIrd ventricular fusion in 2 patients, while a hypothalamus elevation is present in 3 of them. The authors point out the absence of autonomic disturbances in these patients, whereby we can only agree that even in the most dysplastic ventricles of our series, fenestration was innocuous and no hypothalamus alteration was seen. Now, it is important to emphasize that the thalamic fusion together with this hypothalamic increase in the resonance is verified, regardless of the low frequency of this series, thus confirming that the septations and ventricle floor abnormalities could be a manifestation of different degrees of dyencephalic dysplasia that associates the two phenomena: the medial fusion of the thalamus and the hypothalamus elevation.

A new anatomic factor included in this review is the enlargement of the basal cistern compartments that was identified in two patients. This observation represents an obvious advantage for endoscopic purposes, and even if it was not part of our original description, on several occasions it was possible to reach the cisterns through the fenestration stoma, showing a beautiful posterior circulation anatomy.

Likewise, the presence of cerebral heterotopy as subependymal nodules in the lateral ventricle walls was identified in one patient. Similar abnormalities were not observed spontaneously with the endoscope. We do not know what results a directed search would have yielded in this respect.

Table **3** Cerebral alterations present in myelomeningocele.

	Pavez et al [this work] n = 10	*Gilbert et al. [5] n = 25*	*Babcock and Han [9] n = 29*	*Zimmerman et al. [10] n = 47*	*Kawamura et al. [13] n = 10*
Ventricular abnormalities	100 %	92 %	96 %	89 %	80 %
Hydrocephalus	100 %		92 %	85 %	70 %
Septal absence	90 %	12 %	55 %	50 %	60 %
III ventricle floor abnormalities	70 %	52 %	5 %	0 %	30 %
Diencephalic fusion	50 %	8 %	17 %	2 %	20 %

The report includes patients with myeloschisis and lumbar lipomas, but we can conclude that in an important subgroup, intellectual evaluation is normal, e. g., in half of the hydrocephalus patients and in half of the corpus callosum agenesis patients.

Final comments

Although this paper does not have the main objective of doing a statistical analysis of the different parameters eventually provided in the different publications covering this topic because – among other reasons – the number of patients included in each study differ widely and because, depending on when the study was performed and the methods used, there are logical differences in sensibility, it is interesting to mention some facts that show a clear tendency of cerebral alterations present in myelomeningocele (Table **3**).

First of all, the ventricular system abnormalities are present in most lumbosacral MMC patients. Gilbert et al. [5] describe 92 % in autopsy exams. Babcock and Han [9] present 96 % in echographic evaluation. Zimmermann et al. [10] record 89 % in tomography, while Kawamura [13] reports an 8/10 rate of ventricular abnormalities in magnetic resonance images. If, in general, 90 % of the patients develop hydrocephalus; it should not be surprising that our series yields 10/10 alterations, as our aim is to solve this condition.

The absence of the septum pellucidum stands out as the first constant correlated figure in anatomical and imaging descriptions. Babcock and Han [9] describe it in 55 % of the ultrasound series; Zimmerman et al. [10] in 50 % with the scanner. Gilbert et al. [5] and Kamamura et al. [13] describe corpus callosum agenesis in 12 % and 6/10 respectively. In addition, the autopsy report details the almost constant presence of thinning of the corpus callosum associated to a severe dilatation of the lateral ventricles. Our series reports only one case with septum presence. Since the development of the corpus callosum is in the anterior-posterior direction – except the rostrum – which is at the end together with splenius – the absence of the septum septations in the endoscopic area of interest (frontal horns), supports the idea of the septum destruction mechanism, as long as the most frequently described agenesis is partial, so the septum should be present at the anterior portion.

The third ventricular abnormalities include atresia, aqueduct malformations, and intermediate mass prominence, also known as the thickening of the gray or interthalamus commissure. Gilbert et al. [5] found 16 % of thalamic fusion, and Kawamura [13] presents 2/10 of the same finding. Babcock and Han [9] refer to intermediate mass prominence in 17 %. As mentioned previously, some endoscopic third ventricle abnormalities can be correlated with those already described, in which case our ratios would tend to become more distant (4 – 6/10). This could be understood if the 3/10 cases of Kawamura et al. [13] were also considered with respect to the hypothalamus elevation which, in our opinion, represents the anatomical scenery together with the thalamus fusion, and our intraventricular septations and floor alterations are nothing more than the endoscopic version of the same.

Some findings described without endoscopic correlation include the colpocephalia (atrioventricular dilatation) and the modification of the frontal horns. The first figures are 62 % of the echographic series of Babcock and Han [9] and 89 % by Zimmermann et al. [10]. Findings in frontal horns appear with 86 % of the echographic series, 50 % in TAC and 4/10 in magnetic resonance. Heterotopies like subependimary focus, not described in the ultrasound or in the TAC, reach 44 % in Gilbert et al.'s [5] series. Kawamura [13] describes this in myeloschisis but not in MMC. It is important to remember that even if these parameters were not part of the original description, the nature of an observation method defines at least part of the resulting morphology. So the technical and two-dimensional character of a magnetic resonance image or TAC allows verification of the details of a frontal horn, or of all the ventricular regions at once. On the contrary, the dynamic and visual profile of endoscopy enables a comparison of the foramen of Monro, an endoscopic anatomical factor not mentioned in any of the series checked.

This variety of the different approaches gives an even more interesting connotation to the task of figuring out the meaning of these alterations.

Conclusion

There are categorical structural alterations in the ventricular system of myelomeningocele patients that are well correlated with previous necropsy and imaging reports. These alterations do not necessarily predict intellectual disturbances or specific neurological conditions. For this reason, it is appropriate to disagree with some authors who maintain that the patients included correspond to a selection with more severe damage, thereby overestimating the frequency of these alterations.

This specific ventricular configuration of dysraphism adds an operative factor of difficulty that should be well known to the neurosurgeon who indicates and executes an ETVC.

Acknowledgements

The authors wish to thank Miss Lorena Troncoso, whose talent for web navigation was a special contribution to this manuscript. We also want to thank the outstanding translation of Miss Angelica Ovando.

References

[1] Hopf N, Grunert P, Fries G, Resch K, Perneczky A. Endoscopic third ventriculostomy: outcome analysis of 100 consecutive procedures. Neurosurgery 1999; 44: 795 – 806
[2] Teo C, Jones R. Management of hydrocephalus by endoscopic third ventriculostomy in patients with myelomeningocele. Pediatr Neurosurg 1996; 25: 57 – 63
[3] Natelson SE. Early third ventriculostomy in myelomeningocele infants: Shunt independence. Child's Brain 1981; 8: 321 – 325
[4] Sayers MP, Kosnik EJ. Percutaneous third ventriculostomy: Experience and technique. Child's Brain 1976; 2: 24 – 30
[5] Gilbert J, Keneth J, Rorke L, Chernoff G, James H. CNS anomalies associated with myelomeningocele, hydrocephalus, and Arnold-Chiari malformations: Reappraisal of posterior neural tube closure defects. Neurosurgery 1986; 18: 559 – 564
[6] Sainte-Rose C. Third ventriculostomy. In: Manwaring KH, Crone KR (eds). Neuroendoscopy. New York: Mary Ann Liebert, 1992; Vol. 1: 47 – 62
[7] Valenzuela S. Neuroendoscopia. Revista Chilena de Neurocirugia 1998; 12: 9 – 14
[8] Lang J. Topographic anatomy of preformed intracranial spaces. Minimally invasive neurosurgery I. Acta Neurochir (TACHAR) 1993; Suppl. 54: 1 – 10, Springer Verlag
[9] Babcock D, Han B. Cranial monographic findings in myelomeningocele. AJR 1981; 136: 563 – 569
[10] Zimmermann RD, Brockbill D, Dennis M, David M. Cranial CT findings in patients with myelomeningocele. AJR 1979; 132: 623 – 629
[11] De La Cruz R, Milan JM, Miracles M, Munoz MJ. Cranial monographic evaluation in children with myelomeningocele. Childs Nerv Syst 1989; 5: 94 – 98
[12] Walker M. Editorial Comment. Pediatr Neurosurg 1996; 25: 63
[13] Kawamura T, Morioka T, Nishio S, Mihara F, Fukui M. Cerebral abnormalities in lumbosacral neural tube closure defect: MR imaging evaluation. Childs Nerv Syst 2001; 17: 405 – 410
[14] Morota N, Watabe T, Inukai T, Hongo K, Nakagawa H. Anatomical variants in the floor of the third ventricle; implications for endoscopic third ventriculostomy. JNNPs 2000; 69: 531 – 534
[15] Salazar C. Tercer Ventriculocisternostomia en el tratamiento de la hidrocefalia en la edad pediatrica. Revista Chilena de Neurocirugia 1999; 14: 35 – 43

The Role of Intraoperative Monitoring of Oculomotor and Trochlear Nuclei – Safe Entry Zone to Tegmental Lesions

H. Ishihara[1]
M. Bjeljac[1]
D. Straumann[2]
Y. Kaku[1]
P. Roth[1]
Y. Yonekawa[1]

Original Article

Abstract

Objective: A safe entry zone to tegmental lesions was identified based on intraoperative electrophysiological findings, the compound muscle action potentials (CMAP) from the extraocular muscles, and anatomic considerations. This entry zone is bordered caudally by the intramesencephalic path of the trochlear, laterally by the spinothalamic tract, and rostrally by the caudal margin of the brachium of the superior colliculus. **Methods:** Four intrinsic midbrain lesions were operated upon via the safe entry zone using the infratentorial paramedian supracerebellar approach. All lesions involved the tegmentum and included an anaplastic astrocytoma, a metastatic brain tumor, a radiation necrosis, and a cavernous angioma. CMAP were bilaterally monitored from the inferior recti (for oculomotor function) and superior oblique (for trochlear nerve function) muscles. **Results:** In three of four cases, CMAP related to the oculomotor nerve were obtained upon stimulation at the cavity wall after removal of the tumor. Stimulation at the surface of the quadrigeminal plate, however, did not cause any CMAP response. Using this monitoring as an indicator, the lesions were totally removed. **Conclusions:** In the surgery of tegmental lesions, CMAP monitoring from extraocular muscles is particularly helpful to prevent damage to crucial neural structures during removal of intrinsic lesions, but less so to select the site of the medullary incision. The approach via the lateral part of the colliculi is considered to be a safe route to approach the tegmental lesions.

Key words

Intraoperative monitoring · oculomotor complex · trochlear nerve

Introduction

Intraoperative monitoring of cranial nerves has become indispensable to preserve cranial nerve functions in skull base surgery [1,2]. This technique has also been applied to the direct surgery of pontine lesions. In combination with precise anatomic exploration, this technique has minimized operative morbidity, especially at the floor of the 4th ventricle [3–6]. The use of intraoperative monitoring during midbrain surgery, however, is still under debate. In this publication, we present our experience of electrophysiological monitoring during midbrain surgery, and describe a safe entry zone to approach dorsal tegmental lesions.

Patients and Methods

Anesthesia and placement of the recording electrodes

General anesthesia was induced with thiopental sodium, and the fast-acting muscle relaxant pancronium bromide was administered for orotrachial intubation. Isoflurane (0.1–1.0 vol%) was used to maintain balanced anesthesia, while patients breathed 30% oxygen and 70% nitrous oxide without further muscle relaxation. The recording platinum needle electrodes were placed percutaneously in the inferior recti and superior oblique muscles on both sides. The reference electrode was placed on the ipsilateral shoulder, and the ground electrode was placed on the sternum.

Affiliation
[1] Department of Neurosurgery, University Hospital of Zurich, Zurich, Switzerland
[2] Department of Neurology, University Hospital of Zurich, Zurich, Switzerland

Correspondence
Hideyuki Ishihara, M. D. · Department of Neurosurgery · Yamaguchi University School of Medicine · 1-1-1 Minamikogushi · Ube · Yamaguchi 755–8505 · Japan · Tel.: +81/836/222295 · Fax: +81/836/222294 · E-mail: sara20021209@yahoo.co.jp

Bibliography
Minim Invas Neurosurg 2006; 49: 168–172 © Georg Thieme Verlag KG Stuttgart · New York
DOI 10.1055/s-2006-944239
ISSN 0946-7211

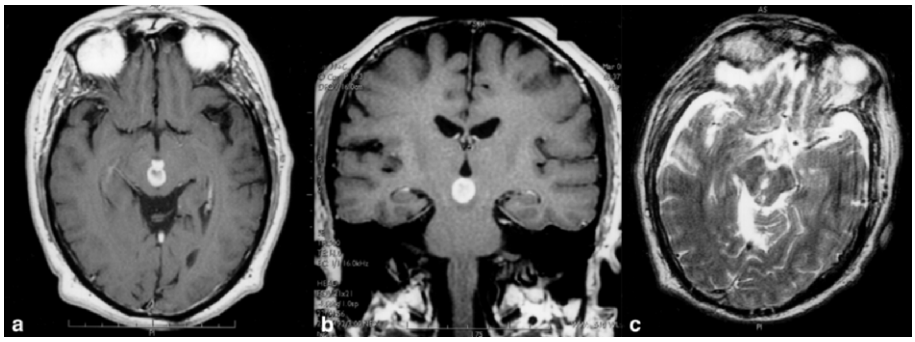

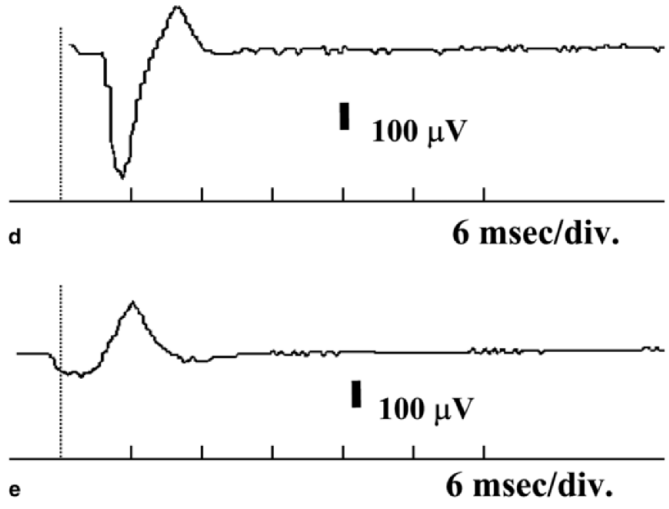

Fig. **1** Case 1: a 31-year-old male. Preoperative axial (**a**) and coronal (**b**) enhanced MRI scans revealing a cystic enhanced mass 12 mm in diameter in the tegmentum. Postoperative axial T_2-weighted image (**c**) showing the surgical corridor. CMAP was obtained from the right inferior rectus muscle (**d**) when the right rostral border of the tumor was stimulated with 0.30 mA intensity. CMAP from the left superior oblique muscles (**e**) was elicited by stimulation with 0.45 mA intensity on the right caudal border of the tumor.

Electrical stimulation and recording

A monopolar stimulation electrode (bare tip) was used to elicit responses at the brainstem. Electrical stimulation was at constant current with rectangular pulses of 0.2 msec duration and a repetition rate of 3 Hz. The intensity of the stimulus varied from 0.15 up to 0.5 mA. The apparatus for both electrical stimulation and analysis of CMAP was a Nerve Integrity Monitor type 2 (NIM-2, manufactured by XOMED, Florida, USA). Initial electrical stimulations were performed at the surface of the tectal plate. During surgical removal of the lesions, especially during manipulation at the boundaries between tumor and neural tissue, electrical stimulations were repeated.

Illustrative cases

Case 1: A 51-year-old man presented with a 5-month history of a progressive oculomotor paresis on the right side including an anisocoria (wider pupil on the right side) and intermittent headache. Neurological examination at admission revealed, in addition to the right-sided external and internal oculomotor palsy, bradydiadochokinesis of the left hand. MRI showed a cystic gadolinium-enhanced mass lesion (diameter: 12 mm) in the tegmentum of the midbrain (Fig. **1a** and **b**). The operation was performed through a right paramedian infratentorial supracerebellar approach. A 4 mm longitudinal medullary incision was made 5 mm laterally from midline in the recess between superior and inferior colliculus, after confirming that no CMAP could be elicited by surface stimulation. The capsule of the tumor was recognized 3 mm below the surface. Xanthochromic liquid was aspirated and solid material was removed. During the removal of the mass, electrical stimulation was repeatedly applied at the cavity wall, since the border between tumorous and normal tissue was not distinct. When the neural tissue adjacent to the right rostral border of the tumor was stimulated with 0.30 mA intensity, CMAP was recorded from the right inferior rectus muscle (Fig. **1d**). Similarly, CMAP was recorded from the left inferior rectus muscle by the stimulation of neural tissue at the left rostral border of the tumor (Fig. **1e**). Then, the lower portion of the tumor was removed. Its caudal border was detected by eliciting CMAP from the superior oblique muscles on both sides. Finally, the tumor was completely removed by avoiding areas where CMAP could be evoked (Fig. **1c**). The pathological diagnosis was adenocarcinoma. Postoperatively, the patient developed transient tetraparesis, which was completely reversible within 4 weeks, but required a ventriculo-peritoneal shunt. The right-sided ptosis had improved, but there was an additional slight internal oculomotor palsy on the left side. Further radiological examination failed to detect the primary lesion. The patient went back home 7 weeks after the operation.

Case 2: A 7-year-old boy developed sudden headache, right ptosis and left hemiparesis, and was admitted our hospital. He had already been operated on twice for a right thalamic hemorrhage in 1991 and a midbrain hemorrhage in 1993. Both times the diagnosis was cavernous angioma. After the second operation, the patient had recovered well, and only a slight right oculomotor palsy and left upper limb dominant hemiparesis (Weber's syndrome) had remained. A neurological examination at admission revealed an increase of the known right-sided oculomotor palsy. Consciousness was not affected. MRI showed two hemorrhagic lesions, one in the right tegmentum of midbrain with low inten-

sity rim in T_1- and T_2-weighted images (diameter: 16 mm), the other in left frontal lobe (Fig. **2a** and **b**). Following removal of the left frontal lobe lesion, the right dorsal part of the midbrain was exposed through a paramedian, infratentorial-supracerebellar approach. First, electrical stimulations were applied to the surface of the quadrigeminal plate, but no CMAPs were recorded. A 4 mm longitudinal medullary incision was made 5 mm laterally from midline in the recess between superior and inferior colliculus. The capsule of a hematoma was recognized 1 mm below the surface. The small vessels in the medial wall of the hematoma were not removed although no CMAP was recorded with electrical stimulation in this part. The hematoma was totally removed (Fig. **2c**). Stimulation of the wall of the hematoma did not elicit CMAP in the recorded eye muscles. The pathological diagnosis of both lesions was cavernous angioma. Postoperatively, the right oculomotor palsy was slightly improved. The patient was discharged from the hospital 10 days after the operation.

Discussion

Intraoperative electrophysiological monitoring of the ocular motor neurons in the midbrain (nuclei and axons of the IIIrd and IVth nerves) was successfully performed in four patients who underwent surgery for midbrain lesions. Stimulation using a monopolar electrode with a current intensity up to 0.5 mA was safely carried out, and proved to be helpful in avoiding postoperative morbidity. CMAP from extraocular muscles could be obtained on the stimulation of the cavity wall after the removal of the lesion, except in case 2 where the wall probably consisted of small vessels. Stimulation from the surface of the quadrigeminal plate, the posterior commissure and the floor of the posterior third ventricle did not elicit any eye muscle response. Our results indicate that the role of electrophysiological monitoring in surgery for midbrain lesions is slightly different from that for pontine lesions. In the context of surgery on midbrain lesions, CMAP does not play a role in identifying the medullary incision, but is useful for the removal of the tumor. The safe entry zone, however, has to be identified based on the precise anatomic considerations and preoperative evaluation of the tumor's location.

Anatomic considerations for safe entry zone

The midbrain is the shortest segment of the brainstem; its longitudinal dimension is less than 2 cm. Like in other parts of the brainstem, important neural structures are densely contained. The dorsal surface of the midbrain consists of the four colliculi situated caudally to the posterior commissure and rostrally to the superior medullary velum. The brachium of the inferior colliculus ascends to reach the medial geniculate body. The brachium of superior colliculus runs underneath the brachium of inferior colliculus to the lateral geniculate body. The dorsal part, the tectum, and central part, the tegmentum, contain important relay nuclei of the auditory and the ocular motor systems. The trochlear and oculomotor nuclei lie in the dorsomedial part of the tegmentum. When tegmental lesions are surgically approached from the dorsal surface of the midbrain, these important structures should be given thorough consideration.

Caudal midbrain: The inferior colliculi receive input from every nuclear group within the auditory brain stem. They are the secondary relay structures of the ascending auditory system, and are densely connected with each other by the commissure of the inferior colliculus. The auditory nuclei, including cochlear nuclei, superior olivary complex and nuclei of the lateral lemniscus, have bilateral ascending projections. This might be the reason why Bognar et al. and Kaku et al. could resect the inferior colliculus on one side without adverse effects on hearing [7, 8].

The trochlear nuclei lie in the ventral region of the central gray matter, just below the rostral part of the inferior colliculus. The respective fibers descend dorsolaterally around the central gray matter at the level of the caudal part of the inferior colliculus, and reach the superior medullary velum, where they decussate to emerge at the lateral side of the frenulum veli [9]. Therefore, a unilateral lesion in the area of the caudal part of the inferior colliculus produces a contralateral trochlear nerve palsy. In case 1, electric stimulation of the caudal cavity wall in this area elicited CMAP of the superior oblique muscle, which was probably due to the activation of intrinsic trochlear nerve fibers. When the inferior colliculus is chosen for an approach to a tegmental lesion, one should restrict possible damage to the lateral and rostral parts of inferior colliculus to spare the commissure of the inferior colliculus and the trochlear nerve fibers.

Rostral midbrain: The superior colliculus (SC) is an important structure in the control of visual fixation and the generation of saccadic eye movements. This is reflected in the anatomic connections to other structures with oculomotor functions. The deeper layers of the SC project mainly to premotor structures of the ocular motor system, such as the paramedian pontine reticular formation (PPRF) and the rostral interstitial nucleus of the medial longitudinal fasciculus (riMLF). By superficial electrical stimulation, however, no eye movements can be evoked [10], because the superficial layers of SC connect to the visual system by

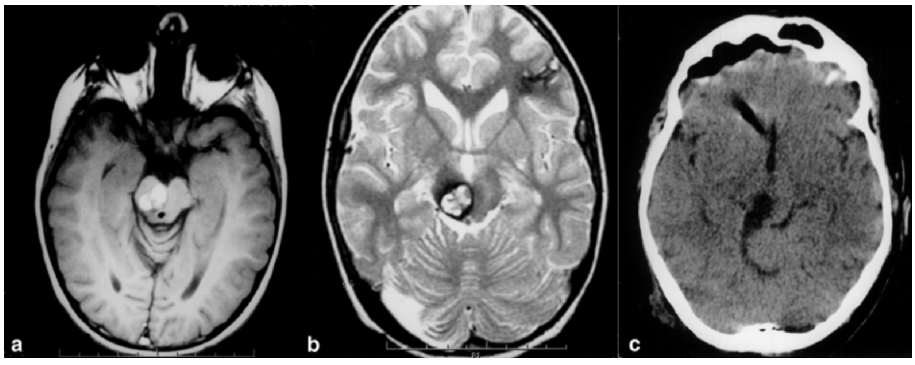

Fig. **2** Case 2: a 7-year-old boy. Preoperative axial T_1-weighted image (**a**) and T_2-weighted image (**b**), revealing hematomas with low intensity rim in the right tegmentum and left frontal lobe. Postoperative CT (**c**) showing the surgical corridor.

projection to the thalamus and the lateral geniculate nuclei. This lack of ocular motor responses is in agreement with our findings. More recent studies have revealed that the superior colliculus fixation neurons which are located in the rostral pole of the SC control saccades by suppressing or activating omnipause neurons which are located in the nucleus raphe interpositous [11,12].

The rostral interstitial nucleus of the MLF (riMLF) and the accessory oculomotor nuclei are closely connected with the oculomotor complex. The accessory oculomotor nuclei comprise the interstitial nucleus of Cajal (INC), the nucleus of Darkschewitsch and the nuclei of the posterior commissure. The INC is situated ventrolaterally to the MLF at the mesodiencephalic junction, and plays an important role in the integration of eye-velocity signals into eye-position signals and in eye-head coordination [13,14]. The riMLF lies adjacent to the rostral border of the INC and is wing-shaped. This nucleus contains neurons with vertical (upward, downward) and torsional (ipsitorsional) eye movement on-directions. In the monkey, unilateral lesions are characterized by a loss of all rapid eye movements with an ipsitorsional component, and downward movements are slowed. In bilateral lesions all vertical and torsional rapid eye movements are abolished [15]. Similar deficits can be seen after a lesion of the INC [16]. This anatomic location of these crucial structures related to vertical eye movements suggests that dorsal tegmental lesions should not be approached from the rostral part of the SC, but rather from the caudal and lateral parts.

Safe entry zone for tegmental lesion: In order to minimize the postoperative morbidity, we identified a safe entry zone from the dorsolateral mesencephalon on the basis of our electrophysiological findings and anatomic considerations. This "inferior brachial triangle" (Fig. **3**) is bordered caudally by the trochlear nerve fibers inside the brainstem, laterally by the spinothalamic tract, and rostrally by the caudal margin of the brachium of the superior colliculus. Although a medullary incision in this triangle compromises unilateral ascending projections from the inferior colliculus, this approach preserves the trochlear tract, the connection between the inferior colliculi on both sides, the superior colliculus, the accessory oculomotor nuclei and the oculomotor complex.

The paramedian infratentorial supracerebellar approach has advantages to access lateral parts of the quadrigeminal plate [17–19], and therefore is a suitable approach for the "inferior brachial triangle".

Midbrain monitoring

Intraoperative monitoring of motor nuclei has been applied and has established its importance in surgery through the rhomboid fossa [6,20]. The facial colliculus is the main target in the mapping of the 4th ventricle floor, because the abducens nuclei and facial nerve tracts lie just beneath. In the midbrain, however, it is difficult to identify the oculomotor complex and the trochlear nuclei from the surface of the midbrain, since they are embedded in the ventral border of the periaqueductal gray matter. Therefore, electrophysiological monitoring in the midbrain should mainly be applied during the removal of lesions rather than to decide on the location of the medullary incision.

There are two reasons why we used lower current for stimulation. One is for the purpose of avoiding neural damage by the electrical stimulation itself. Neuronal damages due to electrical stimulation were shown in animal models. Asanuma and Arnold showed that currents above 0.04 mA (at 0.2 ms duration) and up to 0.08 mA transiently damaged pyramidal tract neurons [21,22]. It is considered that a higher current can damage neural tissue, and also can give false negative results, although the character of the current is surely important.

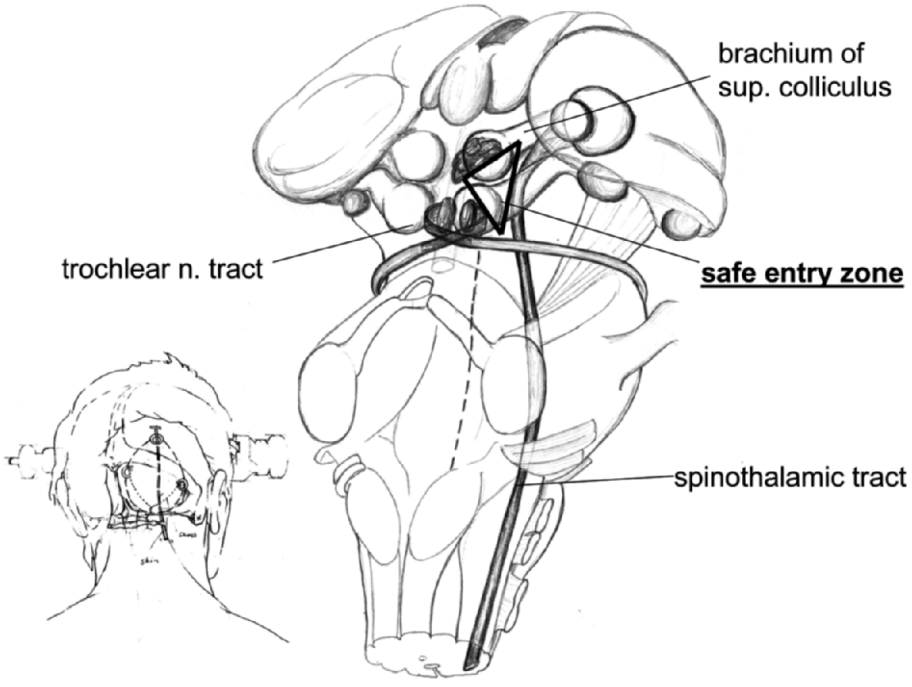

Fig. **3** Schematic drawing of the dorsolateral midbrain anatomy and the safe entry zone.

The other reason is for the purpose of reducing the false positive results of monitoring. At the brainstem, the threshold intensity to obtain the CMAPs required is only 0.05 to 0.20 mA when the stimulation probe is directly applied to motor nuclei or tracts [20,23]. The current-distance estimates of several neurons have been shown in animal models [24,25]. According to these experiments, the relation between the current intensity that evoked an action potential from neurons and the distance from stimulation probe is: current = K (distance)^2 where K is the current-distant constant, and it can range from 0.1 to 4.0 mA/mm^2 depending on the neural elements. The current intensity necessary to activate a neuron 1 mm away from the electrode tip would be 0.1 mA for a low and 4.0 mA for a high threshold neuron. For example, when a 1 mA current is applied to neural tissue, a low threshold neuron more than 3 mm away from the electrode would be activated. We therefore prefer low currents repeatedly for the electrical stimulation in order to reduce false positive results of the monitoring.

Recently, Sekiya et al. reported the usefulness of oculomotor nuclei monitoring to avoid surgical injury to ocular motor functions during midbrain surgery [26]. This study corresponds well with our results. Our aim of ocular motor monitoring in the midbrain, however, is not only to preserve ocular motor function but also to support surgical orientation. The midbrain is tightly packed with many important nuclei and neural tracts, for instance, the central tegmental tract which connects the reticular formation to the cerebral cortex is crucial for consciousness. This tract is located just lateral to the part of the oculomotor nucleus that contains neurons innervating the inferior rectus muscle. To confirm the location of the oculomotor nucleus is hence important to avert surgical damages to other crucial structures.

Conclusion

In conclusion, anatomic considerations and our results indicate that the lateral part of the tectal plate, the “inferior brachial triangle”, is a safer entry zone to tegmental lesions. Furthermore, the intraoperative monitoring of CMAP from extraocular muscles using lower current stimulation is useful to preserve ocular motor function as well as the function of other neural structures.

Acknowledgements

The authors thank Mr. Roland Stillhard and Mr. Andre Roth for the preparation of photographs, and Ms. Rosmarie Frick for her assistance.

References

[1] Moller AR, Jannetta PJ. Preservation of facial function during removal of acoustic neuromas. Use of monopolar constant-voltage stimulation and EMG. J Neurosurg 1984; 61: 757 – 760
[2] Sekhar LN, Moller AR. Operative management of tumors involving the cavernous sinus. J Neurosurg 1986; 64: 879 – 889
[3] Kyoshima K, Kobayashi S, Gibo H, Kuroyanagi T. A study of safe entry zones via the floor of the fourth ventricle for brain-stem lesions. J Neurosurg 1993; 78: 987 – 993
[4] Matsushima T, Rhoton AL, Lenkey C. Microsurgery of the fourth ventricle: Part 1. Microsurgical anatomy. Neurosurgery 1982; 11: 631 – 667
[5] Strauss C, Lutjen-Drecoll E, Fahlbusch R. Pericollicular surgical approaches to the rhomboid fossa. Part I. Anatomical basis. J Neurosurg 1997; 87: 893 – 899
[6] Strauss C, Romstöck J, Nimsky C, Fahlbusch R. Intraoperative identification of motor areas of the rhomboid fossa using direct stimulation. J Neurosurg 1993; 79: 393 – 399
[7] Bognar L, Fischer C, Turjman F, Michel F, Villanyi E, Mottolese C, Guyotat J, Lapras C. Tectal plate gliomas. Part III: Apparent lack of auditory consequences of unilateral inferior collicular lesion due to localized glioma surgery. Acta Neurochir (Wien) 1994; 127: 161 – 165
[8] Kaku Y, Yonekawa Y, Taub E. Transcollicular approach to intrinsic tectal lesions. Neurosurgery 1999; 44: 338 – 344
[9] Mansour AM, Reinecke RD. Central trochlear palsy. Surv Ophtalmol 1986; 30: 279 – 297
[10] McHaffie JG, Stein BE. Eye movements evoked by electrical stimulation in the superior colliculus of rats and hamsters. Brain Res 1982; 247: 243 – 253
[11] Everling S, Pare M, Dorris MC, Munoz DP. Comparison of the discharge characteristics of brain stem omnipause neurons and superior colliculus fixation neurons in monkey: implications for control of fixation and saccade behavior. J Neurophysiol 1998; 79: 511 – 528
[12] Gandhi NJ, Keller EL. Spatial distribution and discharge characteristics of superior colliculus neurons antidromically activated from the omnipause region in monkey. J Neurophysiol 1997; 78: 2221 – 2225
[13] Fukushima K, Kaneko CRS, Fuchs AF. The neuronal substrate of integration in the oculomotor system. Prog Neurobiol 1992; 39: 609 – 639
[14] Kaneko CRS, Fukushima K. Discharge characteristics of vestibular saccade neurons in alert monkeys. J Neurophysiol 1998; 79: 835 – 847
[15] Suzuki Y, Buttner-Ennever JA, Straumann D, Hepp K, Hess BJ, Henn V. Deficits in torsional and vertical rapid eye movements and shift of Listing’s plane after uni- and bilateral lesions of the rostral interstitial nucleus of the medial longitudinal fasciculus. Exp Brain Res 1995; 106: 215 – 232
[16] Helmchen C, Rambold H, Fuhry L, Buttner U. Deficits in vertical and torsional eye movements after uni- and bilateral muscimol inactivation of the interstitial nucleus of Cajal of the alert monkey. Exp Brain Res 1998; 119: 436 – 452
[17] Ogata N, Yonekawa Y. Paramedian supracerebellar approach to the upper brain stem and peduncular lesions. Neurosurgery 1997; 40: 101 – 105
[18] Rhoton AL. Tentrial incisura. Neurosurgery 2000; 47: S131 – 153
[19] Vishteh AG, David CA, Marciano FF, Coscarella E, Spetzler RF. Extreme lateral supracerebellar infratentorial approach to the posterolateral mesencephalon: Technique and clinical experience. Neurosurgery 2000; 46: 384 – 389
[20] Eisner W, Schmid UD, Reulen HJ, Oeckler R, Olteanu-Nerbe V, Gall C, Kothbauer K. The mapping and continuous monitoring of the intrinsic motor nuclei during brain stem surgery. Neurosurgery 1995; 37: 255 – 265
[21] Asanuma H, Arnold AP. Noxious effects of excessive currents used for intracortical microstimulation. Brain Res 1975; 96: 103 – 107
[22] Tehovnik EJ. Electrical stimulation of neural tissue to evoke behavioral responses. J Neurosci Methods 1996; 65: 1 – 17
[23] Silverstein H, Rosenberg S. Intraoperative facial nerve monitoring. Otolaryngol Clin North Am 1991; 24: 709 – 725
[24] Hentall ID, Zorman G, Kansky S, Fields HL. Relations among threshold, spike height, electrode distance, and conduction velocity in electrical stimulation of certain medullospinal neurons. J Neurophysiol 1984; 51: 968 – 977
[25] Stoney SD, Thompson WD, Asanuma H. Excitation of pyramidal tract cells by intracortical microstimulation: Effective extent of stimulating current. J Neurophysiol 1968; 31: 659 – 669
[26] Sekiya T, Hatayama T, Shimamura N, Suzuki S. Intraoperative electrophysiological monitoring of oculomotor nuclei and their intramedullary tracts during midbrain tumor surgery. Neurosurgery 2000; 47: 1170 – 1177

T. Yamamoto
Y. Nakao
K. Mori
M. Maeda

Endoscopic Hematoma Evacuation for Hypertensive Cerebellar Hemorrhage

Abstract

Object: The management of spontaneous cerebral hemorrhage remains controversial, particularly the surgical indications. Endoscopic surgery was evaluated for the treatment of spontaneous cerebellar hemorrhage. **Methods:** The records of 69 patients with hypertensive cerebral hemorrhage were retrospectively reviewed. Patients treated by endoscopic surgery (n = 10) were compared with patients treated by conventional surgical hematoma evacuation (n = 10) under the same surgical indications. **Results:** The surgical procedure time, duration of ventricular drainage, extent of hematoma evacuation, necessity for cerebrospinal fluid (CSF) shunt, surgical complications, and outcome at discharge and at 3 months after onset were compared. The extent of hematoma evacuation was greater in the endoscopic group (95.2%) than in the craniectomy group (90.6%) but without significant difference. The endoscopic technique (64.5 min) took significantly less time than the craniectomy method (230.6 min, $p < 0.0001$). The period of ventricular drainage was significantly shorter in the endoscopic group (2.6 days) compared to the craniectomy group (12.3 days, $p < 0.01$). CSF shunt surgery was required in no patient in the endoscopic group compared to three in the craniectomy group. **Conclusion:** Endoscopic hematoma evacuation is a rapid, effective, and safe technique for the removal of hypertensive cerebellar hemorrhage. Reduction of the mass effect can be accomplished with low risk of recurrent hemorrhage. Release of obstructive hydrocephalus in the early stage may improve the patient's outcome and decrease the requirement for permanent shunt emplacement.

Key words

Cerebellar hemorrhage · endoscope · surgical indication · minimally invasive surgery

Introduction

The surgical indications for hypertensive intracerebral hemorrhage remain controversial, as early surgical treatment within 24 hours did not improve the outcome for patients with spontaneous supratentorial intracerebral hematoma [1]. In contrast, neurosurgical treatment is widely accepted to evacuate cerebellar hematoma of more than 3 cm in diameter causing mass effects in the posterior fossa [2–4]. The surgical indications also consider the need for resolution of hydrocephalus, which may be caused by intraventricular hemorrhage or fourth ventricle compression. Cerebellar hematoma should be evacuated before neurological deterioration occurs [5]. In particular, cerebellar hemorrhage with a mass effect causing compression of the fourth ventricle and the brain stem should be surgically treated, although many of the patients could be considered for conservative medical treatment.

Hypertensive cerebellar hemorrhage can be evacuated through a suboccipital craniectomy, but the surgical indication remains debatable. Recently, stereotactic hematoma aspiration has generally been performed for hypertensive intracerebral and cerebellar hemorrhage. Such burr hole surgery may be better than craniect-

Affiliation
Department of Neurosurgery, Juntendo University Shizuoka Hospital, Izunokuni City, Shizuoka, Japan

Correspondence
Takuji Yamamoto, M. D. · Department of Neurosurgery ·
Juntendo University Shizuoka Hospital · 1129 Nagaoka · Izunokuni City · Shizuoka 410–2295 · Japan
Tel.: +81/55/948/3111 · Fax: +81/55/946/0516 · E-mail: tyamamoto@med-juntendo.jp

Bibliography
Minim Invas Neurosurg 2006; 49: 173–178 © Georg Thieme Verlag KG Stuttgart · New York
DOI 10.1055/s-2006-944242
ISSN 0946-7211

omy surgery for elderly patients or high-risk patients. Suboccipital craniectomy also requires extensive procedures for decompression of the posterior fossa or to prevent postoperative cerebrospinal fluid (CSF) leakage. Recently, endoscopic surgery for hypertensive putaminal hemorrhage has been widely performed [6–8]. Endoscopic surgery can access the hematoma through the burr hole and safely evacuate it under endoscopic control. The use of the coagulation system enables effective hemostasis [9].

This study describes the endoscopic technique for evacuation of cerebellar hemorrhage via a single burr hole and compares the procedure with craniectomy for the treatment of patients with spontaneous/hypertensive cerebellar hemorrhage.

Materials and Methods

The records of 69 patients with hypertensive cerebral hemorrhage treated in the Department of Neurosurgery, Juntendo University Shizuoka Hospital were retrospectively reviewed. The treatment guidelines of our university require alert patients with hematoma measuring less than 30 mm in maximum diameter to be treated by conservative therapy; and patients with hematoma larger than 30 mm in maximum diameter to be treated by hematoma evacuation with decompressive suboccipital craniectomy, or hematoma evacuation by the endoscopic technique since 2002, with ventricular drainage preceding the craniectomy for associated intraventricular hematoma and/or hydrocephalus. Twenty patients without brain stem damage were surgically treated: 10 patients by using the endoscopic technique (endoscopic group), and 10 patients by hematoma evacuation with craniectomy and extended posterior decompression (craniectomy group). All patients with abnormal vascular diseases such as aneurysm and arteriovenous malformation were excluded based on angiographic findings. All patients were admitted within 24 hours of onset.

The level of consciousness and the outcome were assessed using the Glasgow Coma Scale and the intracerebral hemorrhage score which is related to the severity of intracerebral hemorrhage [10] at admission, and the Glasgow Outcome Scale and modified National Institutes of Health scale at discharge and at 3 months after onset. The size of the hematoma was taken as the maximum diameter and volume measured on computed tomography (CT) scans. Postoperative CT was performed just after surgery to evaluate the extent of hematoma evacuation, and the day after surgery to check for rebleeding. Shunt surgery was performed if hydrocephalus was identified.

The surgical procedure time, duration of ventricular drainage, extent of hematoma evacuation, necessity for CSF shunt, surgical complications, period of hospitalization, and outcome at discharge and at 3 months after onset were compared for the two groups.

Surgical technique

The patient is positioned in a lateral position after induction of general anesthesia. Ventricular drainage is placed prior to hematoma evacuation, if necessary. The skin incision and single burr hole are made at the point closest to the hematoma cavity (Fig. **1A**). Venous sinus injury must be avoided. A transparent sheath with metal stylet (MACHIDA, Tokyo, Japan) is inserted into the hematoma cavity. The 2.7-mm rigid endoscope (Olympus, Tokyo, Japan) and 2.5-mm suction tube designed for hematoma evacuation are inserted through the sheath. The hematoma is aspirated through the suction tube under endoscopic control (Fig. **1B**). If a bleeding point is identified, monopolar coagulation is applied through the coated suction device [9]. In patients with intraventricular hematoma, the clear sheath is advanced into the fourth ventricle under endoscopic control, and the intraventricular hematoma is gently removed without brain stem injury (Fig. **1C, D**). Finally, a drainage tube is placed into the fourth ventricle and hematoma cavity.

Illustrative cases

Case 1: A 72-year-old female presented with severe headache, vertigo, and nausea. CT revealed cerebellar hemorrhage with intraventricular hemorrhage and acute hydrocephalus (Fig. **2** upper panel). On admission, bilateral external ventricular drainages were placed for acute hydrocephalus. Angiography was performed to confirm the absence of vascular malformations. Endoscopic hematoma evacuation was then performed. Most of the cerebellar hematoma was removed without major bleeding problems (Fig. **2**, lower panel). The endoscope was passed into the fourth ventricle and the hematoma was evacuated. After surgery, her consciousness recovered to alert. The hydrocephalus was immediately resolved, and no shunt operation was required.

Case 2: A 71-year-old man suffered from a consciousness disturbance. CT revealed a hematoma in the cerebellum and acute hydrocephalus without vascular anomaly (Fig. **3**, upper panel). The hematoma volume was 20.4 mL. Endoscopic hematoma evacuation surgery was performed under a diagnosis of hypertensive cerebellar hemorrhage. The cerebellar hematoma was successfully removed with no surgical complications (Fig. **3**, lower panel). The obstructive hydrocephalus was resolved by fourth ventricular drainage.

Case 3: A 68-year-old man was transferred to our institute with a diagnosis of cerebellar hemorrhage. The enlarged hematoma had a maximum diameter of 4.3 cm (Fig. **4**, upper panel). The cerebellar hematoma was effectively removed by the endoscopic technique (Fig. **4**, lower panel). CSF drainage was continued for 2 days. He was treated in our hospital for 20 days, and discharged with mild cerebellar ataxia.

Results

Table **1** shows the characteristics of the patients. There was no statistical difference between the endoscopic group and the craniectomy group.

Table **2** shows the surgical results. The extent of hematoma evacuation was greater in the endoscopic group (95.2%) than in the craniectomy group (90.6%) but without the difference being significant. The endoscopic technique (64.5 min) took significantly less time than the craniectomy method (230.6 min, $p < 0.0001$). Six of the 10 patients treated by the endoscopic technique presented with intraventricular hematoma and hydrocephalus.

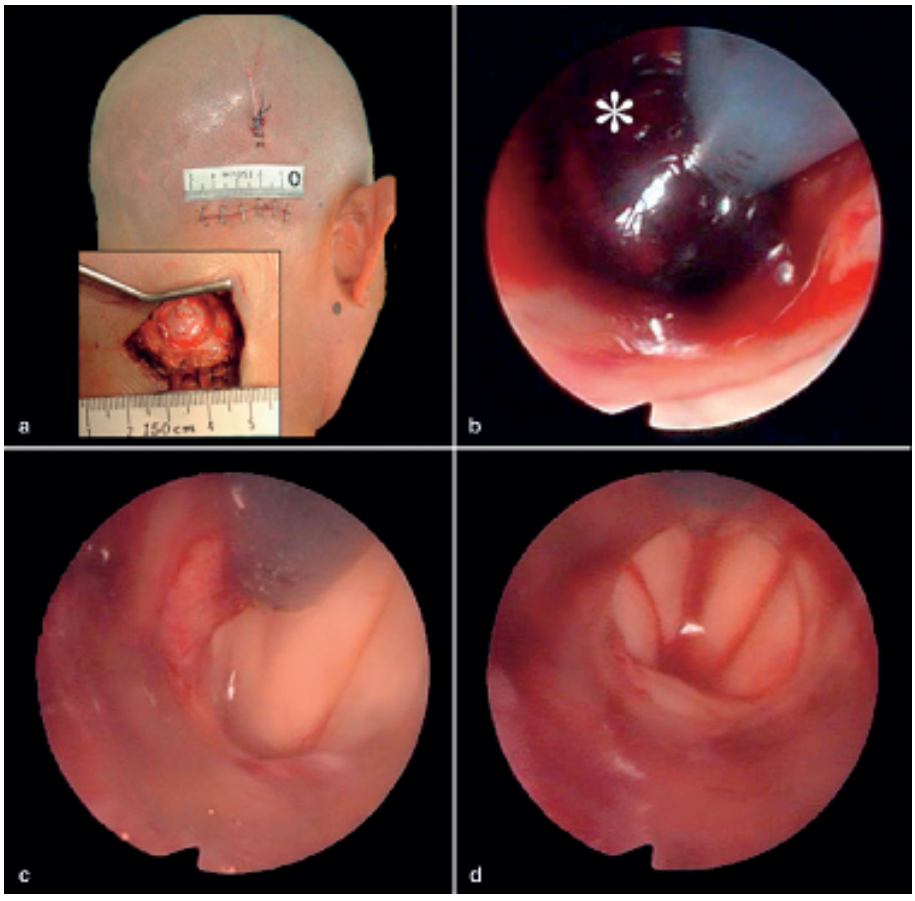

Fig. **1** Intraoperative photographs showing the skin incision and single burr hole made at the closest point to the hematoma (**A**). Hematoma (*) was gently aspirated under endoscopic control (**B**). After removal of the hematoma in the fourth ventricle, the floor of the fourth ventricle (**C**) and CSF outflow from the aqueduct (**D**) could be observed.

Nine of the 10 patients underwent ventricular drainage. No patient required shunt surgery. No complications with the ventricular drainage such as meningitis were observed. Seven of the 10 patients in the craniectomy group had intraventricular hemorrhage and nine patients had hydrocephalic status. All 10 patients underwent ventricular drainage. Three patients required ventriculoperitoneal shunting for post-intraventricular hemorrhage hydrocephalus ($p = 0.06$). No severe systemic complication such as pneumonia, deep-seated vein thrombosis, or cardiac failure occurred. One patient worsened because of major tranquilizer administration for the treatment of schizophrenia. The period of ventricular drainage was significantly shorter in the endoscopic group (2.6 days) compared to the craniectomy group (12.3 days, $p < 0.01$). Two patients in the craniectomy group were treated for meningitis caused by long-term drainage. Rebleeding occurred in one patient in the craniectomy group but none in the endoscopic group.

Table **3** shows the outcomes of the patients. Eight patients in the endoscopic group had a good recovery or moderate disability, compared to three in the craniectomy group, but there was no significant difference between the groups.

Table **1** Patient characteristics*

	Endoscopic Group	*Craniectomy Group*
No. of patients	10	10
female/male	4/5	4/5
mean age (range)	69.3 (54 – 82) years	67.3 (53 – 86) years
mean GCS score (range)	12.7 (5 – 15)	10.7 (5 – 15)
mean ICH score (range)	2.0 (1 – 4)	2.3 (1 – 5)
CT findings		
mean hematoma volume	15.9 mL	22.3 mL
intraventricular hematoma	6 patients	7 patients
hydrocephalus	6 patients	9 patients

*GCS = Glasgow coma scale; ICH = intracerebral hemorrhage; CT = computed tomography.

Table **2** Surgical results

	Endoscopic Group	*Craniectomy Group*
mean duration of surgery	64.5 min*	230.6 min
mean extent of hematoma evacuation	95.2 %	90.6 %
rebleeding after surgery	0 patients	1 patient
external ventricular drainage	9 patients	10 patients
mean period of drainage	2.6 days*	12.3 days
meningitis	0 patients	2 patients
ventriculoperitoneal shunt	0 patients**	3 patients

*$p < 0.05$; **$p = 0.06$.

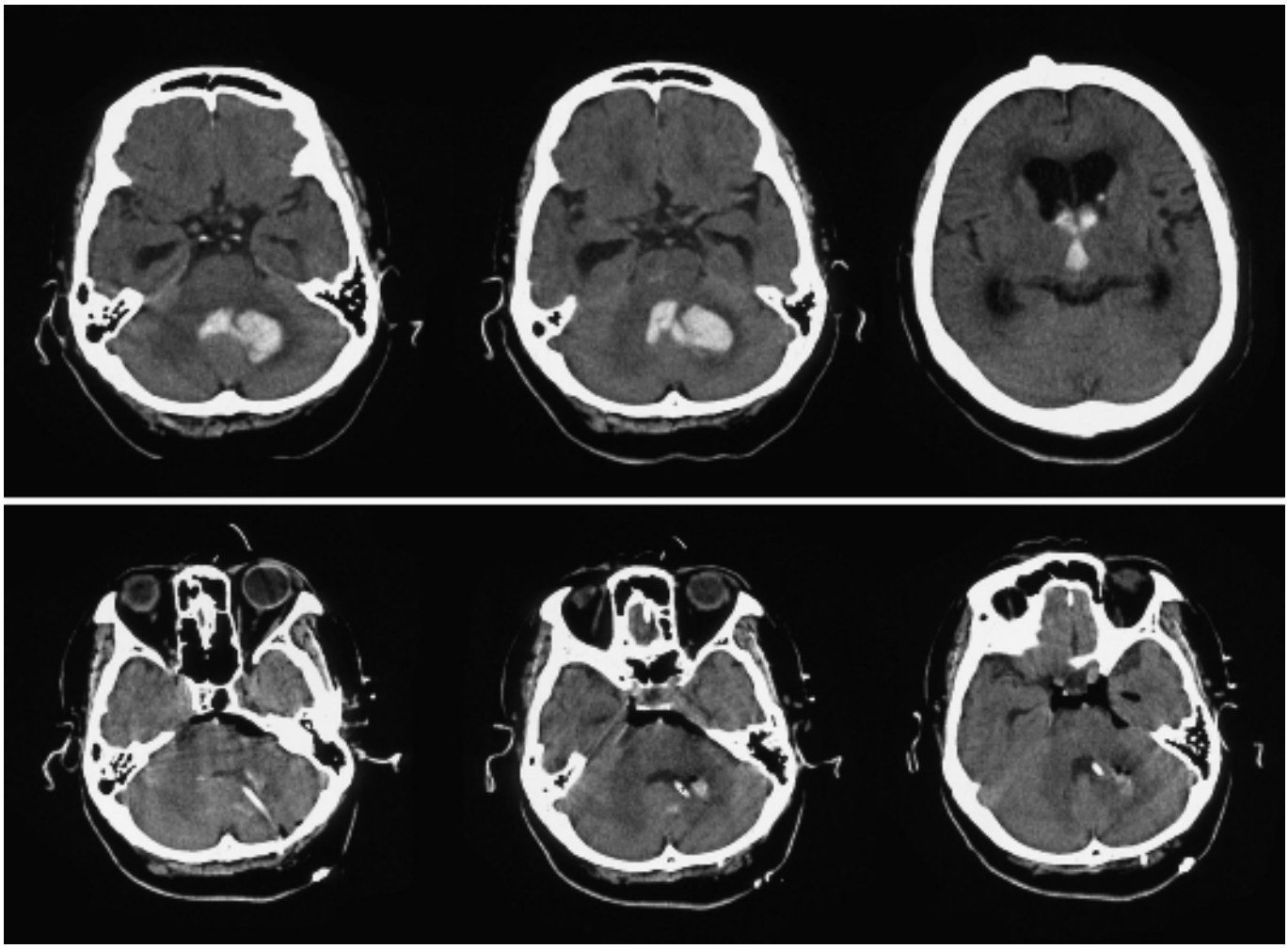

Fig. **2** Case 1. Upper panel: Preoperative CT scans revealing left cerebellar hemorrhage with intra-fourth ventricular hematoma causing obstructive acute hydrocephalus. Lower panel: Postoperative CT scans showing removal of the hematoma in both the cerebellum and fourth ventricle.

Discussion

In our opinion, hypertensive intracerebral or cerebellar hematoma should be directly and immediately removed by surgery. The surgery should be rapid and simple, and provide a high evacuation rate with a low risk of complications. Aspiration surgery via a burr hole or drainage using fibrinolytic agents has been described as less-invasive surgery to treat hypertensive cerebellar hemorrhage [11,12]. However, this method involves a risky blind procedure in the hematoma cavity, and a reduction of intracranial pressure is not obtained immediately. Recurrent hemorrhage after hematoma aspiration is an important complication [13]. The reported rebleeding risk after stereotactic hematoma aspiration ranges between 1.6% and 10% [14,15]. Such a complication might be caused by excessive aspiration without any hemostatic device.

Table **3** Clinical outcomes*

Glasgow Outcome Scale	*Endoscopic Group*	*Craniectomy Group*
GR	4	2
MD	4	1
SD	2	7
VS	0	0
D	0	0

*GR = good recovery; MD = moderate disability; SD = severe disability; VS = vegetative state; D = dead.

The endoscopic technique facilitates the precise localization of the hematoma so that surgical trauma can be minimized. More than 90% of the hematoma can be directly removed, and hemostasis confirmed under endoscopic control. The procedure takes approximately 60 to 90 minutes, which is much quicker than the conventional surgical technique. This shortening of operation time may bring a decline in surgical systemic complications. No recurrent hemorrhage was observed in the present series of 10 patients, indicating that hemostasis could be effectively achieved with the monopolar coagulation device combined with a suction tube [9]. It is important to first exclude particular diseases requiring surgery with craniectomy, such as a ruptured aneurysm, arteriovenous malformation, or hemorrhagic brain tumor.

The objective of conventional surgery with posterior decompression is to reduce the compression of the brain stem. In this series,

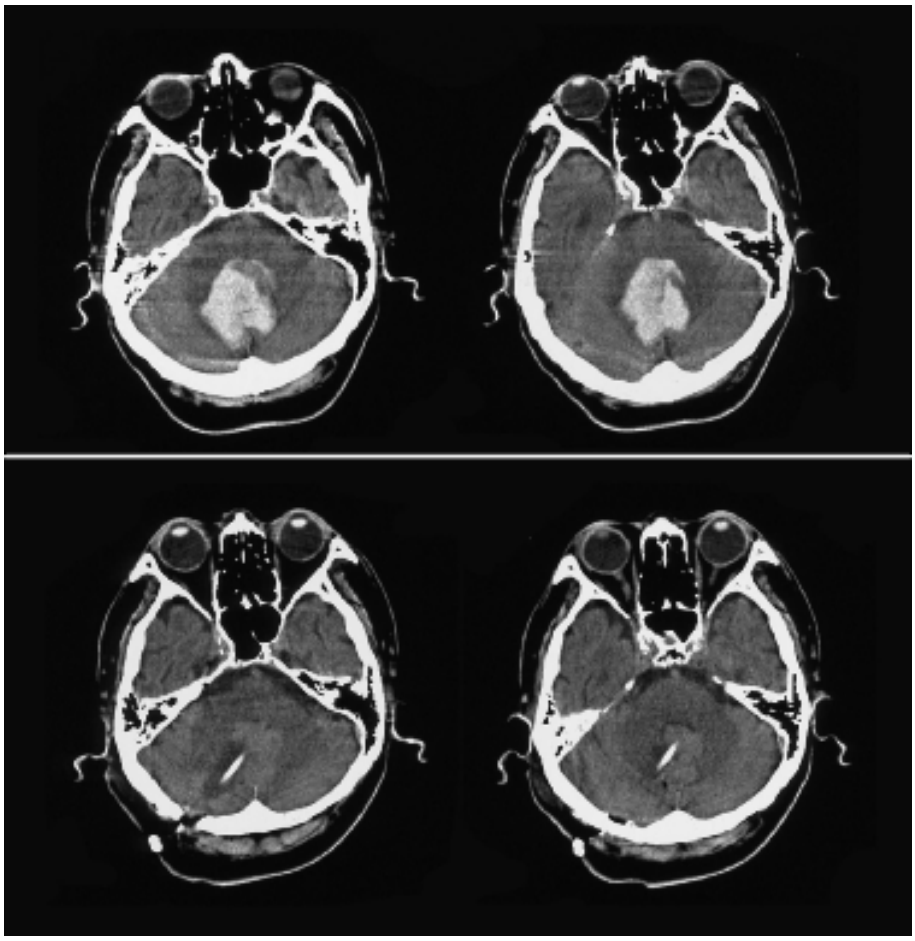

Fig. **3** Case 2. Upper panel: Preoperative CT scans revealing cerebellar hemorrhage measuring 4.5 × 3.5 × 3.0 cm, and volume of 20.4 mL. Lower panel: Postoperative CT scans showing that more than 95 % of the hematoma was removed which took 55 minutes.

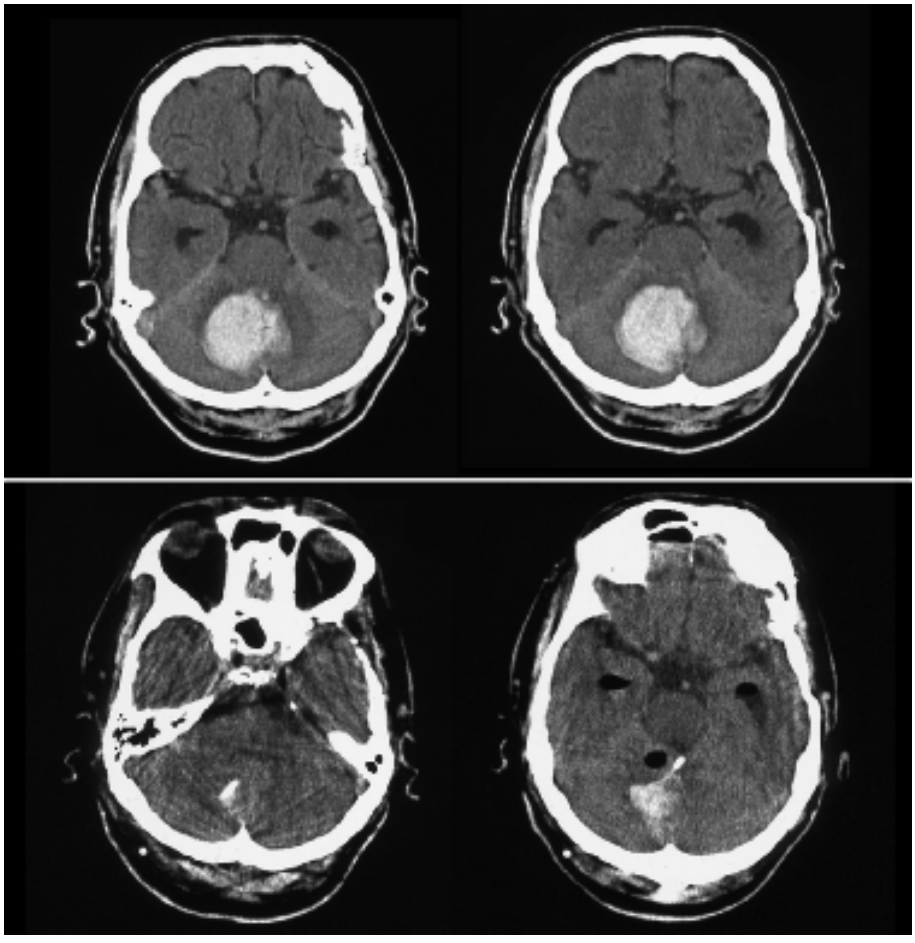

Fig. **4** Case 3. Upper panel: Preoperative CT scans revealing cerebellar hemorrhage and the enlarged hematoma with a maximum diameter of 4.3 cm. Lower panel: Postoperative CT scans showing most of the hematoma was removed. Acute hydrocephalus was managed by short-term ventricular drainage.

CT after surgery showed that the brain stem was decompressed in all patients. All patients recovered consciousness after surgery. Therefore, endoscopic hematoma evacuation via a small burr hole was effective for a reduction of the mass effect on the brain stem.

The endoscopic method may also reduce the need for shunt surgery. No patients treated by the endoscopic technique required shunt surgery, despite the presence of intraventricular hemorrhage. The endoscopic technique can both reduce the compression of the fourth ventricle and directly remove hematoma from the fourth ventricle. As a result, obstructive hydrocephalus can be resolved and the CSF circulation can be normalized immediately after surgery. Progressive hydrocephalus is a known predictor of poor outcome [5]. Immediate CSF drainage can reduce the requirement for permanent shunt emplacement and the risk of meningitis.

This study did not demonstrate that endoscopic surgery provides a better outcome than conservative treatment. Conservative therapy is generally more effective than surgery for small hematomas. In contrast, the surgical indications for patients with severe damage of the brain stem caused by huge hematomas remain controversial [2]. The present study suggests that endoscopic surgery provides a less-invasive method for the removal of cerebellar hematoma compared with conventional craniectomy with external decompression, and also reduces elevated intracranial pressure faster than simple hematoma evacuation. Moreover, hemostasis can be effectively performed and confirmed using the monopolar coagulation system under endoscopic control.

We conclude that endoscopic hematoma evacuation is an effective, rapid, and safe technique for the removal of hypertensive cerebellar hemorrhage. Reduction of the mass effect can be accomplished with a low risk of recurrent hemorrhage. Release of obstructive hydrocephalus in the early stage may improve the patient's condition and decrease the requirement for permanent shunt emplacement.

References

[1] Mendelow AD, Gregson BA, Fernandes HM, Murray GD, Teasdale GM, Hope DT et al. Early surgery versus initial conservative treatment in patients with spontaneous supratentorial intracerebral haematomas in the International Surgical Trial in Intracerebral Haemorrhage (STICH): a randomized trial. Lancet 2005; 29: 387 – 397

[2] Kobayashi S, Sato A, Kageyama Y, Nakamura H, Watanabe Y, Yamaura A. Treatment of hypertensive cerebellar hemorrhage – surgical or conservative management? Neurosurgery 1994; 34: 246 – 250

[3] Little JR, Tubman DE, Ethier R. Cerebellar hemorrhage in adults. Diagnosis by computerized tomography. J Neurosurg 1978; 48: 575 – 579

[4] Waidhauser E, Hamburger C, Marguth F. Neurosurgical management of cerebellar hemorrhage. Neurosurg Rev 1990; 13: 211 – 217

[5] Kirollos RW, Tyagi AK, Ross SA, Hille PT van, Marks PV. Management of spontaneous cerebellar hematomas: a prospective treatment protocol. Neurosurgery 2001; 49: 1378 – 1386

[6] Auer LM, Deinsberger W, Niederkorn K, Gell G, Kleinert R, Schneider G et al. Endoscopic surgery versus medical treatment for spontaneous intracerebral hematoma: a randomized study. J Neurosurg 1989; 70: 530 – 535

[7] Hsieh PC, Cho DY, Lee WY, Chen JT. Endoscopic evacuation of putaminal hemorrhage: how to improve the efficiency of hematoma evacuation. Surg Neurol 2005; 64: 147 – 153

[8] Nakano T, Ohkuma H, Ebina K, Suzuki S. Neuroendoscopic surgery for intracerebral hemorrhage – comparison with traditional therapies. Minim Invas Neurosurg 2003; 46: 278 – 283

[9] Nishihara T, Teraoka A, Morita A, Ueki K, Takai K, Kirino T. A transparent sheath for endoscopic surgery and its application in surgical evacuation of spontaneous intracerebral hematomas. Technical note. J Neurosurg 2000; 92: 1053 – 1055

[10] Hemphill 3rd JC, Bonovich DC, Besmertis L, Manley GT, Johnston SC. The ICH score: a simple, reliable grading scale for intracerebral hemorrhage. Stroke 2001; 32: 891 – 897

[11] Takanashi Y, Shinonaga M. Usefulness of aspiration surgery for elderly patients with hypertensive cerebellar hemorrhage. No To Shinkei 1998; 50: 751 – 754 (in Japanese)

[12] Yokote H, Komai N, Nakai E, Ueno M, Hayashi S, Terashita T. Stereotactic evacuation of hypertensive cerebellar hemorrhage using plasminogen activator. No Shinkei Geka 1989; 17: 421 – 426 (in Japanese)

[13] Marquardt G, Wolff R, Seifert V. Multiple target aspiration technique for subacute stereotactic aspiration of hematomas within the basal ganglia. Surg Neurol 2003; 60: 8 – 13

[14] Lippitz BE, Mayfrank L, Spetzger U, Warnke JP, Bertalanffy H, Gilsbach JM. Lysis of basal ganglia haematoma with recombinant tissue plasminogen activator (rtPA) after stereotactic aspiration: initial results. Acta Neurochir (Wien) 1994; 127: 157 – 160

[15] Niizuma H, Otsuki T, Yonemitsu T, Kitahara M, Katakura R, Suzuki J. Experiences with CT-guided stereotaxic biopsies in 121 cases. Acta Neurochir Suppl (Wien) 1988; 42: 157 – 160

D. Gurkanlar[1]
E. Yucel[2]
U. Er[3]
S. Keskil[4]

Spontaneous Regression of Cervical Disc Herniations

Abstract

The spontaneous regression of cervical disc herniations is a rare occurrence. Six herniated cervical discs that had regressed spontaneously are presented. All radiological disc regressions correlated well with clinical improvements. We want to underscore the potential for regression that should be considered in the evaluation and management of any patient with a herniated cervical disc.

Key words

Extruded disc · non-surgical · radiculopathy

Introduction

Guinto et al. had first documented the spontaneous herniated nucleus pulposus (HNP) regression in 1984 [1]. Spontaneous regression of herniated lumbar disc herniations has been well documented and discussed [2–5], but spontaneous regression of cervical intervertebral disc herniations is rarely reported, which is possibly non-representative of the general population. Here we present the spontaneous regression of herniated cervical discs in six cases. The scans of all the patients were obtained using 1.5-T magnetic resonance imaging (MRI) scanners and interpreted independently by all the authors.

Case Reports

Case 1

A 49-year-old woman suffering from neck pain had been admitted to our hospital without any brachial pain or hypesthesia. Her neurological examination was normal although the cervical MRI revealed a C5–6 right posterolateral extruded HNP (Figs. **1a** and **c**). An operation was not recommended and the patient was referred to the physical therapy department. After three weeks while still on the waiting list, her symptoms improved and her follow-up cervical MRI obtained five years later revealed a total regression of the cervical disc herniation (Figs. **1b** and **d**).

Case 2

A 34-year-old woman suffering from neck and right brachial pain with C7 distribution was admitted to our hospital. Her neurological examination revealed no muscle weakness but only C6 and C7 hypesthesia. She was managed conservatively with oral analgesics and physical therapy leading to marked improvement of her symptoms. Although the initial MRI revealed C6–7 posterocentral HNP, her follow-up MRI obtained two years later showed regression of the herniated cervical disc (Figs. **2a–d**).

Case 3

A 33-year-old man suffering from right brachial pain was admitted to our outpatient clinic and his neurological examination revealed motor weakness of the right forearm and wrist flexion to-

Affiliation
[1] Department of Neurosurgery, Akderiz University, Antalya, Turkey
[2] Department of Neurosurgery, Zonguldak County Hospital, Zonguldak, Turkey
[3] Department of Neurosurgery, SSK Social Security Hospital, Ankara, Turkey
[4] Department of Neurosurgery, Bayendar Medical Center, Ankara, Turkey

Correspondence
Prof. Dr. Semih Keskil, M.D., Ph.D. · Fethiye Sokak No: 4/6 · Gazi Osman Pasa · 06700 Ankara · Turkey
Tel.: +90/532/615/8422 · Fax: +90/318/225/2819 · E-mail: sk06-k@tr.net

Bibliography
Minim Invas Neurosurg 2006; 49: 179–183 © Georg Thieme Verlag KG Stuttgart · New York
DOI 10.1055/s-2006-932194
ISSN 0946-7211

Fig. **1** **a** T_2-weighted sagittal MRI showing C5 – 6 extruded disc herniation. **b** T_1-weighted sagittal MRI showing spontaneous regression of the C5 – 6 extruded disc herniation. **c** T_2-weighted axial MRI showing C5 – 6 left posterolateral extruded disc herniation. **d** T_2-weighted axial MRI showing spontaneous regression of the C5 – 6 left posterolateral extruded disc herniation.

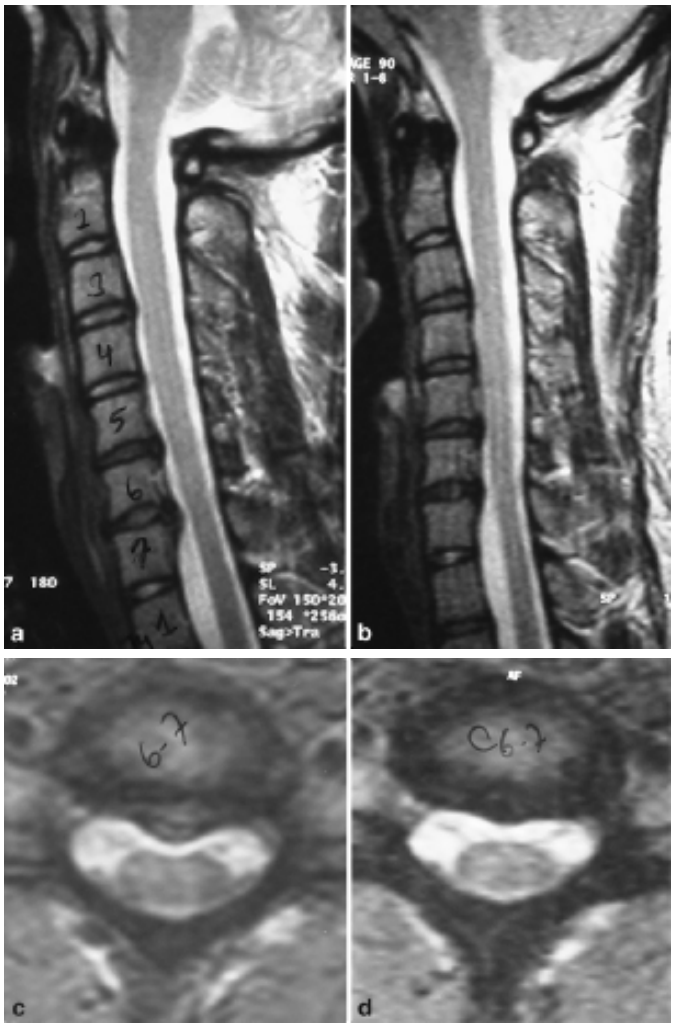

Fig. **2** **a** T_2-weighted sagittal MRI showing C6 – 7 extruded disc herniation. **b** T_2-weighted sagittal MRI showing spontaneous regression of the C6 – 7 extruded disc herniation. **c** T_2-weighted axial MRI showing C6 – 7 posterocentral extruded disc herniation. **d** T_2-weighted axial MRI showing spontaneous regression of the C6 – 7 posterocentral extruded disc herniation.

gether with right C5 and C6 hypesthesia. His initial MRI revealed C5 – 6 right posterolateral intraforaminal disc herniation (Figs. **3a** and **c**). He was managed conservatively with oral analgesics and physical therapy. His symptoms improved in two months time and the follow-up MRI showed spontaneous regression of the herniated cervical disc (Figs. **3b** and **d**).

Case 4

A 36-year-old woman suffering from neck and left brachial pain was admitted to our hospital and her neurological examination revealed motor weakness of left forearm extension and diminished triceps reflex. The MRI revealed a C6 – 7 left foraminal HNP (Fig. **4a**). She was offered surgery but refused to undergo the operation. After four weeks without receiving any specific therapy, she showed clinical improvement and her neurological examination was intact. The follow-up MRI obtained one year later revealed complete regression of the herniated intervertebral disc (Fig. **4b**).

Case 5

A 49-year-old man presented to our hospital with one-week history of neck and bilateral brachial pain. His neurological examination revealed marked weakness in right forearm extension, C6 – 7 hypesthesia and absent right triceps reflex, together with mild left forearm weakness, absent left biceps reflex and left C5 – 6 hypesthesia. MRI of the cervical spine revealed C4 – 5 left paramedian, C5 – 6 diffuse posterior and C6 – 7 posterocentral HNP (Figs. **5a** and **c – e**). He was offered an anterior cervical discectomy but refused the operation. Within two weeks time, his symptoms showed improvement. Six months later, control MRI revealed regression of the disc herniation at the C4 – 5 level (Figs. **5b** and **f**), but no regression of the herniations at the CS-6 and C6 – 7 levels (Figs. **5b**, **g** and **h**).

Case 6

A 32-year-old women who had been suffering from right brachial pain for 8 months was admitted to our outpatient clinic. Her neurological examination revealed motor weakness of the right wrist flexion and C6 hypesthesia. Her MRI revealed C6 – 7

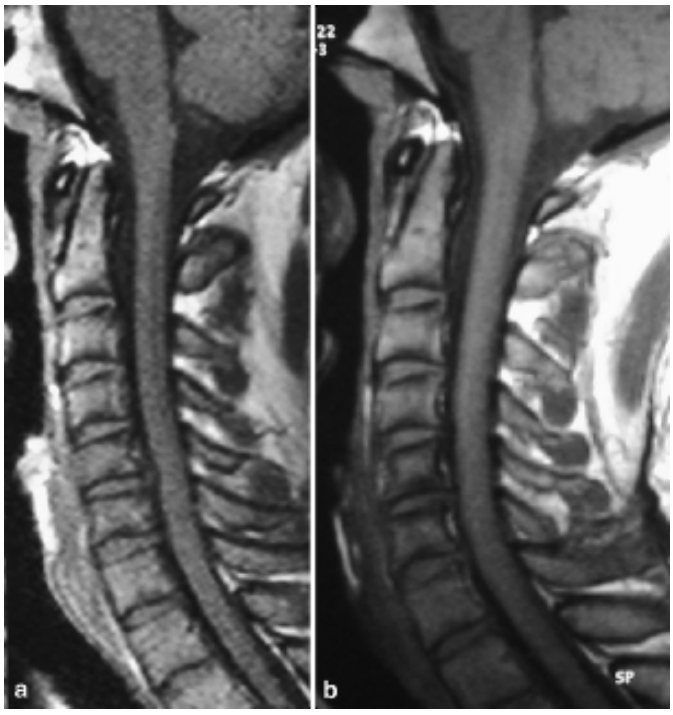

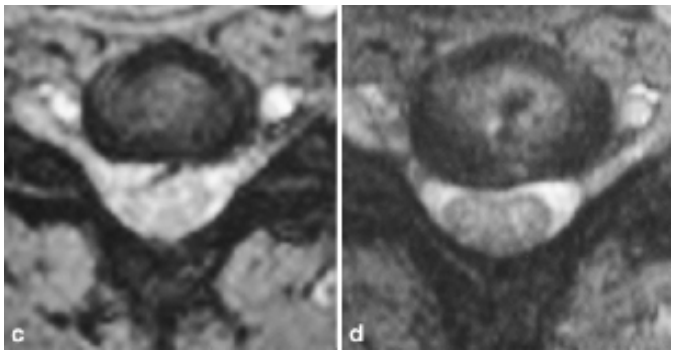

Fig. **3** **a** T_1-weighted sagittal MRI showing C5 – 6 disc herniation. **b** T_1-weighted sagittal MRI showing spontaneous regression of the C5 – 6 protrusion. **c** T_2-weighted axial MRI showing C5 – 6 right posterolateral intraforaminal disc herniation. **d** T_2-weighted axial MRI showing marked spontaneous regression of the CS – 6 right posterolateral-intraforaminal disc herniation.

right posterolateral disc herniation (Figs. **6a**, **c** and **e**). Although she did not undergo any conservative therapy, her symptoms showed marked improvement after two months and now she is free of pain and hypesthesia. Her control MRI showed spontaneous regression of the aforementioned disc herniation (Figs. **6b**, **d** and **f**).

Discussion

Since the initial documentation of the spontaneous herniated nucleus pulposus (HNP) regression in early 1980s by Guinto et al. [1] and Teplick et al. [5], the spontaneous resolution in cervical disc herniations has been documented only in 12 cases [6 – 13] up to now. We report six more patients. Formerly CT and recently MRI, which provides much more detailed information, have been used to document this regression in different spinal compartments [1,2,4,14 – 16].

However, the mechanism of spontaneous regression is still controversial, and in migrated or sequestrated type herniation, dehydration of expanded nucleus pulposus, resorption of hematoma neovascularization, phagocytosis, preinflammatory chemokines (MCP-1 and IL-8) are all factors suggested to be responsible [4,8,17 – 20]. All of our patients are not elderly, had extruded migrated-type posterolateral herniations without calcification, and underwent imaging procedures immediately after the onset of symptoms, similar to the patients reported in the literature. It would be inappropriate to make generalizations using the results of only a few cases and we do not advocate conservative management of a large herniated cervical disc that presents with myelopathy. However, non-surgical conservative observation for at least two or three months may be considered as an option for the treatment of patients with even significantly sized cervical disc herniations, even with radiculopathy and neurological deficits; especially for patients with a complicated medical situation.

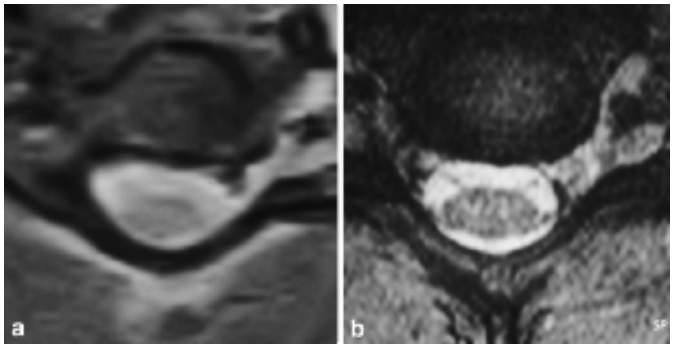

Fig. **4** **a** T_2-weighted axial MRI showing C6 – 7 left intraforaminal disc herniation. **b** T_2-weighted axial MRI showing spontaneous regression of the C6 – 7 left intraforaminal disc herniation.

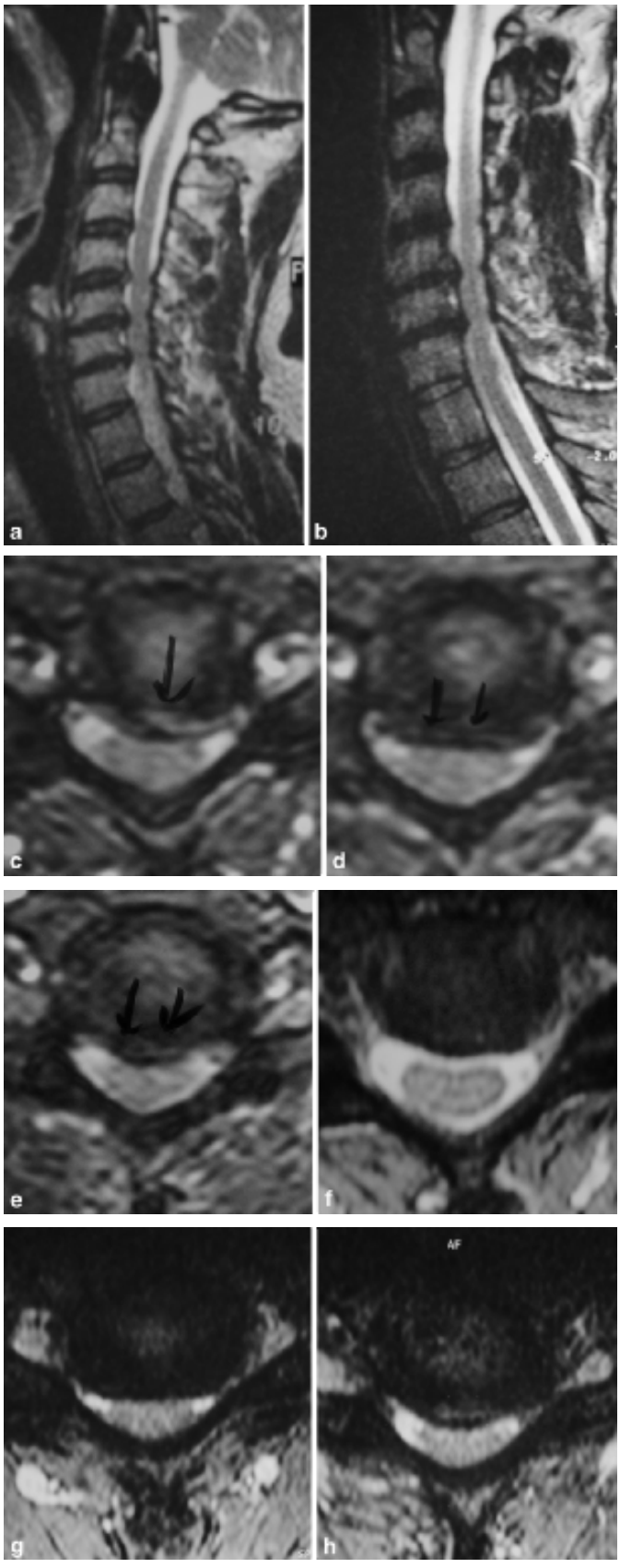

Fig. **5** **a** T_2-weighted sagittal MRI showing C4 – 5, C5 – 6, C6 – 7 disc herniations. **b** T_2-weighted sagittal MRI showing spontaneous regression of the C4 – 5 disc herniation but no regression in the C5 – 6 and C6 – 7 levels. **c** T_2-weighted axial MRI showing C4 – 5 left paramedian extruded disc herniation. **d** T_2-weighted axial MRI showing C5 – 6 diffuse posterior extruded disc herniation. **e** T_2-weighted axial MRI showing C6 – 7 posterocentral extruded disc herniation. **f** T_2-weighted axial MRI showing spontaneous regression of the C4 – 5 left paramedian extruded disc herniation. **g** T_2-weighted axial MRI showing no regression of the C5 – 6 diffuse posterior extruded disc herniation. **h** T_2-weighted axial MRI showing no regression (even worsening) of the C6 – 7 posterocentral extruded disc herniation.

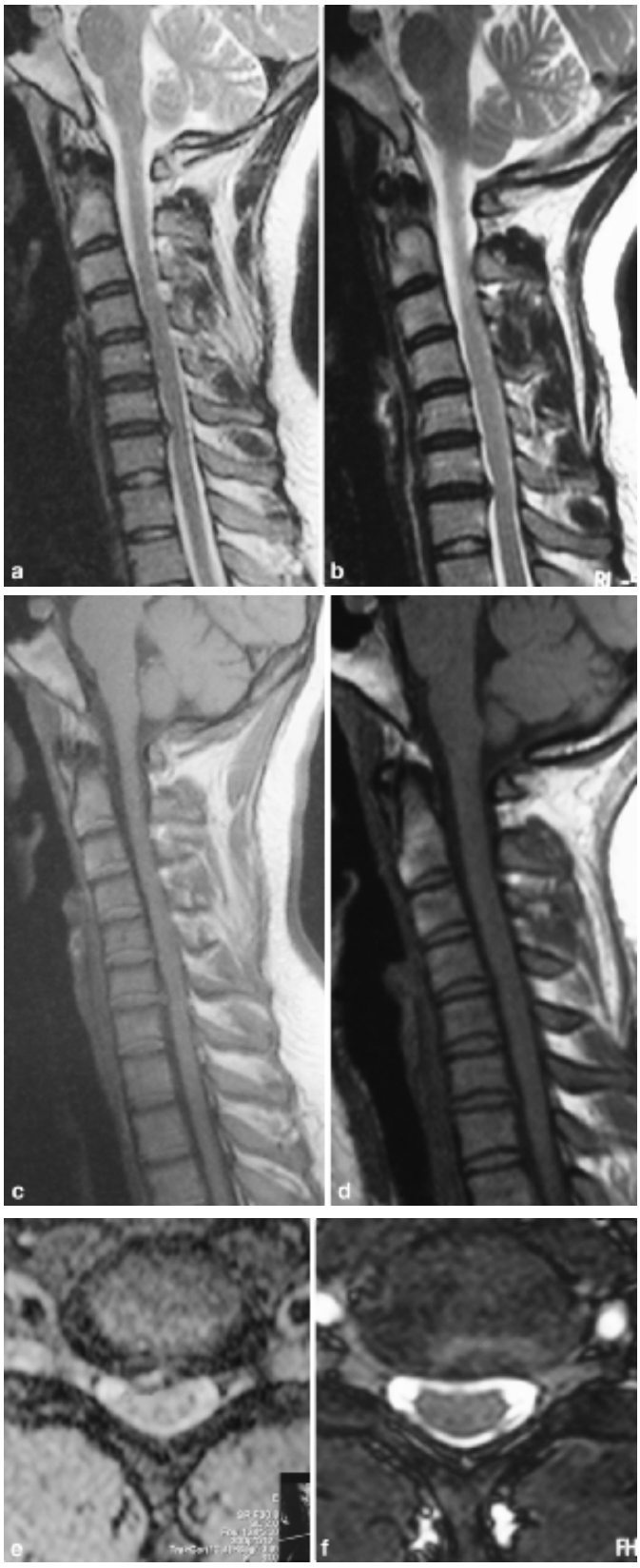

Fig. **6** **a** T_2-weighted sagittal MRI showing C6 – 7 disc herniation. **b** T_2-weighted sagittal MRI showing spontaneous regression of the C6 – 7 disc herniation. **c** T_1-weighted sagittal MRI showing C6 – 7 disc herniation. **d** T_1-weighted sagittal MRI showing spontaneous regressions of the C6 – 7 disc herniation. **e** T_2-weighted axial MRI showing right posterolateral C6 – 7 extruded disc herniation. **f** T_2-weighted axial MRI showing spontaneous regression of the right posterolateral C6 – 7 extruded disc herniation.

References

[1] Guinto FG, Hashim H, Stumer M. CT demonstration of disc regression after conservative therapy. AJNR 1984; 5: 632 – 633
[2] Keskil S, Ayberk G, Evliyaoglu C, Kızartıcı T, Yücel E, Anbarcı H. Spontaneous resolution of "protruded" lumbar discs. Minim Invas Neurosurg 2004; 47: 226 – 229
[3] Komori H, Okawa A, Haro H et al. Contrast-enhanced magnetic resonance imaging in conservative management of lumbar disc herniation. Spine 1998; 23: 67 – 73
[4] Komori H, Shinomiya K, Nakai O et al. The natural history of a herniated nucleus pulposus with radiculopathy. Spine 1996; 21: 225 – 229
[5] Teplick JG, Haskin ME. Spontaneous regression of herniated nucleus pulposus. AJR 1985; 145: 371 – 375
[6] Kobayashi N, Asamoto S, Doi H, Ikeda Y, Matusmoto K. Spontaneous regression of herniated cervical disc. Spine J 2003; 3: 171 – 173
[7] Krieger AJ, Maniker AH. MRI-documented regression of a herniated cervical nucleus pulposus: a case report. Surg Neurol 1992; 37: 457 – 459
[8] Mochida K, Komori H, Okawa A et al. Regression of cervical herniation observed on magnetic resonance images. Spine 1998; 23: 990 – 997
[9] Reddy PK, Sathyanarayana S, Nanda A. MRI-documented spontaneous regression of cervical disc herniation. A case report and review of the literature. La State Med Soc 2003; 155: 97 – 98
[10] Saal JS, Saal JA, Yurth EF. Nonoperative management of herniated cervical intervertebral disc with radiculopathy. Spine 1996; 21: 1877 – 1883
[11] Song JH, Park HK, Shin KM. Spontaneous regression of a herniated cervical disc in a patient with myelopathy. Case report. J Neurosurg (Spine 1) 1999; 90: 138 – 140
[12] Vinas FC, Wilner H, Rengachary S. The spontaneous resorption of herniated cervical discs. J Clin Neurosci 2001; 8: 542 – 546
[13] Westmark RM, Westmark KD, Sonntag VKH. Disappearing cervical disc. Case report. J Neurosurg 1997; 86: 289 – 290
[14] Ellenberg M, Reina N, Ross M, Chorodoff G, Honet JC, Gross N. Regression of herniated nucleus pulposus: two patients with lumbar radiculopathy. Arch Phys Med Rehab 1989; 70: 842 – 844
[15] Miller S, Casden AM. Spontaneous regression of a herniated disc. A case report with a four year follow-up. Bul Hosp Joint Dis 1998; 57: 99 – 101
[16] Weber H. Lumbar disc herniation. A controlled, prospective study with ten years of observation. Spine 1983; 8: 131 – 140
[17] Burke JG, Watson RW, McCormack D et al. Spontaneous production of monocyte chemoattractant protein-1 and interleukin-8 by the human lumbar intervertebral disc. Spine 2002; 27: 1402 – 1407
[18] Haro K, Shinomiya K, Komori H et al. Upregulated expression of chemokines in herniated nucleus pulposus resorption. Spine 1996; 21: 1647 – 1652
[19] Hirabayashi S, Kumano K, Tsuiki T, Eguchi M, Ikeda S. A dorsally displaced free fragment of lumbar disc herniation and its interesting histologic findings. A case report. Spine 1990; 15: 1231 – 1233
[20] Minamide A, Hashizume H, Yoshida M et al. Effects of basic fibroblast growth factor on spontaneous resorption of herniated intervertebral discs. Spine 1999; 24: 940 – 945

Unilateral Hydrocephalus Due to Foramen of Monro Stenosis

G. Dastgir[1]
A. Awad[2]
A. Salam[2]
M. Attia[2]

Case Report

Abstract

Unilateral lateral ventricular dilatation due to foramen of Monro stenosis or constriction can present with headache. Fundoscopy can be normal. This condition is congenital, radiological appraisal can disclose the diagnosis, and treatment depends upon the symptomatology. The condition can be treated well with insertion of a ventriculoperitoneal shunt.

Key words

Foramen of Monro · stenosis · lateral ventricle · dilatation

Introduction

Partial obstruction of one of the foramina of Monro may cause hydrocephalus that is limited to one whole lateral ventricle provided that there is no further partition inside the respective ventricle [1]. This condition can be congenital [2,3] and acquired. The acquired form can be a result of inflammatory disease, growth or because of intraventricular surgery [4].

Case Report

This patient was an eighteen-year-old female. She presented with headache very severe in intensity generally all over the head, but it was not constant, routine clinical examination was normal and there was no evidence of even early papilloedema. We investigated the brain with computed tomography (CT) and magnetic resonance imaging (MRI) and found that there was comparatively more dilatation of the right lateral ventricle along with calcification of the falx cerebri as shown in Fig. **1** and a thick choroid plexus as shown in Fig. **2**. We inserted a ventriculoperitoneal shunt on the right side and patient experienced relief from the headache and she is still pain-free one year after the operation.

Discussion

Stenosis or constriction of the foramen of Monro can be congenital or acquired and can appear in children and adults. The foramen of Monro can be blocked by a thin avascular membrane [5] and in these cases fenestration by endoscopic ventriculostomy (EV) is successful in almost all cases. But if the pathology is other than the thin membrane then one needs much proficiency in the endoscopic surgery as described by Cohen for the successful neuroendoscopic fenestration of an occluded foramen of Monro due to postoperative adhesions [6]. Thus, the selected operative strategy should be according to the expertise available. Other reports show unsuccessful EV in those cases where there is pathology other than a thin membrane for unilateral hydrocephalus and later on a shunt has to be inserted [7]. But this does not mean that here we are advocating shunt placement, our implication is only that one should look at the whole available setting both in relation to modern equipment and operative proficiency. Also, one can go for the EV and if no thin membrane is present it is better to come out and insert the shunt. As in this case there was a thick choroid plexus on CT findings and more handling with this can complicate the operative site.

Affiliation
[1] Neurosurgery Department, King Fahd General Hospital, Jeddha, Saudi Arabia
[2] Neurosurgery Department, King Khalid Civilian Hospital, Tabuk, Saudi Arabia

Correspondence
Dr. Ghulam Dastgir · Haki Kot · Shadara · Lahore · Pakistan · Tel.: +966/50 25 31104 ·
E-mail: safadast@hotmail.com

Bibliography
Minim Invas Neurosurg 2006; 49: 184–186 © Georg Thieme Verlag KG Stuttgart · New York
DOI 10.1055/s-2005-919162
ISSN 0946-7211

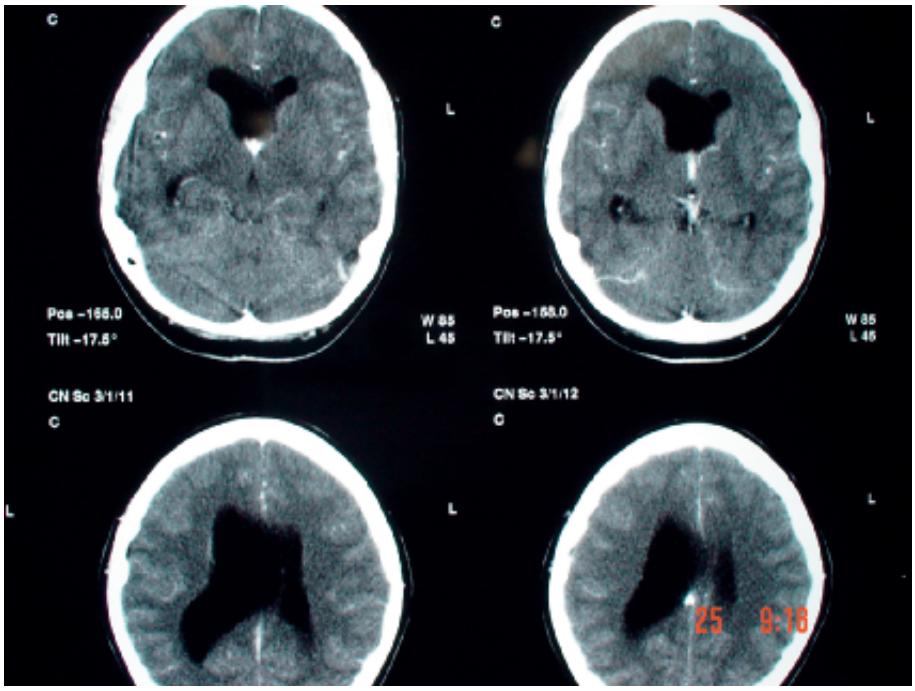

Fig. **1** CT scan of the brain shows the enlarged lateral ventricle on the right side along with calcification of the falx cerebri.

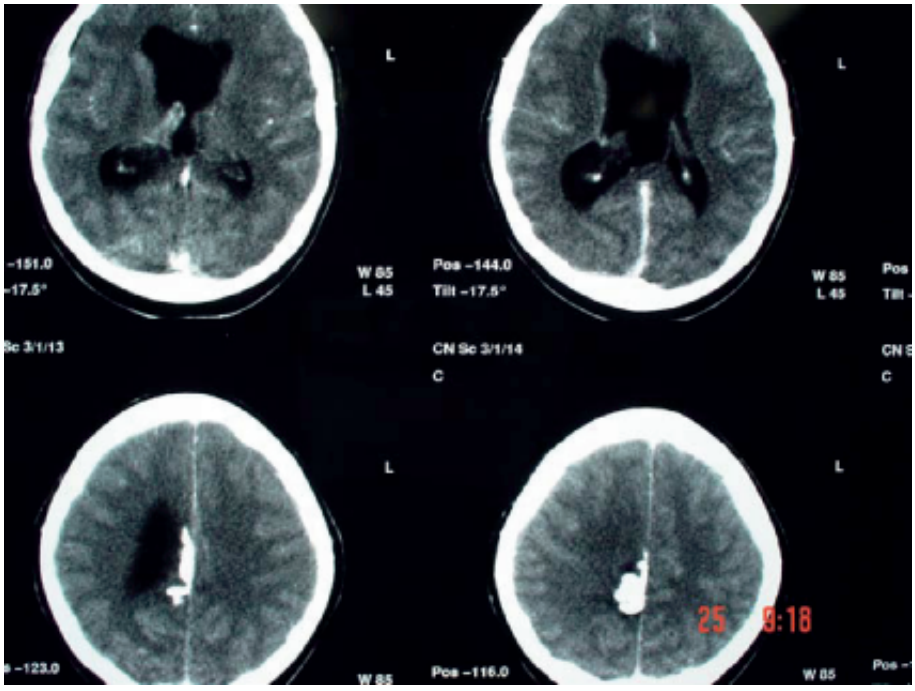

Fig. **2** CT scan of the brain with intravenous contrast shows comparative thick choroid plexus.

Conclusions

Unilateral hydrocephalus can be congenital or acquired. In those cases which are due to thickened choroids plexus the insertion of a ventriculoperitoneal shunt is the better option.

Acknowledgements

We acknowledge the support of our department team in organizing and reviewing this subject.

References

[1] Boyer B, Ildan F, Bagdatoglu H et al. Unilateral hydrocephalus resulting from occlusion of foramen of Monro. Surg Neurol 1993; 39: 110 – 114
[2] Mampalam TJ, Harsh GR IV, Tien RD et al. Unilateral hydrocephalus in adults. Surg Neurol 1991; 35: 14 – 19
[3] Marions O, Boethius J. Congenital constriction of foramen of Monro. Neuroradiology 1986; 28: 275 – 278
[4] Milhorat TH, Hammock MK, Brekhill DK. Acute unilateral hydrocephalus resulting from oedematous occlusion of foramen of Monro – complication of intraventricular surgery. J Neurol Neurosurg Psychiatry 1975; 38: 745 – 748
[5] Mohanty A, Das BS, Sastry KVR et al. Neuroendoscopic fenestration of occluded foramen of Monro causing unilateral hydrocephalus. Paediatr Neurosurg 1996; 25: 248 – 251
[6] Cohen AR. Endoscopic ventricular surgery. Paediatr Neurosurg 1993; 19: 127 – 134
[7] Kumar R. Unilateral hydrocephalus in paediatric patients, a trial of endoscopic fenestration. Neurology India 1999; 47 : 4: 282 – 285